Calhoun
Institutional Archive of the Naval Postgraduate School

Calhoun: The NPS Institutional Archive

DSpace Repository

Theses and Dissertations | 1. Thesis and Dissertation Collection, all items

2003-12

Modeling of the ring-hybrid dipole antenna and mutual coupling in a small antenna array

Ong, Chee Hwee

Monterey, California. Naval Postgraduate School

Copyright is reserved by the copyright owner.

Downloaded from NPS Archive: Calhoun

http://www.nps.edu/library

Calhoun is the Naval Postgraduate School's public access digital repository for research materials and institutional publications created by the NPS community. Calhoun is named for Professor of Mathematics Guy K. Calhoun, NPS's first appointed -- and published -- scholarly author.

Dudley Knox Library / Naval Postgraduate School
411 Dyer Road / 1 University Circle
Monterey, California USA 93943

NAVAL POSTGRADUATE SCHOOL

MONTEREY, CALIFORNIA

THESIS

MODELING OF THE RING-HYBRID DIPOLE ANTENNA AND MUTUAL COUPLING IN A SMALL ANTENNA ARRAY

by

Chee Hwee Ong

December 2003

Thesis Advisor:	David C. Jenn
Second Reader:	Roberto Cristi

Approved for public release; distribution is unlimited.

THIS PAGE INTENTIONALLY LEFT BLANK

REPORT DOCUMENTATION PAGE			Form Approved OMB No. 0704-0188
Public reporting burden for this collection of information is estimated to average 1 hour per response, including the time for reviewing instruction, searching existing data sources, gathering and maintaining the data needed, and completing and reviewing the collection of information. Send comments regarding this burden estimate or any other aspect of this collection of information, including suggestions for reducing this burden, to Washington headquarters Services, Directorate for Information Operations and Reports, 1215 Jefferson Davis Highway, Suite 1204, Arlington, VA 22202-4302, and to the Office of Management and Budget, Paperwork Reduction Project (0704-0188) Washington DC 20503.			
1. AGENCY USE ONLY *(Leave blank)*	**2. REPORT DATE** December 2003	**3. REPORT TYPE AND DATES COVERED** Master's Thesis	
4. TITLE AND SUBTITLE: Title (Mix case letters) Modeling of the Ring-Hybrid Dipole Antenna and Mutual Coupling in a Small Antenna Array			**5. FUNDING NUMBERS**
6. AUTHOR(S) Chee Hwee Ong			
7. PERFORMING ORGANIZATION NAME(S) AND ADDRESS(ES) Naval Postgraduate School Monterey, CA 93943-5000			**8. PERFORMING ORGANIZATION REPORT NUMBER**
9. SPONSORING /MONITORING AGENCY NAME(S) AND ADDRESS(ES) N/A			**10. SPONSORING/MONITORING AGENCY REPORT NUMBER**
11. SUPPLEMENTARY NOTES The views expressed in this thesis are those of the author and do not reflect the official policy or position of the Department of Defense or the U.S. Government.			
12a. DISTRIBUTION / AVAILABILITY STATEMENT Approved for public release; distribution is unlimited.			**12b. DISTRIBUTION CODE**

13. ABSTRACT (maximum 200 words)

This thesis project modeled a microstrip ring-hybrid dipole that is capable of simultaneously producing a sum pattern and difference pattern using the method of moments (MoM) based on the Rao-Wilton-Glisson (RWG) edge elements. The ring-hybrid dipole is simply a ring-hybrid coupler driving a dipole antenna. A two-feed point dipole model was developed and its antenna parameters were found to be a good representation of the ring-hybrid dipole actual values. In the feed network modeling, the matrix solution combined the MoM equations on the antenna surfaces and a magic-tee scattering matrix by applying Kirchhoff's voltage and current laws at the terminals of the antenna. Once the excitation is specified, the complete system of equations was solved to yield the MoM current expansion coefficients and the signals in the feed network.

The effect of mutual coupling in an array of three ring-hybrid dipoles was examined by extending the model. In the receive mode, the direction and polarization of the incidence plane wave were varied. The phases for both the sum port and difference port outputs were observed to change smoothly, except during situations of cross polarization and zero phase difference. The array model will form the foundation for the design and analysis of a mutual coupling compensation network.

14. SUBJECT TERMS Method of Moments, RWG Basis Function, Scattering and Radiation, Matlab, Dipole Antenna, Antenna Feed Network, Scattering Parameters, Transmission Line, Magic-Tee, Ring Hybrid, Phased Array Antenna, Mutual Coupling.			**15. NUMBER OF PAGES** 119
			16. PRICE CODE
17. SECURITY CLASSIFICATION OF REPORT Unclassified	**18. SECURITY CLASSIFICATION OF THIS PAGE** Unclassified	**19. SECURITY CLASSIFICATION OF ABSTRACT** Unclassified	**20. LIMITATION OF ABSTRACT** UL

NSN 7540-01-280-5500 Standard Form 298 (Rev. 2-89)
Prescribed by ANSI Std. 239-18

THIS PAGE INTENTIONALLY LEFT BLANK

Approved for public release; distribution is unlimited.

MODELING OF THE RING-HYBRID DIPOLE ANTENNA AND MUTUAL COUPLING IN A SMALL ANTENNA ARRAY

Chee Hwee Ong
MAJ, Republic of Singapore Navy
B.E. (Honors), University of Edinburgh, UK, 1998

Submitted in partial fulfillment of the
requirements for the degree of

**MASTER OF SCIENCE IN ENGINEERING SCIENCE
(ELECTRICAL ENGINEERING)**

from the

**NAVAL POSTGRADUATE SCHOOL
December 2003**

Author: Chee Hwee Ong

Approved by: David C. Jenn
Thesis Advisor

Roberto Cristi
Second Reader

John P. Powers
Chairman, Department of Electrical and Computer Engineering

THIS PAGE INTENTIONALLY LEFT BLANK

ABSTRACT

This thesis project modeled a microstrip ring-hybrid dipole that is capable of simultaneously producing a sum pattern and difference pattern using the method of moments (MoM) based on the Rao-Wilton-Glisson (RWG) edge elements. The ring-hybrid dipole is simply a ring-hybrid coupler driving a dipole antenna. A two-feed point dipole model was developed and its antenna parameters were found to be a good representation of the ring-hybrid dipole actual values. In the feed network modeling, the matrix solution combined the MoM equations on the antenna surfaces and a magic-tee scattering matrix by applying Kirchhoff's voltage and current laws at the terminals of the antenna. Once the excitation is specified, the complete system of equations was solved to yield the MoM current expansion coefficients and the signals in the feed network.

The effect of mutual coupling in an array of three ring-hybrid dipoles was examined by extending the model. In the receive mode, the direction and polarization of the incidence plane wave were varied. The phases for both the sum port and difference port outputs were observed to change smoothly, except during situations of cross polarization and zero phase difference. The array model will form the foundation for the design and analysis of a mutual coupling compensation network.

THIS PAGE INTENTIONALLY LEFT BLANK

TABLE OF CONTENTS

I. INTRODUCTION....1
A. MOTIVATION....1
B. OBJECTIVES....3
C. OUTLINE OF CHAPTER....4

II. METHOD OF MOMENTS AND THE RWG BASIS FUNCTIONS....5
A. CHAPTER OVERVIEW....5
B. RWG BASIS FUNCTIONS....5
C. THE RECEIVING ALGORITHM....7
1. Introduction....7
2. Matlab Code Sequence....8
3. Creating the Antenna Structure....10
4. RWG Edge Elements....10
5. Impedance Matrix....12
6. Moment Equations and Surface Currents....14
D. THE TRANSMITTING ALGORITHM....15
1. Introduction....15
2. Strip Model of a Wire....16
3. Feed Model....16
4. Input Impedance....18
E. CHAPTER SUMMARY....19

III. ANTENNA MODELING....21
A. CHAPTER OVERVIEW....21
B. CONVERGENCE TEST....21
C. ANTENNA PARAMETERS FOR CENTER-FED DIPOLE....22
1. Antenna Impedance and Gain....22
2. Transmitted and Received Power....24
D. MODELING OF THE RING-HYBRID DIPOLE FEED....27
E. TWO-FEED POINT DIPOLE....28
1. Antenna Impedance and Gain....29
2. Feed Power and Radiated Power....29
F. CHAPTER SUMMARY....33

IV. ANTENNA BEAMFORMING NETWORK MODELING....35
A. CHAPTER OVERVIEW....35
B. BASIC THEORY....35
C. CENTER-FED DIPOLE CONNECTED TO A TRANSMISSION LINE....37
D. TWO-FEED POINT DIPOLE CONNECTED TO TWO TRANSMISSION LINES....40
E. TWO-FEED POINT DIPOLE CONNECTED TO A MAGIC-TEE....43
F. CHAPTER SUMMARY....45

V. MUTUAL COUPLING IN SMALL ANTENNA ARRAY 47
A. CHAPTER OVERVIEW 47
B. MUTUAL COUPLING FOR AN ARRAY OF THREE CENTER-FED DIPOLES 47
C. MUTUAL COUPLING FOR AN ARRAY OF THREE CENTER-FED DIPOLES OVER A GROUND PLANE 51
D. MUTUAL COUPLING FOR AN ARRAY OF THREE CENTER-FED DIPOLES CONNECTED TO TRANSMISSION LINES OVER A GROUND PLANE 55
E. MUTUAL COUPLING FOR AN ARRAY OF THREE TWO-FEED POINT DIPOLES CONNECTED TO MAGIC-TEES OVER A GROUND PLANE 57
F. CHAPTER SUMMARY 61

VI. CONCLUSIONS AND RECOMMENDATIONS 63
A. CONCLUSIONS 63
B. RECOMMENDATIONS FOR FUTURE WORK 64

APPENDIX A : MATLAB SCRIPTS RWG1.M TO RWG5.M AND EFIELD1.M TO EFIELD3.M 65

APPENDIX B : MATLAB SCRIPTS FOR THE SIMULATIONS OF CHAPTER IV-V 81

LIST OF REFERENCES 95

INITIAL DISTRIBUTION LIST 97

THIS PAGE INTENTIONALLY LEFT BLANK

LIST OF FIGURES

Figure 1.1. Microstrip ring-hybrid dipole antenna (From Ref. [2].).. 2
Figure 2.1. Schematic of a RWG edge element and dipole interaction (From Ref. [3].).....6
Figure 2.2. (a) Schematic of a receiving antenna; the surface current density is shown by white arrows. (b) Antenna cut to create a voltage gap (From Ref. [3].).....7
Figure 2.3. Flowchart of the receiving algorithm (From Ref. [3].).....9
Figure 2.4. Three RWG edge elements *m*, *m*+1, and *m*+2 (with two triangles each), all containing the same common triangle *T* (From Ref. [3].).. 11
Figure 2.5. Barycentric subdivision of the primary triangle. The subtriangle midpoints are shown by black dots. The primary triangle midpoint is shown by a white circle (From Ref. [3].).....12
Figure 2.6. Incident field geometry for a plate (From Ref. [3].).. 15
Figure 2.7. Thin-strip discretization. Two RWG elements form a current vector **J** directed exactly along the strip (From Ref. [3].).. 16
Figure 2.8. Feeding edge model. Black arrows show the *E*-field direction in the antenna gap. White arrows show the direction of surface current on the antenna surface (From Ref. [3].).....17
Figure 3.1. Thin-wire strip. 21
Figure 3.2. (a) Magnitude and (b) phase of the surface current distribution for a transmitting resonant center-fed dipole. 23
Figure 3.3. Radiation pattern for a transmitting resonant dipole.....24
Figure 3.4. Plane wave illuminating a dipole at TM_z normal incidence. 25
Figure 3.5. (a) Magnitude and (b) phase of the surface current distribution for a receiving resonant dipole. 26
Figure 3.6. Feed model using two thin-wire strips separated by a small gap. 27
Figure 3.7. Patch antenna probe feed model for the dipole feed.....27
Figure 3.8. Feed model using a symmetrical thin-wire strip.....28
Figure 3.9. Sum mode and difference mode for the two-feed point dipole. 28
Figure 3.10 (a) Magnitude and (b) phase of the surface current distribution for the sum mode.....30
Figure 3.11 (a) Magnitude and (b) phase of the surface current distribution for the difference mode. 31
Figure 3.12. Radiation pattern for the sum mode.....32
Figure 3.13. Radiation pattern for the difference mode. 32
Figure 4.1. Antenna feed point connection to the feed network. 37
Figure 4.2. Center-fed dipole connected to a transmission line and its circuit model. 38
Figure 4.3. Two-feed point dipole connected to transmission lines.....40
Figure 4.4. Plane wave illuminating a two-feed point dipole at TM_z 45º incidence.....41
Figure 4.5. (a) Magnitude and (b) phase of the surface current distribution for two-feed point dipole at 45º incidence.....42
Figure 4.6. Two-feed point dipole connected to a magic-tee.....43
Figure 5.1. An array of three dipoles.....48

Figure 5.2. (a) Surface current distribution and (b) radiation pattern for an array of three free-standing center-fed dipoles spaced $\lambda/2$ apart at broadside scan. ..49
Figure 5.3. (a) Surface current distribution and (b) radiation pattern for an array of three free-standing center-fed dipoles spaced $\lambda/2$ apart at 30º off-broadside scan 50
Figure 5.4. An array of three dipoles over a finite ground plane. 51
Figure 5.5. A 2λ square plate with 1248 triangles. 52
Figure 5.6. Input impedance versus scan angle for an array of three center-fed dipoles spaced $\lambda/2$ apart over a 2λ square plate. Resistance is on the left side and reactance on the right side for (a) dipole 1, (b) dipole 2, and (c) dipole 3 53
Figure 5.7. Radiation pattern for an array of three center-fed dipoles spaced $\lambda/2$ apart over a 2λ square plate at (a) broadside scan and (b) 30º off-broadside scan. 54
Figure 5.8. Radiation pattern for an array of three center-fed dipoles spaced $\lambda/2$ connected to 75-Ω transmission lines over a 2λ square plate at (a) broadside scan and (b) 30º off-broadside scan 56
Figure 5.9. Sum port outputs for an array of three two-feed point dipoles spaced $\lambda/2$ apart connected to 50-Ω magic-tees over a 2λ square plate. The scan angle (ϕ) is varied from $\phi = 90°$ to $180°$ with $\theta = 90°$. Magnitude of output is on the left side and phase on the right side for (a) dipole 1, (b) dipole 2, and (c) dipole 3.. 58
Figure 5.10. Sum port outputs for an array of three two-feed point dipoles spaced $\lambda/2$ apart connected to 50-Ω magic-tees over a 2λ square plate. The scan angle (θ) is varied from $\theta = 90°$ to $0°$ with $\phi = 90°$. Magnitude of output is on the left side and phase on the right side for (a) dipole 1, (b) dipole 2, and (c) dipole 3.. 59
Figure 5.11. Difference port outputs for an array of three two-feed point dipoles spaced $\lambda/2$ apart connected to 50-Ω magic-tees over a 2λ square plate. The scan angle (θ) is varied from $\theta = 90°$ to $0°$ with $\phi = 90°$. Magnitude of output is on the left side and phase on the right side for (a) dipole 1, (b) dipole 2, and (c) dipole 3. 60
Figure 6.1. An array of three elements with a compensation network (From Ref. [2].)....64

THIS PAGE INTENTIONALLY LEFT BLANK

LIST OF TABLES

Table 3.1. Input impedance of $\lambda/2$ center-fed dipole with various discretization. 22
Table 3.2. Input impedance and radiation resistance for the sum mode and the difference mode. 29
Table 3.3. Transmitted powers of the two-feed point dipole. 29
Table 4.1. Results for a center-fed dipole driven through an ideal transmission line. 39
Table 4.2. Results for a two-feed point dipole driven through ideal transmission lines. ..40
Table 4.3. Received power for two-feed point dipole at 0º and 45º incidence. 41
Table 4.4. Results for a two-feed point dipole connected to a magic-tee in the receive mode for – 45º incidence. 44
Table 5.1. Input impedance for an array of three center-fed dipoles spaced $\lambda/2$ apart, over a 2λ square plate with various discretization, at broadside scan. 52
Table 5.2. Input impedances, return loss, and gain for an array of three center-fed dipoles spaced $\lambda/2$ apart connected to 75-Ω transmission lines over a 2λ square plate. 55

THIS PAGE INTENTIONALLY LEFT BLANK

ACKNOWLEDGMENTS

I would like to thank Professor David Jenn of the Naval Postgraduate School, Monterey, California for his invaluable guidance to the completion of this thesis project. He adopted an open office concept for the education of his students, never failing to attend to our questions even when he is busy on week days or even week ends.

I would like to thank Professor Roberto Cristi of the Naval Postgraduate School, Monterey, California for agreeing to be the second reader for this thesis project. He is also the mentor to the group of electrical engineering students from the Temasek Defense Systems Institute. I enjoyed working with him on the integrated project for sea base protection.

I would also like to thank my wife Cheong Min Yee and my daughter Ong Shi Yinn for supporting me in my studies from Singapore. I missed Shi Yinn's four years old birthday on 17 November 2003 and promised to organize a late celebration when I return home soon. Min Yee will be attending my graduation on 19 December 2003.

THIS PAGE INTENTIONALLY LEFT BLANK

EXECUTIVE SUMMARY

In the recent years, unmanned air vehicles (UAVs) have been used extensively in military operations to provide surveillance and targeting data. The payload of a UAV is limited and, thus, onboard sensors must be lightweight yet capable of high performance in order to satisfy modern mission requirements. Phased-array antenna systems can provide the beamforming and direction-finding capability required for multiple systems such as synthetic aperture radar (SAR) and moving target indication (MTI). A high performance phased-array antenna has many elements and a complex feed network. It is clear that weight and performance must be balanced in the design of phased-array antenna system for a UAV.

For a large antenna array, elements at the edges are usually assumed to have the same active element pattern as the center element. The rationale is that the number of edge elements in a large array is small compared to the number of non-edge elements, and, therefore, mutual coupling near the edge can be neglected. However, the mutual coupling effect can be severe when there are only a few elements in the antenna. This is because the active elements patterns are severely modified by the mutual coupling and thus differ significantly from one element to the next.

In the design of high-performance direction-finding or scanning system for UAVs using a small antenna array, the effect of the mutual coupling must thus be taken into account. A microstrip ring-hybrid dipole antenna was fabricated and tested at the Naval Postgraduate Schoool, Monterey, California, in early 2003. The ring-hybrid dipole is simply a ring-hybrid four-port network feeding a dipole antenna. The dipole supports currents in both the sum mode (resonant) and the difference mode (anti-resonant). The difference port is provided as a means to sense the interference caused by mutual coupling in an array of ring-hybrid dipoles.

A potential compensation network concept uses feedback circuits to connect from one dipole to the others. The difference ports can be used as a feedback mechanism to adjust how much mutual coupling the dipoles receive. With this information, the dipoles can adjust their voltage to reduce the phase error due to mutual coupling. This is a type of cancellation; signals are coupled from each element and used to cancel the free space coupling.

The design and analysis of the ring-hybrid dipole was carried out using Computer Simulation Technology's Microwave Studio. Although the application is powerful, it is not as suitable for the study of mutual coupling compensation methods in antenna array compared to the method of moments (MoM).

The MoM reduces an integral-differential equation (the electric field integral equation) to a linear system of equations, $\boldsymbol{Z} \cdot \mathbf{I} = \mathbf{V}$; where $\boldsymbol{Z}$ is the impedance matrix that completely simulates the antenna, $\mathbf{V}$ is the voltage excitation vector, and $\mathbf{I}$ is the unknown current coefficient vector. Once the current vector is known, the current distribution on the antenna is defined and all other current-dependent quantities can be determined (for example, input impedance, radiation pattern and gain).

This thesis project developed a suitable antenna model for the ring-hybrid dipole using the method of moments. Next, the feed network was incorporated into the MoM equations to solve the complete system of equations simultaneously. With that, the mutual coupling in an array of ring-hybrid dipoles was studied by extending the model.

The receiving and transmitting algorithms are based on the use of the electric-field integral equation (EFIE) for non-closed structures such as wire strips and plates. In a transmit problem, the antenna excitation is given by a voltage feed instead of an incident electromagnetic wave for the receive problem. Matlab was used to generate the antenna mesh also solve the MoM equation.

A two-feed point dipole model was connected to a magic-tee four-port network to model the complete ring-hybrid dipole. The feed network interaction with the antenna feed was modeled rigorously. In the receive mode, difference power can only be extracted when there is a difference in the incident plane wave path length between the two arms of the dipole. The power relationships (i.e., conservation of energy) between the total captured power, and the total output power in both the sum and difference ports were verified.

The mutual coupling for an array of three center-fed dipoles in the presence of a 2λ square plate was examined. The dipoles were spaced $\lambda/2$ apart along the *x*-axis and lined up with the *z*-axis. The plate was spaced $\lambda/4$ from the antennas. The input impedances were found to vary significantly with scan angle due to mutual coupling. The antennas were then connected to 75-Ω transmission lines. The input impedances were further modified due to additional mutual coupling caused by reflections introduced by mismatched feed condition.

An array of three two-feed point dipoles was connected to 50-Ω magic-tees. The configuration is the same as that for the array of center-fed dipoles. The characteristics for the transmit mode would be similar to those observed for the array of center-fed dipoles. The receive mode was thus examined by varying the direction and the polarization of the incidence plane wave. The phases for both the sum port and the difference port outputs were observed to change smoothly, except during situations of cross polarization and zero phase difference.

A valid antenna model combined with the feed network model has been successfully developed for the ring-hybrid dipole using the method of moments. The effect of mutual coupling in an array of three ring-hybrid dipoles has been studied. The stage is now ready for the design and analysis of compensation networks to reduce the interferences caused by mutual coupling.

.

THIS PAGE INTENTIONALLY LEFT BLANK

I. INTRODUCTION

A. MOTIVATION

In the recent years, unmanned air vehicles (UAVs) have been used extensively in military operations to provide surveillance and targeting data. The payload of a UAV is limited and, thus, onboard sensors must be lightweight yet capable of high performance in order to satisfy modern mission requirements. Phased-array antenna systems can provide the beamforming and direction-finding capability required for multiple systems such as synthetic aperture radar (SAR) and moving target indication (MTI). A high performance phased-array antenna has many elements and a complex feed network. It is clear that weight and performance must be balanced in the design of phased-array antenna system for a UAV.

The existence of mutual coupling between elements in a phased-array antenna affects the final antenna pattern and it cannot be neglected in the design of high performance arrays. It can be significant in applications that demand high accuracy for direction finding. In a large phase array, the coupling effect is generally uniform for most of the elements except for the last few elements near the edge. The variation in mutual coupling near the edges of the array is termed the "edge-effect."

For the majority of the elements in a large array, the active element pattern approach [1] has helped designers to overcome the complicated accountability of the mutual coupling. Elements at the edges are usually assumed to have the same active element pattern as the center element. The rationale is that the number of edge elements in a large array is small compared to the number of non-edge elements and, therefore, mutual coupling near the edge can be neglected. However, the mutual coupling effect can be severe when there are only a few elements in the antenna. This is because the active element patterns are severely modified by the mutual coupling and, thus, differ significantly from one element to the next.

Thus, in the design of high-performance direction-finding or scanning systems for UAVs using a small antenna array, the effect of the mutual coupling must be taken into account. For a small array, it is found that the mutual coupling varies significantly with scan angle. Consequently, a means of controlling or adjusting the mutual coupling as the beam scans is desired. One possibility is to use a compensation or feedback network that allows cancellation of the free-space mutual coupling. Such a network requires an auxiliary antenna or channel.

The ring-hybrid dipole described in [2] and shown in Figure 1.1 is a two-port radiating structure that provides both a main (sum) channel and auxiliary (difference) channel. The ring-hybrid dipole is simply a ring-hybrid coupler feeding a dipole antenna. The dipole supports currents in both the sum mode (resonant) and the difference mode (anti-resonant). The difference port is provided as a means to sense the interference caused by mutual coupling in an array of ring-hybrid dipoles. In [2], a microstrip ring-hybrid dipole antenna was fabricated and tested.

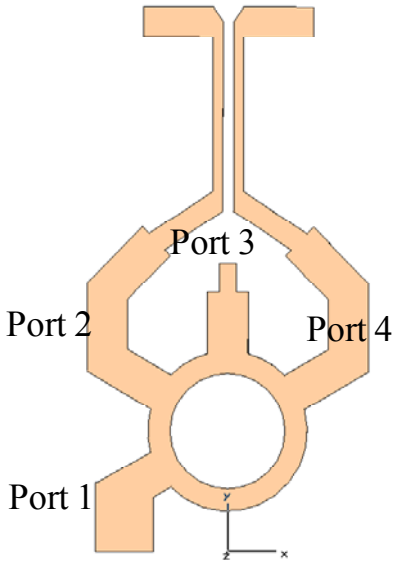

Figure 1.1. Microstrip ring-hybrid dipole antenna (From Ref. [2].).

The design and analysis of the ring-hybrid dipole was carried out using Computer Simulation Technology's Microwave Studio. The application is powerful, but in this case it is not as suitable for the study of mutual coupling compensation methods in an antenna array compared to the method of moments (MoM). The MoM reduces an integral-differential equation (the electric-field integral equation) to a linear system of equations, $\boldsymbol{Z} \cdot \mathbf{I} = \mathbf{V}$; where $\boldsymbol{Z}$ is the impedance matrix, $\mathbf{V}$ is the voltage excitation vector, and $\mathbf{I}$ is the unknown current coefficient vector. Once the current vector is known, the current distribution on the antenna is defined and all other current-dependent quantities can be determined (for example, input impedance, radiation pattern and gain).

In a practical antenna design, the array elements are connected by transmission lines in a beamforming network. Reflections inside of the beamforming network affect the currents on the dipoles, which in turn affect the mutual coupling. Therefore, a precise model of mutual coupling must include the feed network. In this thesis, a scattering matrix representation of the feed network is combined with the MoM to provide a complete, rigorous model of the array and feed. For an *N*-port network, the scattering matrix provides a complete description of the network as seen at its *N* ports (The scattering matrix relates the voltage waves incident on the ports to those reflected from the ports).

B. OBJECTIVES

A suitable antenna feed model is required for the ring-hybrid dipole for use with the method of moments. Next, the feed network should be incorporated into the MoM equations to solve the complete system of equations simultaneously. With that, the mutual coupling in an array of ring-hybrid dipoles can be studied by extending the model created. The final objective is to find a suitable compensation network to reduce interference caused by mutual coupling.

C. OUTLINE OF CHAPTER

Chapter II describes the use of the Rao-Wilton-Glisson basis functions to create the impedance matrix in the method of moments. The scattering algorithm and the radiation algorithm used for antenna modeling with Matlab are also presented.

Chapter III presents the results for the modeling of a center-fed dipole as a test case. The results for a two-feed point dipole that is employed to model the operation of the ring-hybrid dipole are also presented.

Chapter IV presents the basic theory used in the modeling of the feed network connection to the antenna feed. The results for two test cases: (1) center-fed dipole connected to transmission line, and (2) two-feed point dipole connected to transmission lines, are presented. It also presents the results for the two-feed point dipole connected to a magic-tee, which is the model for the complete ring-hybrid dipole.

Chapter V describes the effect of mutual coupling in an array of three center-fed dipoles for the transmit mode. The effect of mutual coupling in an array of three ring-hybrid dipoles is presented for the receive mode.

Chapter VI presents the conclusions and recommendations for future work.

Appendix A contains the Matlab scripts that were modified and appended from [3] to implement the method of moments.

Appendix B contains the Matlab scripts that were developed for the simulations in Chapter IV-V.

II . METHOD OF MOMENTS AND THE RWG BASIS FUNCTIONS

A. CHAPTER OVERVIEW

This chapter describes the use of the Rao-Wilton-Glisson (RWG) basis functions to create the impedance matrix for the method of moments (MoM). The receiving and transmitting algorithms used for antenna modeling are presented. The antenna modeling and visualization of antenna parameters are implemented using Matlab. The materials here are summarized from [3].

B. RWG BASIS FUNCTIONS

The MoM used in this thesis project incorporate the RWG edge elements. First, the surface of a conducting antenna under study is divided into separate triangles as shown in Figure 2.1a. Each pair of triangles having a common edge constitutes a RWG subdomain as shown in Figure 2.1b. One of the triangles has a plus sign and the other a minus sign. A basis function, $\mathbf{f}(\mathbf{r})$, given by

$$\mathbf{f}(\mathbf{r}) = \begin{cases} \dfrac{\ell}{2A^+}\boldsymbol{\rho}^+(\mathbf{r}) & \mathbf{r}\in T^+ \\ \dfrac{\ell}{2A^-}\boldsymbol{\rho}^-(\mathbf{r}) & \mathbf{r}\in T^- \\ 0 & \text{otherwise,} \end{cases} \tag{2.1}$$

is assigned to the edge elements. Here ℓ is the edge length and $A^{\pm}$ is the area of triangle $T^{\pm}$. The vectors $\boldsymbol{\rho}^{\pm}$ are shown in Figure 2.1b. Vectors $\boldsymbol{\rho}^+$ and $\boldsymbol{\rho}^-$ connect the free vertex of the plus triangle T^+ and the minus triangle T^- to the observation point given by the position vector **r**, respectively.

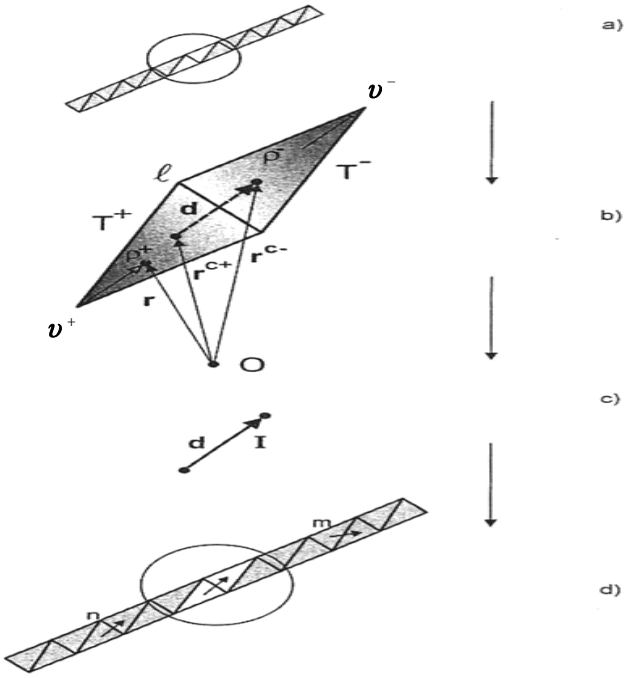

Figure 2.1. Schematic of a RWG edge element and dipole interaction (From Ref. [3].).

The surface electric current on the antenna is a sum of the contributions (2.1) over all edge elements, with unknown coefficients. These coefficients are found from the MoM equations discussed in Section C. The MoM reduces the integral equation for the current to a linear system of equations that can be solved in matrix form. The resulting matrix that characterizes the antenna physical properties is the impedance matrix $\boldsymbol{Z}$.

The basis function of the edge element approximately corresponds to a small but finite electric dipole of length $d = |\mathbf{r}^{c-} - \mathbf{r}^{c+}|$ as shown in Figures 2.1b and 2.1c. The index $c^{\pm}$ denotes the center of the triangle $T^{\pm}$. Thus the division of the antenna structure into RWG edge elements approximately corresponds to the division of the antenna current into small "elementary" electric dipoles as shown in Figure 2.1d. In this sense, the impedance matrix $\boldsymbol{Z}$ describes the interaction between the different elementary dipoles that completely describe the antenna. If the edge elements *m* and *n* are treated as small electric dipoles, then element Z_{mn} describes the effect of dipole *n* (through the radiated field) on the electric current of dipole *m*, and vice versa. Consequently, the interaction between all currents on the body is modeled.

C. THE RECEIVING ALGORITHM

1. Introduction

A receiving antenna may be viewed as a conducting object that collects power from an incident electromagnetic (EM) field. In response to the incident electric field, an electric current appears on the antenna's surface as shown in Figure 2.2a. That current in turn creates a corresponding scattered electric field. If a narrow gap is cut in the body of an antenna, as shown in Figure 2.2b, a voltage difference will appear across the gap. The gap voltage constitutes the received signal. From the viewpoint of energy transfer, an antenna in the receiving mode captures EM energy over a certain area. It then delivers the captured power to the load connected across the gap. Depending on the antenna, a considerable amount of energy may get reflected back to free space.

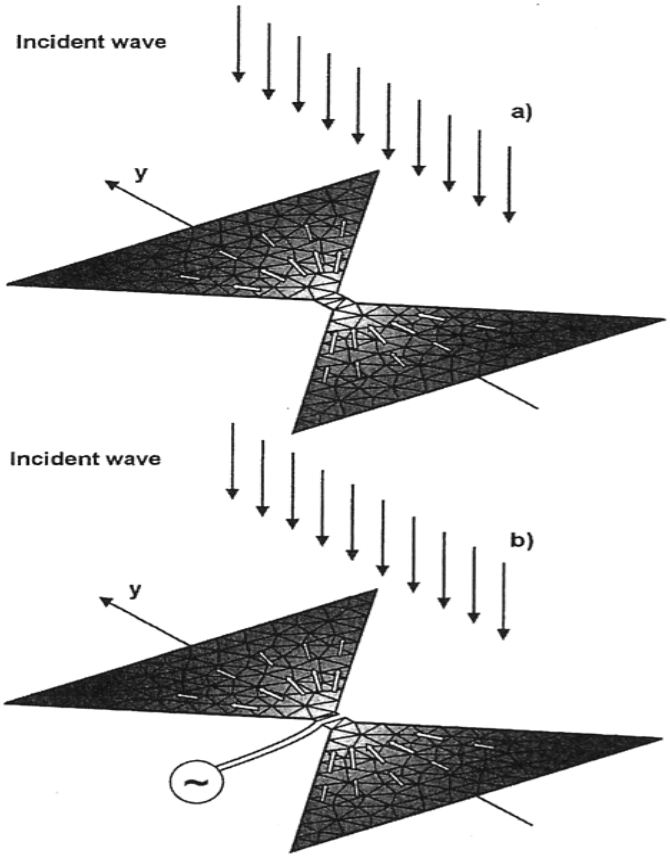

Figure 2.2. (a) Schematic of a receiving antenna; the surface current density is shown by white arrows. (b) Antenna cut to create a voltage gap (From Ref. [3].).

The surface current distribution over the antenna surface is the most critical antenna characteristic. If the current is known, then all other antenna parameters can be computed from it (for example, input impedance, radiation pattern and gain). The receiving algorithm used to compute the current is based on existing Matlab software that uses the electric-field integral equation (EFIE) [4] for non-closed structures such as wire strips and plates. Before discussing the mathematical aspects of the EFIE and its solution using the MoM, the solution procedure and the corresponding Matlab scripts will be outlined first.

2. Matlab Code Sequence

The steps involved in solving for the antenna current using the MoM are depicted in Figure 2.3. Once the current is calculated, all other antenna parameters are easily determined. The source codes in Appendix A include Matlab scripts *rwg1.m* to *rwg5.m*, and also *efield1.m* to *efield3.m* from [3]. The original software was capable of handling only simple structures such as strips and plates. The codes were modified and appended to suit the needs of this thesis project. Figure 2.3 also shows the flowchart for executing the complete code sequence.

The scripts *rwg1.m* to *rwg5.m* implement successive steps of the moment method procedure. The code sequence is applicable to different antenna geometries located in the subdirectory "mesh." To replace one antenna object by another, it is only necessary to replace the corresponding mesh file name in the starting script *rwg1.m*. The frequency, electric permittivity, and magnetic permeability are specified in the script *rwg3.m*. The same sequence of operations is not only valid for antenna reception but also for antenna radiation (discussed in Section D). The only important difference is that the antenna excitation is given by a voltage feed in the latter case and not by the incident EM wave.

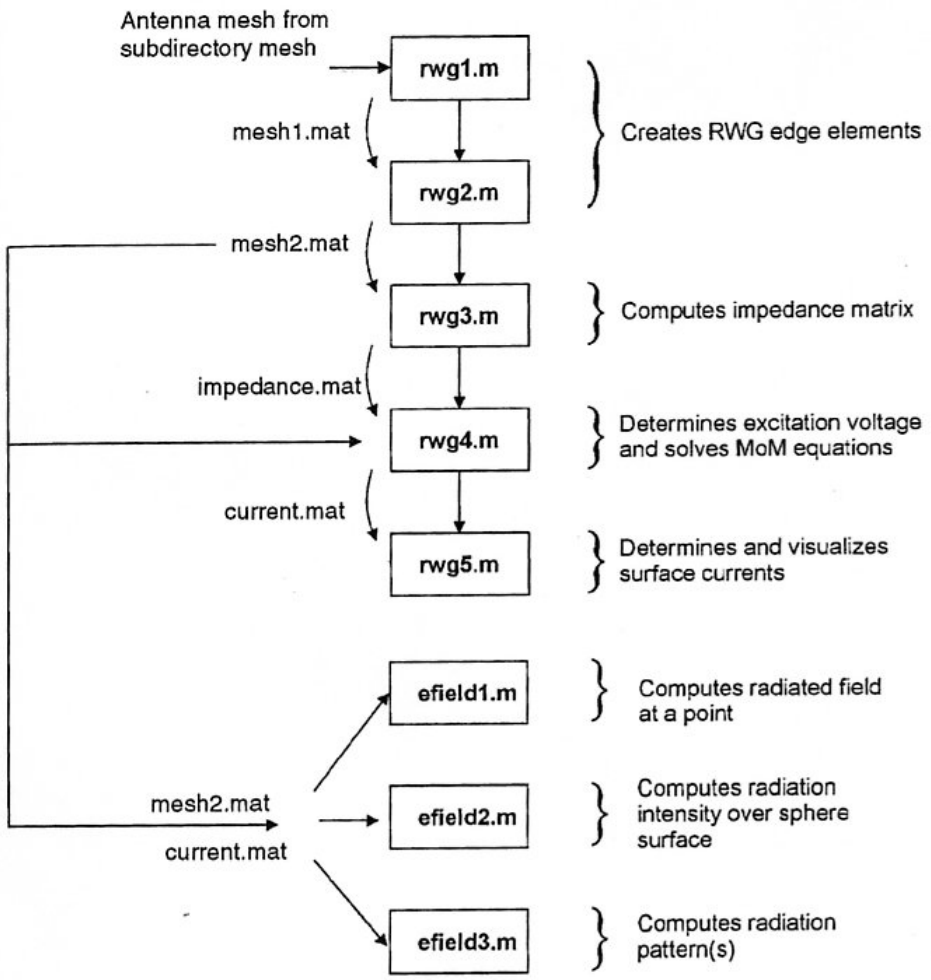

Figure 2.3. Flowchart of the receiving algorithm (From Ref. [3].).

The scripts *efield1.m* to *efield3.m* calculate different parameters of the radiated field due to the surface current distribution on the antenna surface. The script *efield1.m* calculates the electric field and the magnetic field at a point. The script *efield2.m* calculates the radiation intensity distribution over a large spherical surface, as well as the antenna gain and the radiation resistance. The script *efield3.m* calculates the radiation patterns in the azimulthal and polar planes. The algorithms for these scripts can be found in [3].

3. Creating the Antenna Structure

The first step in the solution is to create the antenna structure. Matlab provides several options for doing this. One is to use the built-in mesh generator in the Matlab PDE toolbox. This mesh generator creates planar structures of rectangles, polygons, and circles, using the convenient graphical user interface (GUI). The Delaunay triangulation algorithm is used [5], along with adaptive triangle subdivision. To extend the design to a three-dimensional (3-D) structure it is usually sufficient to write a short Matlab script involving the *z*-coordinate dependency.

Another way to define the antenna is to identify the boundary of the antenna structure analytically. For example, a dipole can be modeled by a thin strip with four edges. The Delaunay triangulation is applied to that structure, using Matlab function *delaunay*. For non-planar structures, the function *delaunay3* may be used. The advantage of this approach is that arbitrary 3-D antenna meshes can be created. Other mesh generation software can also be used and their results imported into Matlab in ASCII format.

4. RWG Edge Elements

A subdomain consists of two triangles sharing a common edge. One of them is labeled by a plus sign and the other by a minus sign. Figure 2.4 shows three edge elements that contain the same triangle *T*. Thus, there are more edges than triangles for a given structure.

Prior to the calculation of the impedance matrix, the edge elements are created by the script *rwg1.m*. The script counts all interior edges of the mesh. For each interior edge *m*, the two triangles $T_m^{\pm}$ attached to it are found using a sweep over all triangles. The triangle area is calculated separately for every single patch using the vector cross-product of two edge vectors.

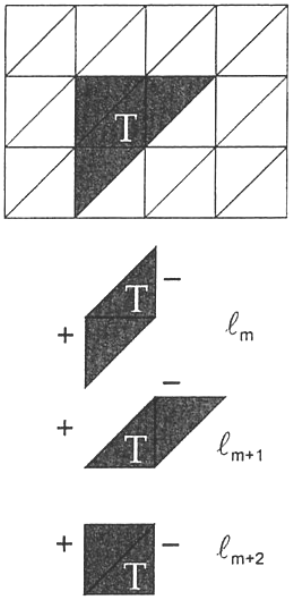

Figure 2.4. Three RWG edge elements *m*, *m*+1, and *m*+2 (with two triangles each), all containing the same common triangle *T* (From Ref. [3].).

Simple space averaging of the triangle's vertex points yields the triangle's midpoint. Any required integration can be approximated at triangle midpoints only. Thus, a numerical integration over a triangle is used. Figure 2.5 shows the so-called barycentric subdivision of an arbitrary triangle. Any primary triangle can be divided into 9 equal small subtriangles by the use of the "one-third" rule. The integrand is assumed to be constant within each small triangle, so that the integral of a function *g* over the primary T_m is approximately equal to

$$\int_{T_m} g(\mathbf{r})\, dS = \frac{A_m}{9} \sum_{k=1}^{9} g\left(\mathbf{r}_k^c\right), \tag{2.2}$$

where points $\mathbf{r}_k^c$, k = 1,…,9, are the midpoints of the nine subtriangles, shown in Figure 2.5 by black dots, and A_m is the area of the primary triangle.

The script *rwg2.m* outputs the subtriangle's midpoints for each triangular patch. After execution of the scripts *rwg1.m* and *rwg2.m*, a binary file *mesh2.mat* is created, which contains all the necessary geometric data for the calculation of the impedance matrix.

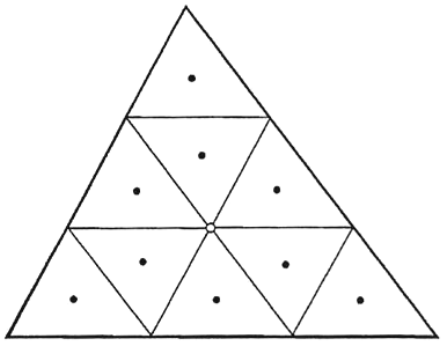

Figure 2.5. Barycentric subdivision of the primary triangle. The subtriangle midpoints are shown by black dots. The primary triangle midpoint is shown by a white circle (From Ref. [3].).

5. Impedance Matrix

The MoM impedance matrix accounts for the electromagnetic interaction between edge elements. If the edge elements *m* and *n* are treated as small electric dipoles, the matrix Z_{mn} describes the contribution of dipole *n* (through the radiated field) to the electric current of dipole *m*, and vice versa. The size of the impedance matrix is equal to the number of the edge elements. The impedance matrix does not depend on the type of excitation (receive or transmit); instead, it depends only on frequency, material composition and geometry.

Frequency, as well as electric permittivity (dielectric constant) ε and the magnetic permeability μ, are specified in the script *rwg3.m*. The impedance matrix calculation is implemented in the form of a Matlab function *impmet* saved in the file *impmet.m*. This function is called from the script *rwg3.m*. The script outputs the frequency and the impedance matrix into the binary file *impedance.mat*.

Quantitatively, the impedance matrix of the electric-field integral equation [4] is given by

$$Z_{mn} = \ell_m \left[j\omega \left(\frac{\mathbf{A}_{mn}^{+} \cdot \boldsymbol{\rho}_m^{c+}}{2} + \frac{\mathbf{A}_{mn}^{-} \cdot \boldsymbol{\rho}_m^{c-}}{2} \right) + \boldsymbol{\Phi}_{mn}^{-} - \boldsymbol{\Phi}_{mn}^{+} \right], \tag{2.3}$$

where indices *m* and *n* correspond to two edge elements. The edge length of the elements *m* is ℓ_m; $\boldsymbol{\rho}_m^{c\pm}$ are vectors between the free vertex point $\boldsymbol{\upsilon}_m^{\pm}$, and the centroid point $\mathbf{r}_m^{c\pm}$, of the two triangles $T_m^{\pm}$ of the edge element *m*, respectively. $\boldsymbol{\rho}_m^{c+}$ is directed away from the vertex of triangle T_m^{+}, whereas $\boldsymbol{\rho}_m^{c-}$ is directed toward the vertex of triangle T_m^{-} (see Figure 2.1). The vectors $\boldsymbol{\rho}_m^{c\pm}$ are expressed through the known quantities using two simple formulas

$$\boldsymbol{\rho}_m^{c+} = \mathbf{r}_m^{c+} - \boldsymbol{\upsilon}_m^{+}, \tag{2.4a}$$

and

$$\boldsymbol{\rho}_m^{c-} = -\mathbf{r}_m^{c-} + \boldsymbol{\upsilon}_m^{-}. \tag{2.4b}$$

The expressions for the magnetic vector potential **A** and the scalar potential $\boldsymbol{\Phi}$ are

$$\mathbf{A}_{mn}^{\pm} = \frac{\mu}{4\pi} \left[\frac{\ell_n}{2A_n^{+}} \int_{T_n^{+}} \boldsymbol{\rho}_n^{+}(\mathbf{r}') g_m^{\pm}(\mathbf{r}')\, dS' + \frac{\ell_n}{2A_n^{-}} \int_{T_n^{-}} \boldsymbol{\rho}_n^{-}(\mathbf{r}') g_m^{\pm}(\mathbf{r}')\, dS' \right], \tag{2.5a}$$

and

$$\boldsymbol{\Phi}_{mn}^{\pm} = -\frac{1}{j4\pi\omega\varepsilon} \left[\frac{\ell_n}{A_n^{+}} \int_{T_n^{+}} g_m^{\pm}(\mathbf{r}')\, dS' - \frac{\ell_n}{A_n^{-}} \int_{T_n^{-}} g_m^{\pm}(\mathbf{r}')\, dS' \right], \tag{2.5b}$$

respectively, where

$$g_m^{\pm}(\mathbf{r}') = \frac{\exp\left(-jk\left|\mathbf{r}_m^{c\pm} - \mathbf{r}'\right|\right)}{\left|\mathbf{r}_m^{c\pm} - \mathbf{r}'\right|}. \tag{2.5c}$$

6. Moment Method Equations and Surface Currents

The surface current density on the surface S of a perfectly electrically conducting (PEC) structure is given by an expansion in terms of the RWG basis functions over the M edge elements

$$\mathbf{J} = \sum_{m=1}^{M} I_m \mathbf{f}_m, \quad \mathbf{f}_m = \begin{cases} \dfrac{\ell_m}{2A_m^+} \boldsymbol{\rho}_m^{\,+}(\mathbf{r}) & \mathbf{r} \in T_m^+ \\ \dfrac{\ell_m}{2A_m^-} \boldsymbol{\rho}_m^{\,-}(\mathbf{r}) & \mathbf{r} \in T_m^- \\ 0 & \text{otherwise.} \end{cases} \tag{2.6}$$

If S is open, $\mathbf{J}$ is regarded as the vector sum of surface currents on opposite sides of S. The units of $\mathbf{J}$ are amperes/meter. The expansion coefficients I_m form the vector $\mathbf{I}$, which is the unique solution of the moment method matrix equation

$$\boldsymbol{Z} \cdot \mathbf{I} = \mathbf{V}, \tag{2.7}$$

where the $M \times M$ impedance matrix $\boldsymbol{Z}$ is computed in script *rwg3.m*. The voltage excitation vector is $\mathbf{V}$. When a plane-wave scattering problem is being solved, the voltage vector is expressed by

$$V_m = \ell_m \left(\frac{\mathbf{E}_m^+ \cdot \boldsymbol{\rho}_m^{c+}}{2} + \frac{\mathbf{E}_m^- \cdot \boldsymbol{\rho}_m^{c-}}{2} \right), \quad \mathbf{E}_m^{\pm} = \mathbf{E}^{inc}\left(\mathbf{r}_m^{c\pm}\right), \quad m = 1, \ldots, M, \tag{2.8}$$

where $\mathbf{E}^{inc}$ is the electric field of the incident EM wave. The voltage excitation vector is similar to the circuit voltage but has units of volts-meter.

The plane wave of amplitude 1 V/m shown in Figure 2.6 has only one E-field component in the x-direction, $\mathbf{E}^{inc} = E_x \hat{\boldsymbol{x}}$. The phasor representation of this component (assuming $\exp(j\omega t)$ time dependence) is equal to $E_x = 1\exp(-jkz)$ V/m, where $k = \omega / c$ is the wave number. If the plate is located at z = 0, then $\mathbf{E}^{inc} = \hat{\boldsymbol{x}}$ V/m. The vector $\hat{\boldsymbol{x}}$ describes the polarization of the plane wave.

In a receive problem, the script *rwg4.m* first determines the excitation voltage vector using (2.8). Next, the system of equations (2.7) is solved via Gaussian elimination. The script outputs the current coefficients I_m, the vector **V**, and the corresponding frequency parameters, into the binary file *current.mat*. The expansion coefficients I_m are not yet the surface current. The surface current density $\mathbf{J}_k$, for a given triangle k, is obtained from

$$\mathbf{J}_k = \sum_{m=1}^{M} I_m \mathbf{f}_m(\mathbf{r}), \quad \mathbf{r} \in T_k. \tag{2.9}$$

A maximum of three edge elements contribute to the current on triangle k. The script *rwg5.m* calculates and plots the resulting surface current density everywhere on the PEC structure.

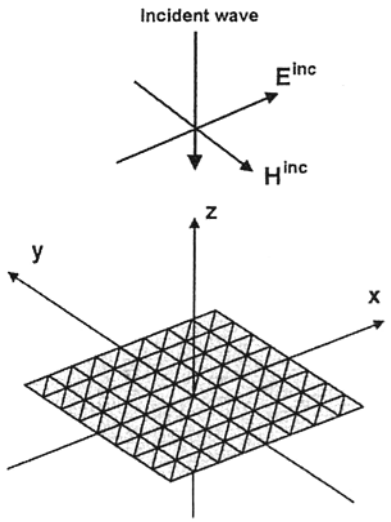

Figure 2.6. Incident field geometry for a plate (From Ref. [3].).

D. THE TRANSMITTING ALGORITHM

1. Introduction

The task of the transmitting algorithm is to find the surface current distribution due to an applied voltage at the antenna feed. The receiving algorithm can easily be modified for antenna radiation. The major challenge related to transmitting antennas is the antenna feed model, which is programmed in the script *rwg4.m*.

2. Strip Model of a Wire

As far as the impedance and radiation pattern are concerned, an electrically thin cylindrical antenna with a noncircular cross-section behaves like a circular cylindrical antenna with an equivalent radius [6]. For a thin strip, the radius of the equivalent cylindrical wire is given by

$$a_{eq} = 0.25w, \tag{2.10}$$

where w is the strip width. A typical RWG boundary element assembly of a strip is shown in Figure 2.7. If $w << \lambda,$ one edge across the width of the strip is sufficient. Two adjoining RWG edge elements are able to support a uniform electric current **J** along the strip axis.

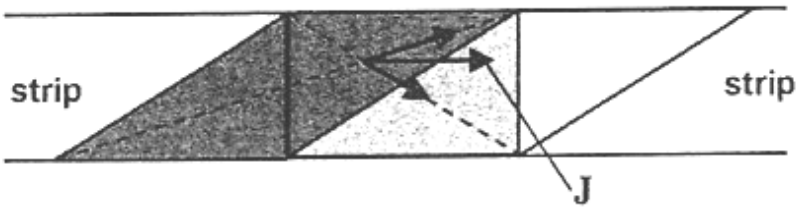

Figure 2.7. Thin-strip discretization. Two RWG elements form a current vector **J** directed exactly along the strip (From Ref. [3].).

3. Feed Model

To account for an applied voltage rather than an incident wave, a feed model is introduced into the antenna structure. An antenna is usually fed by a conventional transmission line at a gap between the two dipole arms. This means that an ideal voltage generator is connected across a gap with a small width along the antenna as shown in Figure 2.8. The feed model that is ideally suited for RWG edge elements is the so-called delta-function generator or the feeding edge model shown in Figure 2.8.

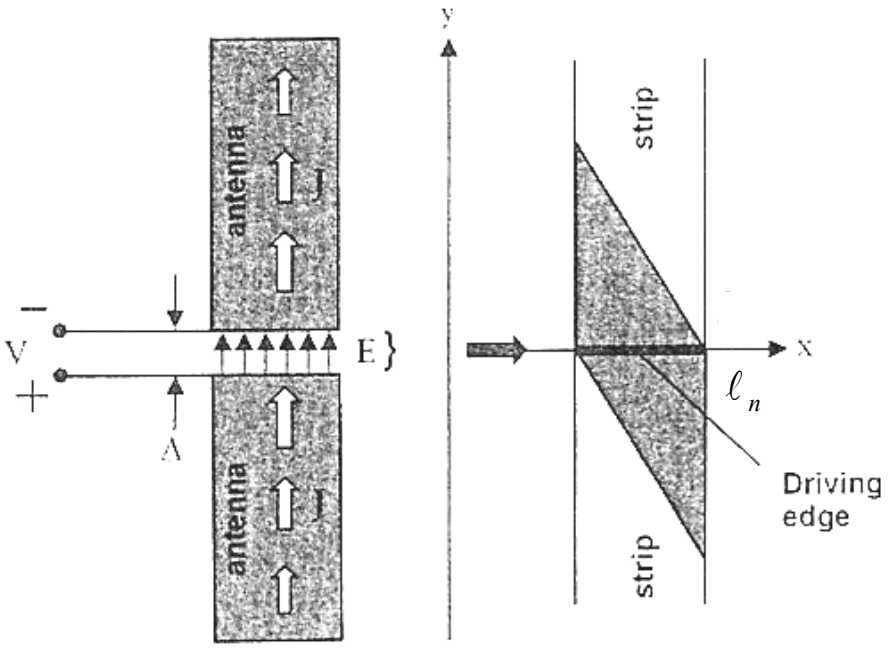

Figure 2.8. Feeding edge model. Black arrows show the *E*-field direction in the antenna gap. White arrows show the direction of surface current on the antenna surface (From Ref. [3].).

In short, this model assumes a gap of negligible width, Δ. If the voltage across the gap is V (from the positive to the negative terminal), then the electric field within the gap becomes

$$\mathbf{E} = -\nabla\mathbf{\Phi} = \frac{V}{\Delta}\mathbf{n}_y, \tag{2.11}$$

where $\mathbf{\Phi}$ is the electric potential and $\mathbf{n}_y$ is a unit vector directed across the gap. When Δ tends to zero, (2.11) predicts infinite values within the gap. For a small gap, the delta-function approximation can be used

$$\mathbf{E} = V\delta(y)\mathbf{n}_y. \tag{2.12}$$

Equation (2.12) simply states that the integral of the electric filed over a gap is equal to the applied voltage, namely

$$\int E_y dy = V. \tag{2.13}$$

It is convenient to associate the gap with an inner edge *n* of the boundary element structure. That is, the structure is broken at edge *n* and a small gap of width Δ inserted. There is only one RWG element corresponding to that edge. Thus the applied electric field will be zero everywhere except for one RWG element, *n*. Therefore, for the transmit problem, the excitation voltage elements are

$$V_m = \begin{cases} \int\limits_{T_n^+ + T_n^-} \mathbf{E} \cdot \mathbf{f}_n dS = V \left(\int\limits_{T_n^+ + T_n^-} \delta(y) \mathbf{n}_y \cdot \mathbf{f}_n dS \right) = \ell_n V \quad m \in T_n \\ \\ 0 \qquad\qquad\qquad\qquad\qquad\qquad\qquad\qquad \text{otherwise.} \end{cases} \tag{2.14}$$

Equation (2.14) uses the fact that a component of the RWG basis function $\mathbf{f}_n$ normal to the edge is always equal to one. A feeding voltage of 1 V is a cosine function of time having phase of zero and an amplitude equal to 1 V. In a transmit problem, only the script *rwg4.m* needs to be modified to account for (2.14). Everything else is directly adopted from the receiving algorithm analysis.

4. Input Impedance

One major parameter of interest is the antenna input impedance. Once the impedance is known, other antenna parameters such as return loss can easily be obtained. The input impedance is defined as the impedance presented by an antenna at its terminals, or the ratio of the voltage to current at a pair of terminals. The feeding edge model determines the impedance to be the ratio of the feeding voltage to the total current normal to the feeding edge, *n*. In the expansion of surface currents over RWG basis functions

$$\mathbf{J} = \sum_{m=1}^{M} I_m \mathbf{f}_m, \tag{2.15}$$

only the basis function $\mathbf{f}_{m=n}$ will contribute to the impedance calculation, since no other basis functions have a component normal to the edge, *n*.

Moreover, since a component of the RWG basis function $\mathbf{f}_n$ normal to the edge is always equal to one, the total normal current across the edge is given by

$$\ell_n I_n, \tag{2.16}$$

where $\ell_n = w$ is the edge length. The antenna impedance is simply

$$Z_{in} = \frac{V}{\ell_n I_n} = \frac{V_n}{\ell_n^2 I_n}, \tag{2.17}$$

according to (2.14). The input impedance is measured in ohm and is a complex quantity in general.

E. CHAPTER SUMMARY

The use of the Rao-Wilton-Glisson (RWG) basis function to create the impedance matrix in the method of moments (MoM) has been described. The RWG basis function is basically an overlapping triangular function that provides continuity of the electric surface current on the antenna structure. The antenna structure is first divided into small triangular patches. Each pair of triangles, having a common edge, constitutes a RWG subdomain element. The electric surface current is a sum of the contributions of the RWG basis functions over all edge elements. The expansion coefficients can be found from the MoM matrix equations for either receive or transmit problem.

The MoM equations are a linear system of equations, $\boldsymbol{Z} \cdot \mathbf{I} = \mathbf{V}$; $\boldsymbol{Z}$ is the impedance matrix, $\mathbf{V}$ is the voltage excitation vector, and $\mathbf{I}$ is the unknown current coefficient vector. The division of the antenna structure into RWG edge elements approximately corresponds to the division of the antenna current into small "elementary" electric dipoles. In this sense, the impedance matrix $\boldsymbol{Z}$ describes the interaction between the elementary component dipoles. If the edge elements *m* and *n* are treated as small electric dipoles, then element Z_{mn} describes the effect of dipole *n* (through the radiated field) on the electric current of dipole *m*, and vice versa. The impedance matrix can be found by applying the MoM procedure to the electric field integral equation (EFIE).

Both the receiving and transmitting algorithms have been presented. Both are based on the use of the EFIE equation for non-closed structures such as wire strips and plates. The only important difference in a transmit problem is that the antenna excitation is given by an applied voltage and not by an incident EM wave as for the receive case. The antenna structure can be created using Matlab PDE toolbox or programmed manually using Matlab. The MoM equations were also solved using Matlab. The Matlab source codes were modified and appended from [3] to suit the needs of this thesis project. Specifically, the antenna modeling of the ring-hybrid dipole will be carried out using these codes.

III. ANTENNA MODELING

A. CHAPTER OVERVIEW

In this chapter, a convergence test based on a center-fed dipole is carried out to determine convergence, i.e., the amount of discretization required. The antenna parameters are then extracted for the center-fed dipole to show that the results are consistent with theory. A symmetrical structure must be employed for the modeling of the ring-hybrid dipole, and the problems encountered with the modeling of the ring-hybrid dipole are discussed briefly. The antenna parameters for a two-feed point dipole used to model the operation of the ring-hybrid dipole are finally extracted. The Matlab codes used for the simulations in this chapter are in Appendix A.

B. CONVERGENCE TEST

A thin-wire strip shown in Figure 3.1 is used to model a dipole antenna. The wire length is l = 2 m and the width is w = 2 cm (i.e., $l >> w$). The equivalent wire radius is $a_{eq} = 0.25w$ = 5 mm. The feed point is located at the origin for a center-fed dipole. The frequency used is f = 75 MHz (i.e., λ = 4 m). The antenna is therefore a half-wave center-fed dipole.

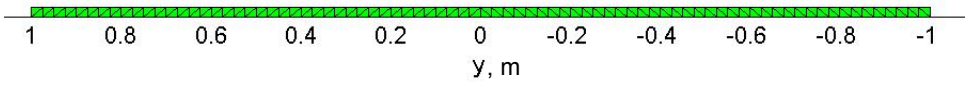

Figure 3.1. Thin-wire strip.

The input impedance, calculated by the simulations, for an increasing number of segments is shown in Table 3.1. It is observed that the phase of the input impedance has stabilized from 80 segments onwards. Thus, a discretization of 80 segments (a total of 159 edges) is selected for the thin-wire strip.

Number of Segments	Dipole Input Impedance		Remarks
10	$87.7988 + j34.4513$	$94.32 \angle 21.42^\circ$	Length = $\lambda/2$
20	$87.5591 + j41.0831$	$96.72 \angle 25.14^\circ$	
30	$87.2588 + j43.2752$	$97.40 \angle 26.38^\circ$	Width = 0.005λ
40	$87.1239 + j44.3880$	$97.78 \angle 27.00^\circ$	
50	$87.0759 + j45.0777$	$98.05 \angle 27.37^\circ$	Non-symmetrical structure
60	$87.0744 + j45.5464$	$98.27 \angle 27.61^\circ$	
70	$87.1006 + j45.8929$	$98.45 \angle 27.78^\circ$	
80	$87.1506 + j46.1642$	$98.62 \angle 27.91^\circ$	
90	$87.2054 + j46.3793$	$98.77 \angle 28.00^\circ$	
100	$87.2683 + j46.5563$	$98.91 \angle 28.08^\circ$	

Table 3.1. Input impedance of $\lambda/2$ center-fed dipole with various discretization.

C. ANTENNA PARAMETERS FOR THE CENTER-FED DIPOLE

In this section, the antenna parameters under a resonance condition are obtained for the center-fed dipole. The parameters are the input impedance, radiation resistance, gain, feed power, radiated power, and received power. The surface current distribution and radiation pattern are also plotted for both the transmit mode and the receive mode.

1. Antenna Impedance and Gain

The half-wave dipole is not exactly resonant. When the wavelength is increased to λ = 4.2114 m, resonance is achieved. The wire length is now shorter than $\lambda/2$ at $l = 0.4749\lambda$. The input impedance becomes Z_{in} = 72.0887 + j0000 Ω, which is purely resistive. The surface current distribution and the radiation pattern for the transmitting dipole at resonance are plotted in Figure 3.2 and Figure 3.3, respectively. Using the computed current distribution, the radiation resistance R_{rad} = 72.6381 Ω and the antenna gain G = 1.6232 or 2.1038 dB are obtained. It is clear that $Z_{in} \approx R_{rad}$, allowing for numerical errors. The computed values of the antenna parameters, the surface current distribution, and radiation pattern, agree very well with the theoretical values [6].

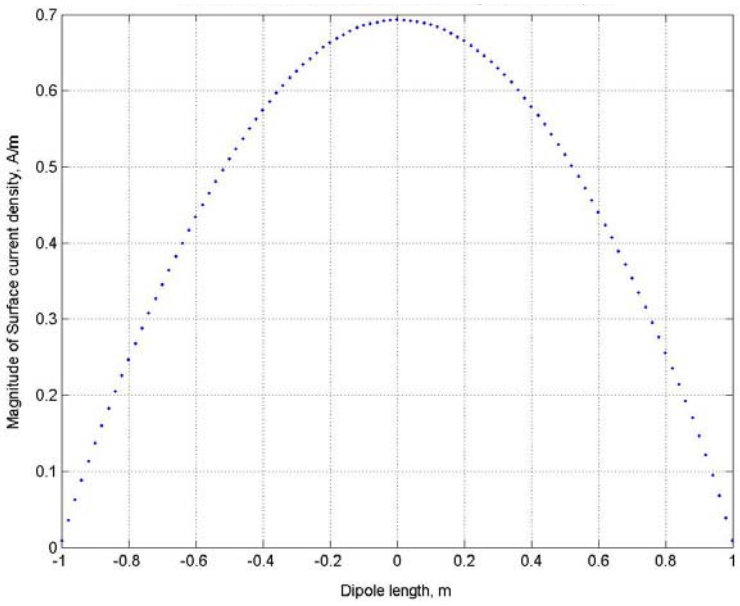

(a)

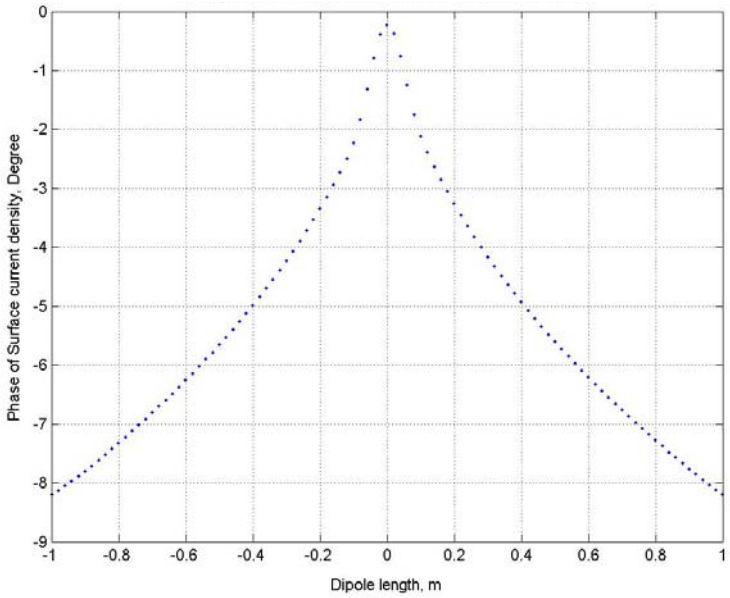

(b)

Figure 3.2. (a) Magnitude and (b) phase of the surface current distribution for a transmitting resonant center-fed dipole.

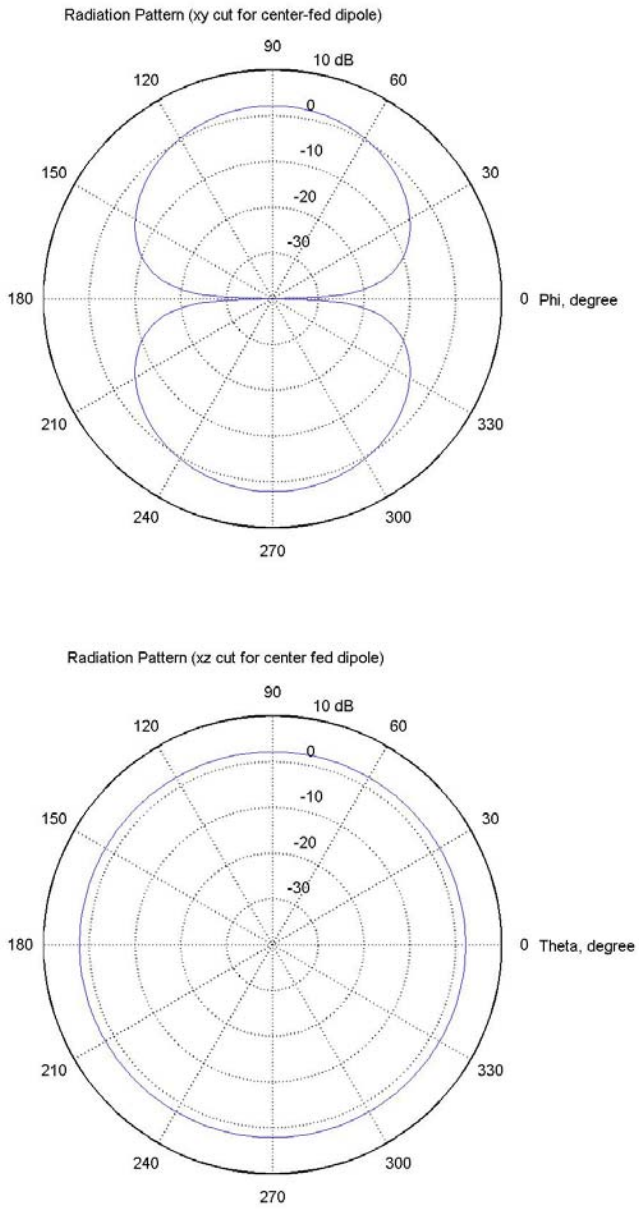

Figure 3.3. Radiation pattern for a transmitting resonant dipole.

2. Transmitted and Received Power

With a feed voltage of $V_f = 1$ V, the feed current $I_f = 13.9$ mA is obtained for a transmitting resonant dipole. Hence, the feed power is $P_t = 0.5\text{Re}\{V_f I_f^*\} = 6.935$ mW. Using the current distribution, the radiated power of $P_{rad} = 6.9888$ mW is obtained. It is clear that $P_t \approx P_{rad}$, allowing for numerical errors.

In the receive mode, a plane wave of 1 V/m is incident in the $-z$ direction and the polarization is parallel to the dipole as shown in Figure 3.4. At the origin, the short-circuited current I_{sc} = 18.384 – j1.43 mA is obtained and the calculated open-circuited voltage is $V_{oc} = I_{sc}Z_{in}$ = 1.3252 – j0.1031 V, where Z_{in} was obtained in the transmit mode. Under a resonance condition, the received power is calculated as $P_r = 0.125|\ V_{oc}\ |^2/\ Z_{in}$ = 3.0636 mW.

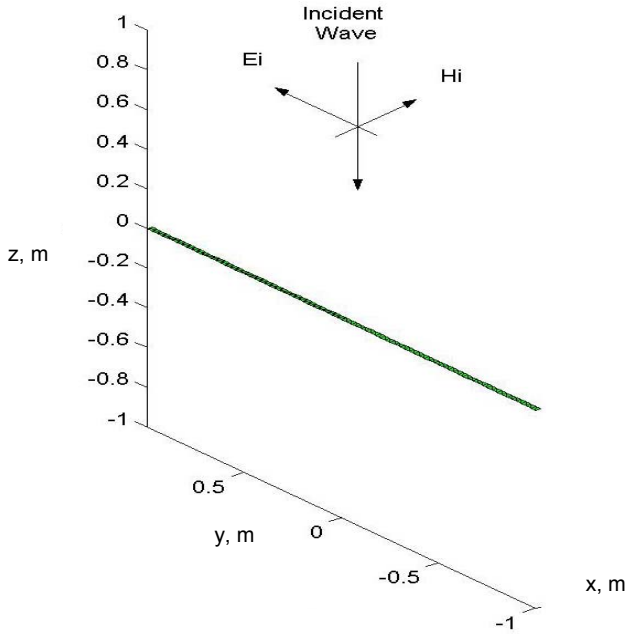

Figure 3.4. Plane wave illuminating a dipole at TM_z normal incidence.

A lumped element of impedance Z_L is connected at the origin (in this case edge number 80) for the receiving resonant dipole by reassigning the impedance matrix elements $Z_{80,80} = Z_{80,80} + l_n^2\ Z_L$, according to [2]. The received power is calculated using the current obtained at the origin, which is flowing through the lumped element load. Under mismatched conditions, the power received when Z_L = 50 Ω and Z_L = 100 Ω is 2.9633 mW and 2.9830 mW, respectively. In a matched condition (i.e., Z_L = 72.0887 + j0000 Ω), the maximum power received is P_r = 3.0636 mW. The surface current distribution for the matched case is shown in Figure 3.5. The reciprocity between the transmit and receive modes is observed. In the receive mode, the magnitude of the surface current density is smaller, due to the property of the effective antenna length. The radiation pattern for the receive mode is the same as that for the transmit mode.

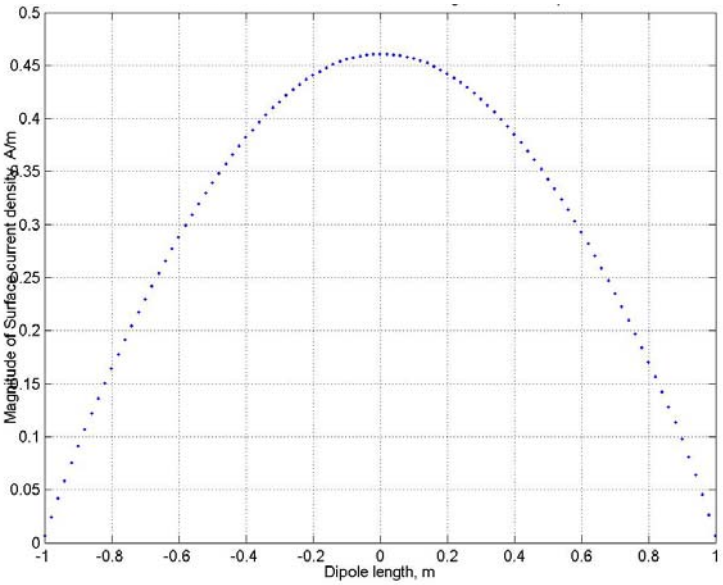

(a)

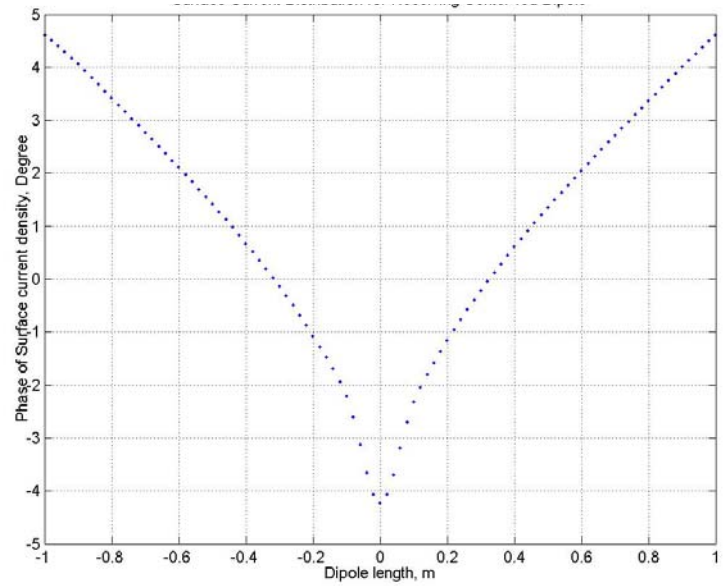

(b)

Figure 3.5. (a) Magnitude and (b) phase of the surface current distribution for a receiving resonant dipole.

D. MODELING OF THE RING-HYBRID DIPOLE FEED

A suitable antenna model used to approximate the operation of the ring-hybrid dipole must be capable of producing simultaneously a resonant pattern, or sum pattern, and an anti-resonant pattern, or difference pattern. The antenna parameters (e.g., impedance) must also be able to represent those of the ring-hybrid dipole.

One possible model is to use two wire strips that are separated by a small physical gap and fed at the edges near the gap, as shown in Figure 3.6. Although the sum pattern and the difference pattern are obtained, the input impedances for both the sum and difference modes are highly capacitive for a $\lambda/2$ structure. This is due to the absence of a common path between the two excitation sources. This model is not adequate, and therefore was discarded.

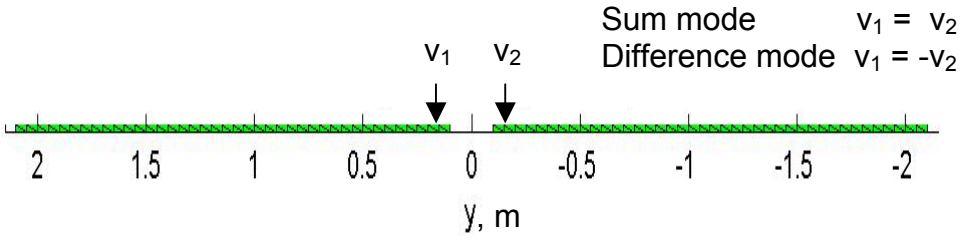

Figure 3.6. Feed model using two thin-wire strips separated by a small gap.

Another possible approach is to use a patch antenna probe feed model [3], as shown in Figure 3.7, to incorporate the common path. However, the feeding strip must extend to $\lambda/4$, in order to model the operation of the ring-hybrid dipole over the ground. The long feeding strip will introduce more mutual coupling as well as radiate. Thus, this model was also discarded.

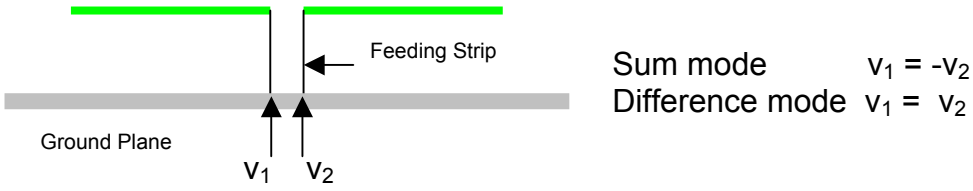

Figure 3.7. Patch antenna probe feed model for the dipole feed.

Finally, a simple and suitable feed model is a continuous wire strip (similar to that used for modeling the center-fed dipole) that incorporates two feed points equally offset from the origin. The common path between the excitation sources is thus established. It is found that a symmetrical structure, as shown in Figure 3.8, must be employed to achieve a correct and balanced operation in both the sum and difference modes. In addition, a minimum offset distance of 12 edges is chosen to ensure that the current distribution is symmetrical about the origin and that the current at the origin is nearly zero, when operating in the difference mode. Subsequently, this configuration will be referred to as a two-feed point dipole.

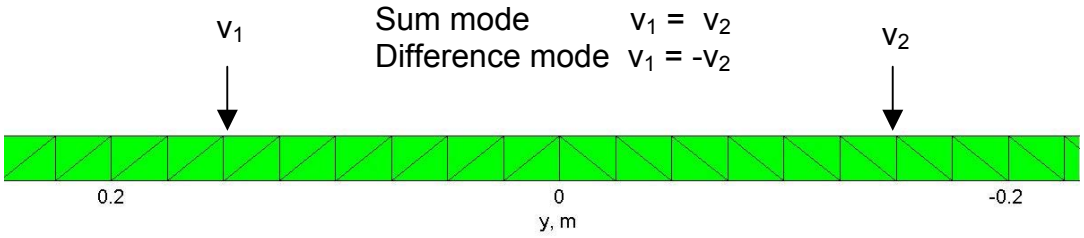

Figure 3.8. Feed model using a symmetrical thin-wire strip.

E. TWO-FEED POINT DIPOLE

In this section, the antenna parameters are obtained for the two-feed point dipole. The parameters are the input impedance, radiation resistance, antenna gain, feed power, and radiated power. For the sum and difference modes, as shown in Figure 3.9, the excitation sources are applied in-phase and 180º out-of-phase, respectively. The surface current distribution and the radiation pattern are also plotted for the transmit case.

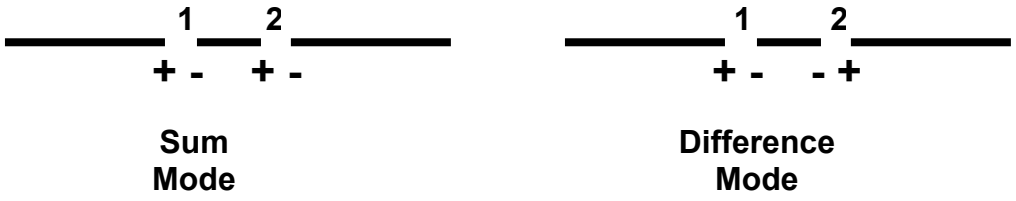

Figure 3.9. Sum mode and difference mode for the two-feed point dipole.

1. Antenna Impedance and Gain

Resonance for the sum mode is achieved when the wavelength is λ = 4.2236 m, and hence the wire length is l = 0.47353 λ. This is shorter than the resonant length l = 0.4749 λ for the center-fed dipole. The input impedance, radiation resistance, and the antenna gain, for the sum mode and the difference mode are shown in Table 3.2. The surface current distributions for the sum mode and the difference mode are shown in Figure 3.10 and Figure 3.11, respectively. The radiation patterns are shown in Figures 3.12 and 3.13. Both the sum mode and the difference mode are balanced and the operating characteristics are a good representation of the actual ring-hybrid dipole values.

Parameters	Sum Mode		Difference Mode		Remarks
	feed 1	feed 2	feed 1	feed 2	
Input Impedance, Z_{in} (Ω)	37.5438	37.5438	1.0885 – *j*886.58	1.0885 – *j*886.58	balanced
Radiation Resistance, R_{rad} (Ω)	75.6541		2.1942		using current distribution
Gain, G	1.6223 or 2.1014 dB		1.8332 or 2.6320 dB		

Table 3.2. Input impedance and radiation resistance for the sum mode and the difference mode.

2. Feed Power and Radiated Power

The feed powers and the radiated powers in the sum and difference modes are shown in Table 3.3. The power in the difference mode is very low due to an anti-resonant antenna. However, the difference mode is useful in the receiving case.

Parameters	Sum Mode		Difference Mode		Remarks
	feed 1	feed 2	feed 1	feed 2	
Feed Voltage	+ 0.5 V	+ 0.5 V	+ 0.5 V	– 0.5 V	
Feed Power	3.3294 mW	3.3294 mW	173.11 nW	173.11 nW	balanced
Radiated Power	6.7091 mW		348.94 nW		

Table 3.3. Transmitted powers of the two-feed point dipole.

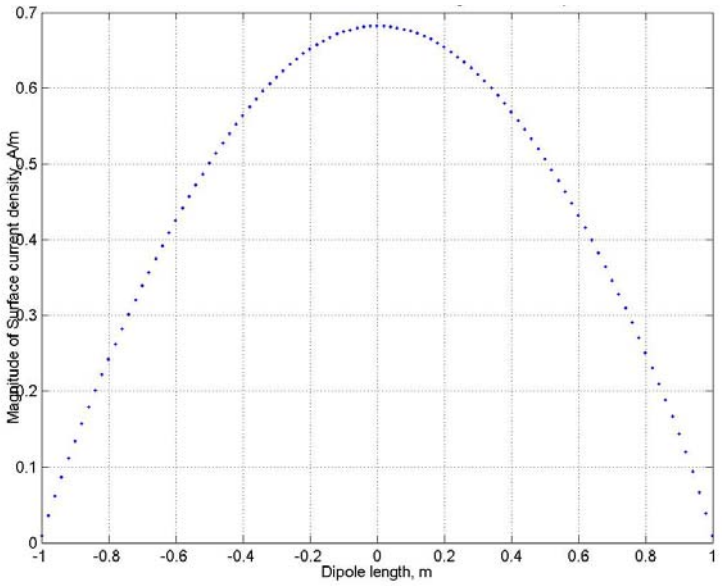

(a)

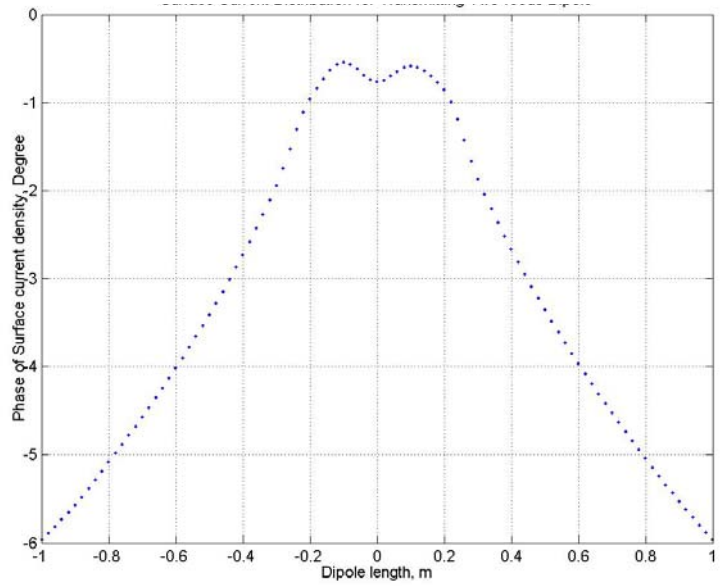

(b)

Figure 3.10. (a) Magnitude and (b) phase of the surface current distribution for the sum mode.

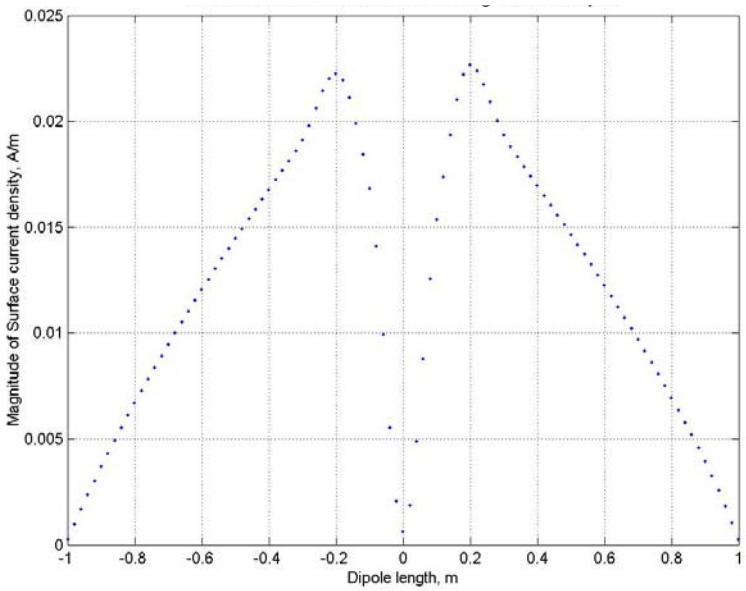

(a)

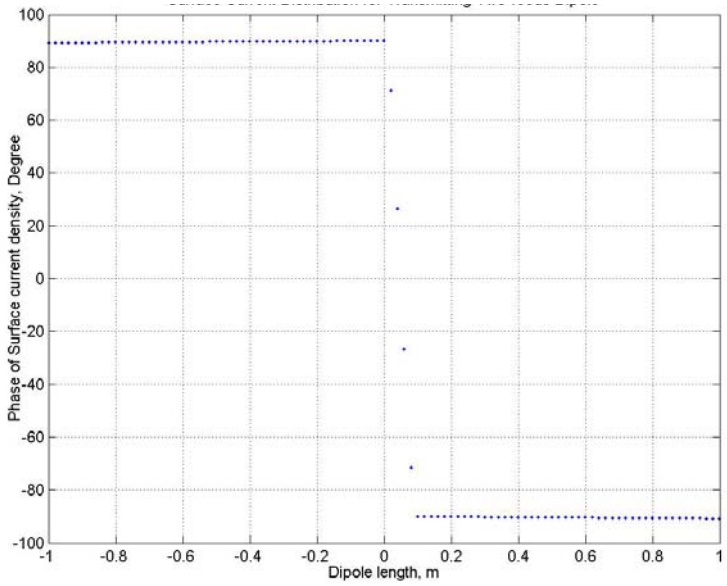

(b)

Figure 3.11. (a) Magnitude and (b) phase of the surface current distribution for the difference mode.

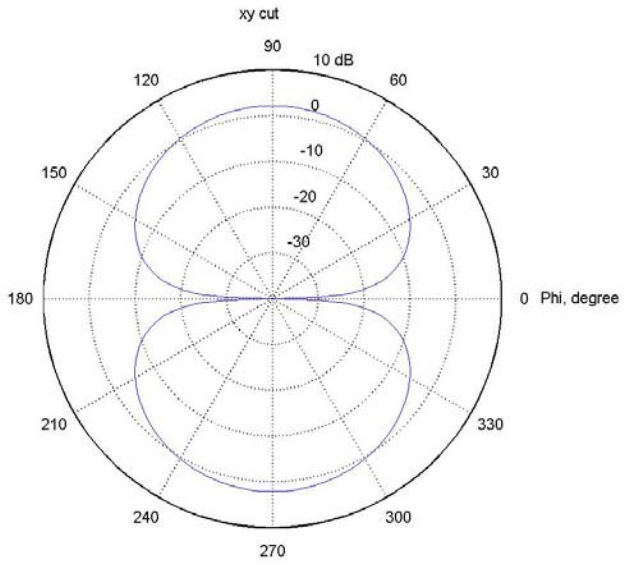

Figure 3.12. Radiation pattern for the sum mode.

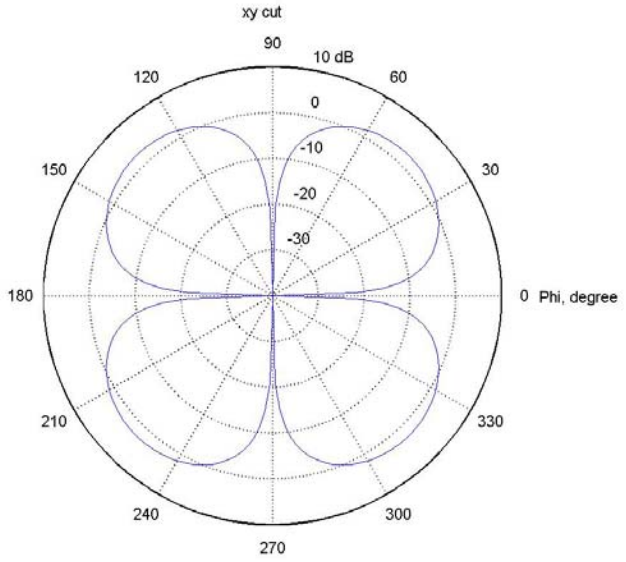

Figure 3.13. Radiation pattern for the difference mode.

F. CHAPTER SUMMARY

A convergence test based on a center-fed dipole was performed to determine the discretization requirement. The dipole was modeled as a thin-wire strip of length *l* that is very much greater than its width *w*. The equivalent wire radius is one quarter of the width. A discretization of 80 segments (or 159 RWG edges) ensured that the phase of the input impedance has stabilized. The antenna parameters for the center-fed dipole in resonance were obtained for both the transmit and receive modes. The surface current distribution, input impedance, antenna gain, and radiation pattern, all agreed very well with antenna theory.

A two-feed point dipole was used to model the ring-hybrid dipole. The two feed points were equally offset by 12 edges from the center of a symmetrical thin-wire strip. The sum mode (resonant) and the difference mode (anti-resonant) were produced by feeding the excitation voltages in-phase and 180º out-of-phase, respectively. The correct radiation pattern for both the sum mode and the difference mode were obtained. These arrangements ensured a correct and balanced operation in both the sum and difference modes. In the sum mode, the input impedance is about 37.5 Ω in each feed. In the difference mode, the input impedance is about 1.1 – j 887 Ω in each feed. The difference mode is thus highly inefficient in the transmit mode but is useful in the receive mode. The antenna parameters obtained for the two-feed point dipole model were a good representation of the actual ring-hybrid dipole values. Thus, this antenna model will be used to combine with a beamforming network model.

THIS PAGE INTENTIONALLY LEFT BLANK

IV. ANTENNA BEAMFORMING NETWORK MODELING

A. CHAPTER OVERVIEW

The beamforming network generally consists of devices such as power dividers and phase shifters, which are used to achieve the desired amplitude and phase distribution at the array aperture. In this chapter, the basic theory used in the modeling of the beamforming network connection to the antenna feed is presented. The reflection coefficient and return loss for the center-fed dipole connected to a transmission line are then obtained. The corresponding analysis is also carried out for the two-feed point dipole that is connected to two transmission lines. Finally, the two-feed point dipole is connected to a magic-tee to model the ring-hybrid dipole. The Matlab codes developed for the simulations (which are modifications of script *rwg4.m*) are in Appendix B.

B. BASIC THEORY

The matrix solution described in [7] uses the method of moments on the antenna surfaces and a scattering matrix formulation for the feed network. The two sets of equations are related by continuity (or joining) relations based on an appropriate form of the conservation of energy. In our case, the Kirchhoff's voltage and current laws must be satisfied at the terminals of the dipole. Once the excitation is specified, the antenna matrix equation is solved to yield the method of moments expansion current coefficients and the signals in the feed network.

From [8], the scattering parameters of a *N*-port device relate the incident and reflected voltages (or currents) at all ports. If V_n^+ and V_n^- are the incident and reflected waves at port *n*, respectively, then for a *N*-port network,

$$V_n^- = S_{n1}V_1^+ + S_{n2}V_2^+ + \cdots + S_{NN}V_N^+, \quad n = 1,\ldots,N, \tag{4.1}$$

or in matrix form

$$\mathbf{V}^- = \boldsymbol{S} \cdot \mathbf{V}^+. \tag{4.2}$$

The S_{nm} are the scattering parameters which give the signal at port n due to an input at port m with all other ports terminated in matched load. Thus, S_{nm} is given by

$$S_{nm} = \left.\frac{V_n^-}{V_m^+}\right|_{V_k^+=0 \text{ for } k\neq m} . \tag{4.3}$$

Hence, S_{nn} is the reflection coefficient seen looking into port n when all other ports are terminated in matched loads, and S_{nm} is the transmission coefficient from port m to port n when all other ports are terminated in matched loads.

In our case, the scattering parameters are combined with the RWG impedance matrix through the joining equations. The magnitude of the total voltage V_n and current I_n at port n must be equal to the magnitude of the voltage V_a and the method of moment expansion current coefficient I_a at the dipole terminal, respectively. Currents I_n and I_a must be in anti-phase based on the reference system defined in Figure 4.1. The two joining equations are thus found to be

$$V_n = V_n^+ + V_n^- = V_a, \tag{4.4}$$

and

$$I_n = \frac{V_n^+ - V_n^-}{Z_{on}} = -I_a. \tag{4.5}$$

The reflection coefficient Γ_L at the dipole terminal is then

$$\Gamma_L = \frac{V_n^-}{V_n^+} = \frac{Z_{in} - Z_{on}}{Z_{in} + Z_{on}}, \tag{4.6}$$

and the return loss RL is thus

$$RL = -10\log_{10}\left|\Gamma_L\right|^2 \text{ dB}. \tag{4.7}$$

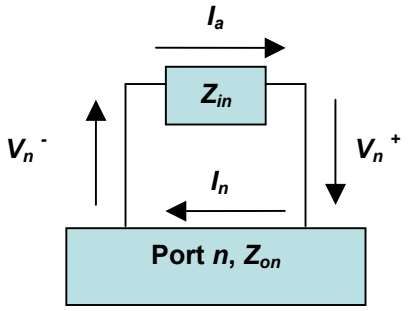

Figure 4.1. Antenna feed point connection to the feed network.

C. CENTER-FED DIPOLE CONNECTED TO A TRANSMISSION LINE

The center-fed dipole is connected to a transmission line as shown in Figure 4.2. The unknown signals c_1, c_2, and c_3, in the feed network are also to be solved. The transmission line is a two-port device with a scattering matrix

$$\boldsymbol{S} = \begin{bmatrix} S_{11} & S_{12} \\ S_{21} & S_{22} \end{bmatrix}. \tag{4.8}$$

Hence, there are two scattering equations

$$\begin{bmatrix} c_1 \\ c_3 \end{bmatrix} = \begin{bmatrix} S_{11} & S_{12} \\ S_{21} & S_{22} \end{bmatrix} \begin{bmatrix} c_2 \\ V_{in} \end{bmatrix}, \tag{4.9}$$

or, rearranging

$$\begin{aligned} c_1 - S_{11}c_2 &= S_{12}V_{in} \\ c_3 - S_{21}c_2 &= S_{22}V_{in} \end{aligned}. \tag{4.10}$$

Using (4.4) and (4.5), the two joining equations are

$$Z_{a1}I_1 + Z_{a2}I_2 + \cdots + Z_{aM}I_M - c_1 - c_2 = 0, \tag{4-11}$$

and

$$I_a - \frac{c_1}{Z_o} + \frac{c_2}{Z_o} = 0. \tag{4.12}$$

where a is the feeding edge number and Z_o is the characteristic impedance of the transmission line.

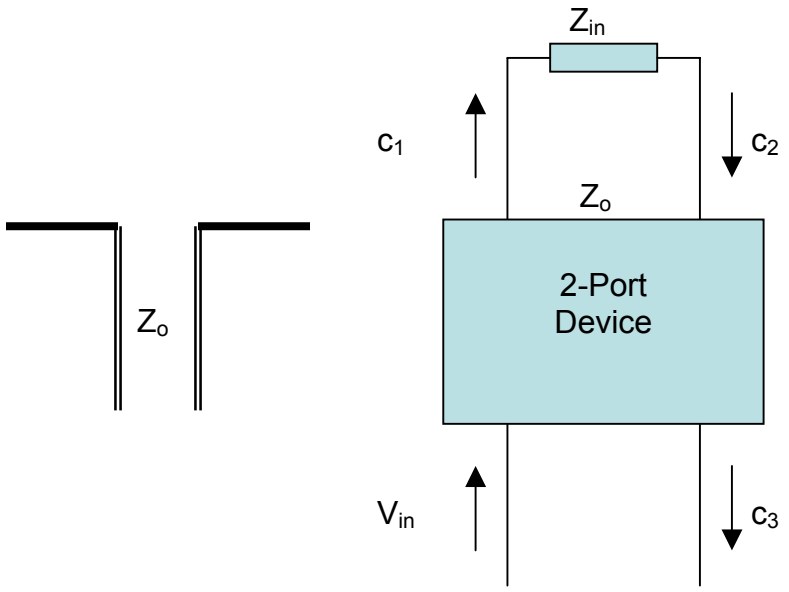

Figure 4.2. Center-fed dipole connected to a transmission line and its circuit model.

The scattering parameters are then combined with the RWG impedance matrix through the two joining equations to obtain one matrix that completely describes the entire antenna and feed network

$$\begin{bmatrix} Z_{11} & \cdots & \cdots & Z_{1a} & \cdots & \cdots & Z_{1M} & 0 & 0 & 0 \\ \vdots & & & \vdots & & & \vdots & \vdots & \vdots & \vdots \\ \vdots & & & \vdots & & & \vdots & 0 & 0 & 0 \\ Z_{a1} & \cdots & \cdots & Z_{aa} & \cdots & \cdots & Z_{aM} & -1 & -1 & 0 \\ \vdots & & & \vdots & & & \vdots & 0 & 0 & 0 \\ \vdots & & & \vdots & & & \vdots & \vdots & \vdots & \vdots \\ Z_{M1} & \cdots & \cdots & Z_{Ma} & \cdots & \cdots & Z_{MM} & 0 & 0 & 0 \\ 0 & \cdots & 0 & 1 & 0 & \cdots & 0 & -1/Z_o & +1/Z_o & 0 \\ 0 & \cdots & 0 & 0 & 0 & \cdots & 0 & 1 & -S_{11} & 0 \\ 0 & \cdots & 0 & 0 & 0 & \cdots & 0 & 0 & -S_{21} & 1 \end{bmatrix} \begin{bmatrix} I_1 \\ \vdots \\ \vdots \\ I_a \\ \vdots \\ \vdots \\ I_M \\ c_1 \\ c_2 \\ c_3 \end{bmatrix} = \begin{bmatrix} V_1 \\ \vdots \\ \vdots \\ V_a \\ \vdots \\ \vdots \\ V_M \\ 0 \\ S_{12}V_{in} \\ S_{22}V_{in} \end{bmatrix}. \quad (4.13)$$

The complete system of equations is solved using

$$\mathbf{I} = \boldsymbol{Z}^{-1} \cdot \mathbf{V}. \quad (4.14)$$

The reflection coefficient at the dipole terminal is computed from

$$\Gamma_L = \frac{c_2}{c_1} = \frac{Z_{in} - Z_o}{Z_{in} + Z_o}, \tag{4.15}$$

and the return loss from

$$RL = -10\log_{10}\left|\Gamma_L\right|^2 \text{ dB}. \tag{4.16}$$

In the transmit mode, V_{in} is the applied voltage. The results for the center-fed dipole driven through a transmission line with characteristic impedance Z_o under matched and mismatched conditions are shown in Table 4.1. The feed network interaction with the antenna is modeled rigorously. An ideal transmission line is used here and its scattering matrix is

$$\boldsymbol{S} = \begin{bmatrix} 0 & 1 \\ 1 & 0 \end{bmatrix}. \tag{4.17}$$

Parameters	Matched	Mismatched		Remarks
	$Z_o = Z_{in} =$ 72.0887 Ω	$Z_o = 50$ Ω	$Z_o = 75$ Ω	
Reflection Coefficient	– 1.8913e–7 – *j*1.6262e–7	0.1809 – *j*0.0000	– 0.0198 – *j*0.0000	resonant antenna
Return Loss (dB)	132.0610	14.8501	34.0698	

Table 4.1. Results for a center-fed dipole driven through an ideal transmission line.

In the receive mode, the source is a plane wave of amplitude 1 V/m and the applied feed voltage V_{in} is set to zero (i.e., the transmission line is connected to a load Z_L matched to the line characteristic impedance). The setup is the same as that shown in Figure 3.4. In a mismatched condition, the power received when $Z_L = 50$ Ω and $Z_L = 100$ Ω is 2.9633 mW and 2.9830 mW, respectively. In a matched condition (i.e., $Z_L = Z_{in}$), the maximum power received is $P_r = 0.5|c_3|^2 / Z_L = 3.0636$ mW. Again, the feed network interaction with the antenna is modeled rigorously. There is no approximation other than the numerical evaluation of the matrix elements.

D. TWO-FEED POINT DIPOLE CONNECTED TO TWO TRANSMISSION LINES

The two-feed point dipole is connected to two transmission lines as shown in Figure 4.3. The same procedure as in Section C is applied. In this case, there are four scattering equations and four joining equations.

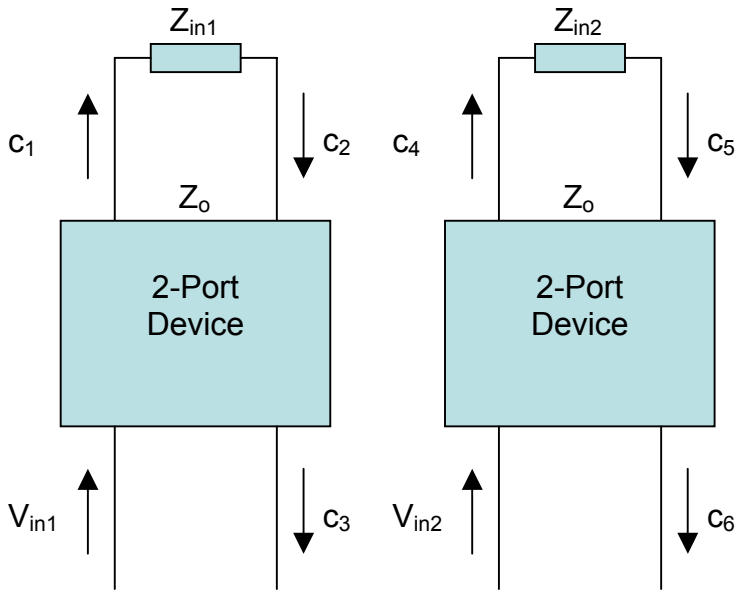

Figure 4.3. Two-feed point dipole connected to transmission lines.

The results for matched and mismatched conditions, when the sum and difference modes are transmitted using ideal transmission lines, are shown in Table 4.2. The return loss for the difference mode is very low when standard 50-Ω transmission lines are used.

Parameters	Sum Mode		Difference Mode		Remarks
	Matched $Z_o = Z_{in}$ = 37.5438 Ω	Mismatched Z_o = 50 Ω	Matched $Z_o = Z_{in}$ = 1.0885 – *j*886.58 Ω	Mismatched Z_o = 50 Ω	
Reflection Coefficient	3.1412e–7 – *j*1.4335e–7	– 0.1423 – *j*0.0000	– 1.5607e–6 + *j*1.7988e–6	0.9935 – *j*0.1124	Same for both feed points
Return Loss (dB)	129.2364	16.9368	116.1332	0.0012	

Figure 4.2. Results for a two-feed point dipole driven through ideal transmission lines.

In the receive mode, two incident directions for a plane wave of 1 V/m are investigated here. The first setup is the same as that shown in Figure 3.4. The second setup is a plane wave incident at 45º as shown in Figure 4.4. The surface current distribution for the second setup is plotted in Figure 4.5.

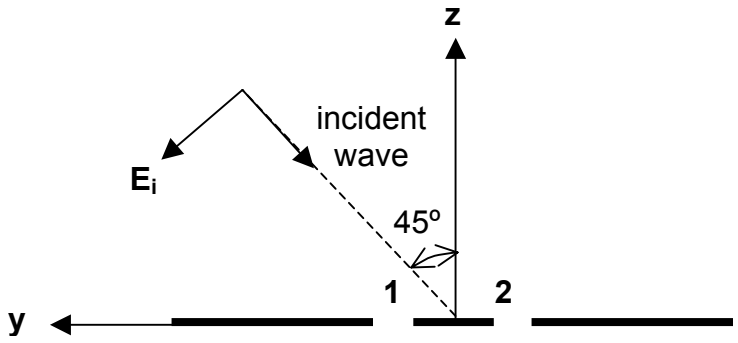

Figure 4.4. Plane wave illuminating a two-feed point dipole at TM_z 45º incidence.

The received powers for both setups are shown in Table 4.3. The difference power can only be extracted when there is a difference in the plane wave path length between the two arms of the dipole.

Plane Wave Incidence	Power received at feed 1	Power received at feed 2	Remarks
0º	1.5399 mW	1.5399 mW	Z_L = 37.5438 Ω for both setups
45º	0.6438 mW	0.5843 mW	

Table 4.3. Received power for the two-feed point dipole at 0º and 45º incidence.

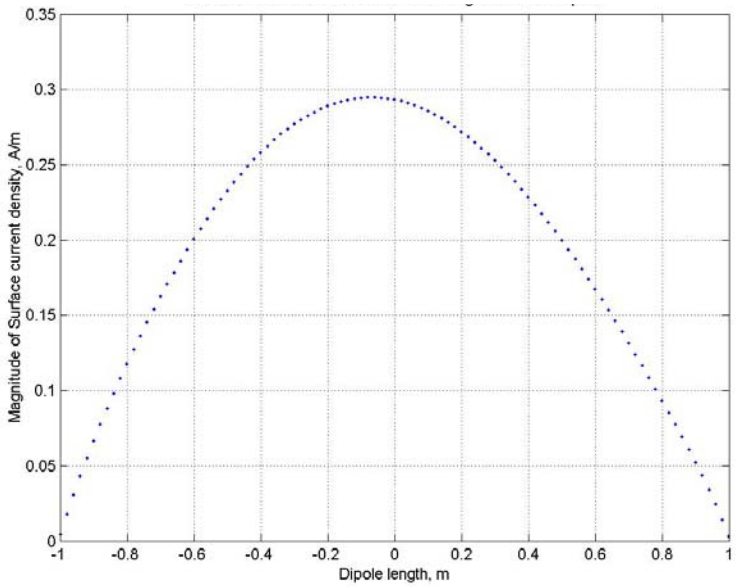

(a)

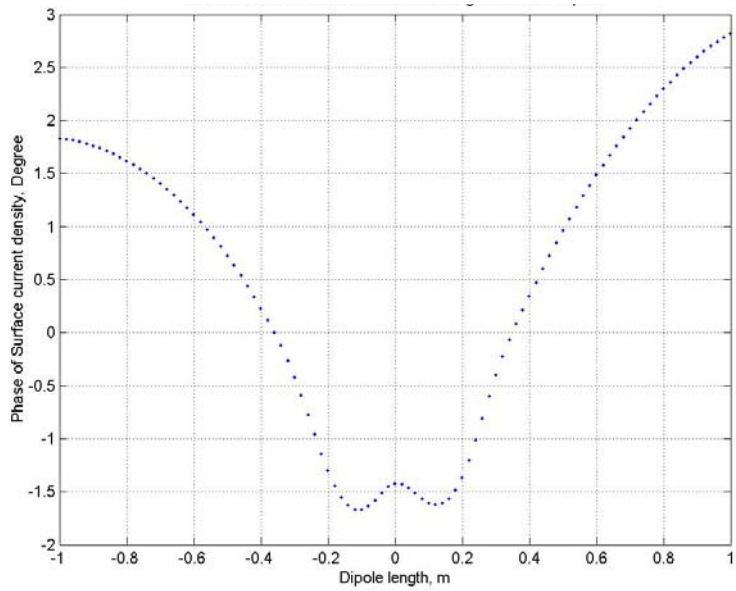

(b)

Figure 4.5. (a) Magnitude and (b) phase of the surface current distribution for two-feed point dipole at 45º incidence.

E. TWO-FEED POINT DIPOLE CONNECTED TO A MAGIC-TEE

The two-feed point dipole is connected to a magic-tee as shown in Figure 4.6. The magic-tee is a four-port power splitting device with the scattering matrix

$$\boldsymbol{S} = A\begin{bmatrix} 0 & 1 & 1 & 0 \\ 1 & 0 & 0 & 1 \\ 1 & 0 & 0 & -1 \\ 0 & 1 & -1 & 0 \end{bmatrix}, \tag{4.18}$$

where $A = 1/\sqrt{2}$ for the lossless case.

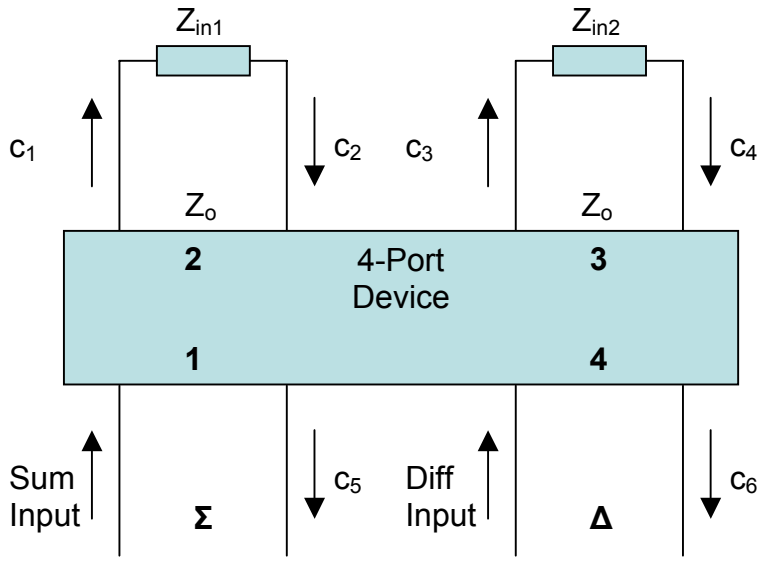

Figure 4.6. Two-feed point dipole connected to a magic-tee.

Port 1 is the sum port and port 4 is the difference port. Port 2 and port 3 are the output ports (referred to as side arms). If a signal is injected into the sum port, equal in-phase signals emerge from port 2 and port 3. If a signal is injected into the difference port, equal 180º out-of-phase signals emerge from port 2 and port 3. The power splits equally when $A = 1/\sqrt{2}$. If $A = 0.5$ is used, one quarter of the power will be absorbed (or lost) in each output.

The same procedure used in Section C is applied. In this case, there are four scattering equations and four joining equations. The receive mode is investigated here and the setup is as shown in Figure 4.4, except that the incident direction is – 45º. The sum input and the difference input are both set to zero. The results for case 1 (where Z_L = 37.5438 Ω with A = 0.5), and case 2 (where Z_L = 50 Ω with $A = 1/\sqrt{2}$), are shown in Table 4.4. In case 1, a quarter of the power is lost in each output. In case 2, the received power is transferred to the sum and difference ports with no loss. The power relationships have been verified (i.e., energy is conserved).

Parameters	Case 1 Z_L = 37.5438 Ω A = 0.5	Case 2 Z_L = 50 Ω $A = 1/\sqrt{2}$	Remarks
Power Received at Feed 1	0.5843 mW	0.5678 mW	
Power Received at Feed 2	0.6438 mW	0.6357 mW	
Total Received Power	1.2281 mW	1.2035 mW	
c_2	– 0.0042 + j0.0002	– 0.0048 + j0.0002	
c_4	– 0.0044 + j0.0002	– 0.0050 + j0.0002	
c_5	– 0.0043 + j0.0002	– 0.0069 + j0.0003	$c_5 = A(c_2 + c_4)$
c_6	1.0384e–4 – j5.0664e–6	1.9528e–4 – j1.2273e–5	$c_6 = A(c_2 – c_4)$
Power at Sum Port	0.6137 mW	1.2025 mW	
Power at Diff Port	359.84 nW	957.08 nW	
Total Power (Σ + Δ)	0.6140 mW	1.2035 mW	Quarter power lost in each output for Case 1

Table 4.4. Results for a two-feed point dipole connected to a magic-tee in the receive mode for – 45º incidence.

F. CHAPTER SUMMARY

The basic theory involved in the modeling of the beamforming network connection to the dipole antenna feed was derived. The matrix solution combined the method of moments equations on the antenna surfaces and a scattering matrix formulation for the feed network. The joining equations were formed by applying Kirchhoff's voltage and current laws (conservation of energy) at the terminals of the dipole antenna. Once the excitation is specified, the complete system of equations was solved to yield the MoM current expansion coefficients and the signals in the feed network.

A test case for a center-fed dipole connected to a transmission line was performed. The feed network interaction with the antenna feed was modeled rigorously. In the transmit mode, the reflection coefficients for both matched and mismatched conditions were computed accurately and in accordance with transmission line theory [8]. In the receive mode, maximum power is received in a matched load condition.

The two-feed point dipole was connected to two 50-Ω transmission lines. There were mismatches in both the sum and difference modes. The return loss is about 17 dB and 0.0012 dB for the sum and difference modes, respectively. In the receive mode, the difference power can only be extracted when there is a difference in the incident wave path length between the two dipole arms.

The two-feed point dipole was connected to a magic-tee to model the complete ring-hybrid dipole. The power relationships (i.e., conservation of energy) between the total captured power, and the total output power in sum port and the difference port were verified for two test cases. The complete ring-hybrid dipole model will thus be extended to create an antenna array model.

THIS PAGE INTENTIONALLY LEFT BLANK

V. MUTUAL COUPLING IN A SMALL ANTENNA ARRAY

A. CHAPTER OVERVIEW

In this chapter, the mutual coupling for a free-standing array of three center-fed dipoles matched at all scan angles is examined first. A ground plane is then introduced and a convergence test is performed to determine the discretization requirement. Next, the mutual coupling in the presence of the ground plane is evaluated. The antenna array is then connected to the beamformer transmission lines, and the mutual coupling is observed. Following that, an array of three two-feed point dipoles over a ground plane are connected to magic-tees simulating an array of three ring-hybrid dipoles. The sum and difference port outputs for different incidence angles in the receive mode are then obtained. The Matlab codes developed for the simulations (which are modifications of script *rwg4.m*) are in Appendix B.

B. MUTUAL COUPLING FOR AN ARRAY OF THREE CENTER-FED DIPOLES

An array of three free-standing dipoles is shown in Figure 5.1. All of the dipoles are directly fed at their center with an ideal voltage source and thus a matched condition is simulated for all scan angles. For the center-fed dipole, the wavelength is λ = 4.2114 m, and the antennas are spaced $\lambda/2$ apart. In order to steer the antenna beam, the phase for the *i*th element relative to the phase of the zeroth element is

$$\gamma_i = -i\, kd \cos\phi, \tag{5.1}$$

where $k = 2\pi/\lambda$, d is the spacing between the elements, and ϕ is the scan angle. For broadside scan, the azimuth and zenith angles are ϕ = 90º (or ϕ = 270º) and $\theta = 90°$, respectively.

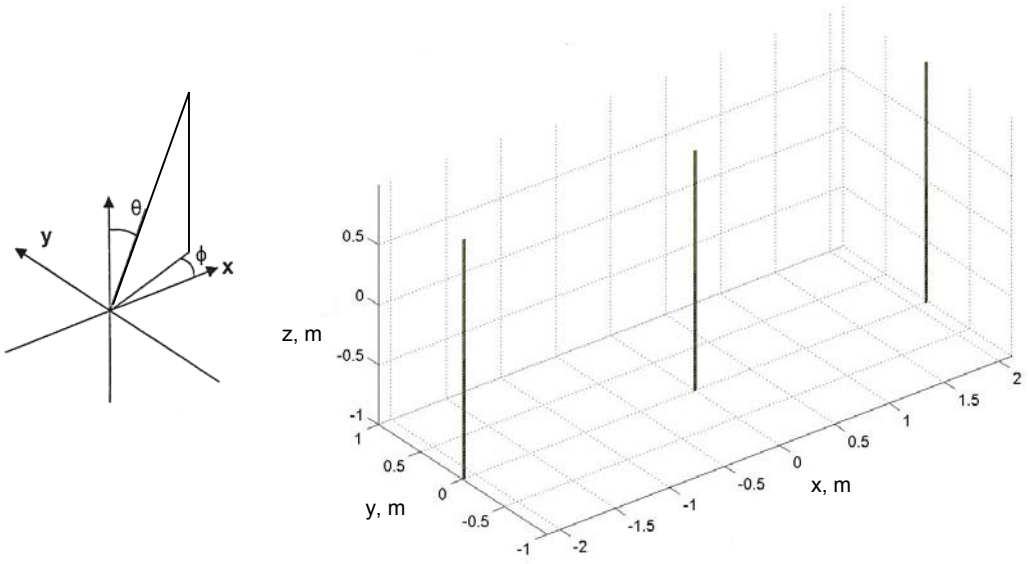

Figure 5.1. An array of three dipoles.

The surface current distribution and the antenna pattern for broadside scan are plotted in Figure 5.2. The current distribution is symmetrical about the middle dipole. The input impedances obtained are Z_{in1} = 67.3465 – j26.5366 Ω, Z_{in2} = 40.7447 – j30.1476 Ω, and Z_{in3} = 67.3451 – j26.5365 Ω. The input impedances are symmetrical about the middle dipole as expected. The input impedances are different from those of a single center-fed dipole due to mutual coupling. Since there are only three antenna elements, the main beam is wide and the gain obtained is G = 5.6763 or 7.5407 dB.

The surface current distribution and the antenna pattern for 30º off-broadside scan (i.e., ϕ = 60º, $\theta = 90°$) are plotted in Figure 5.3. The current distribution is not symmetrical about the middle dipole when the scan is off-broadside. The input impedances obtained are Z_{in1} = 53.8125 – j3.9801 Ω, Z_{in2} = 80.1318 – j23.7998 Ω, and Z_{in3} = 74.5189 – j42.2701 Ω. In accordance with the current distribution, the input impedances are also not symmetrical. The gain obtained is G = 4.9520 or 6.9478 dB, which is reduced from the broadside case.

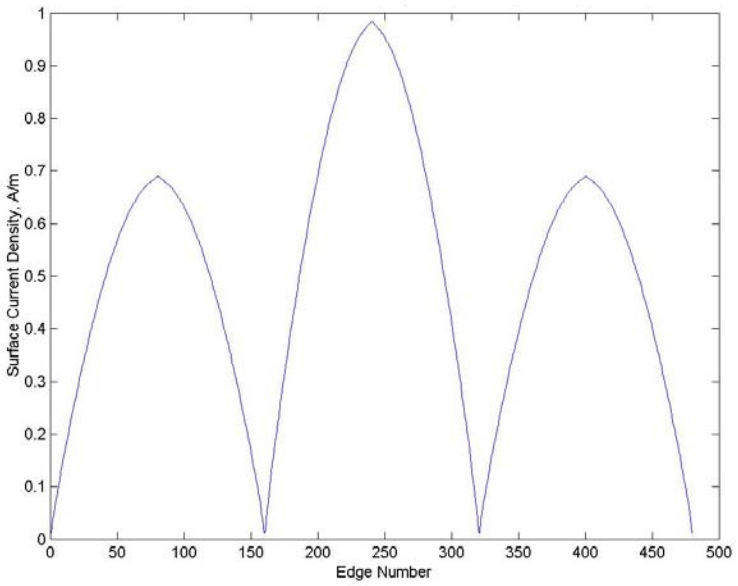

(a)

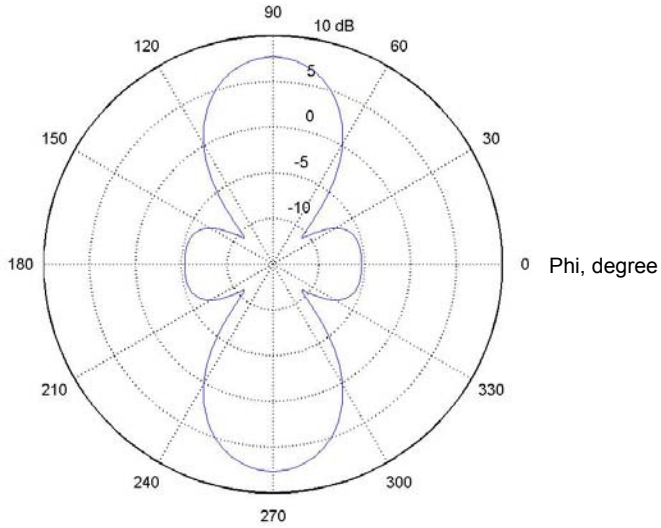

(b)

Figure 5.2. (a) Surface current distribution and (b) radiation pattern for an array of three free-standing center-fed dipoles spaced $\lambda/2$ apart at broadside scan.

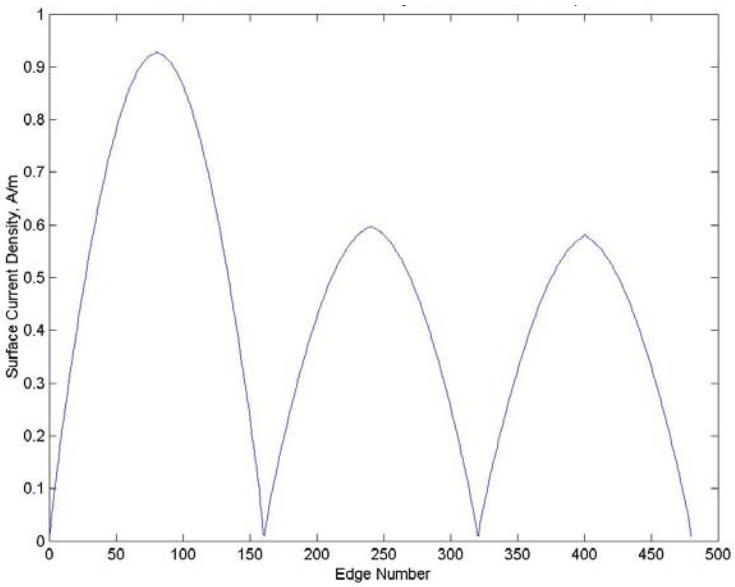

(a)

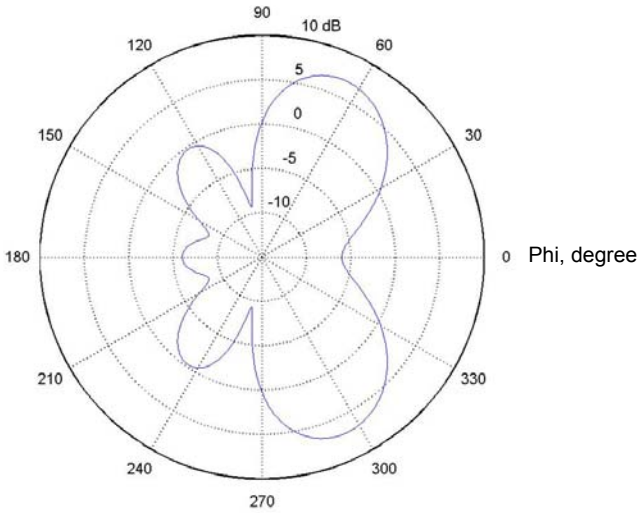

(b)

Figure 5.3. (a) Surface current distribution and (b) radiation pattern for an array of three free-standing center-fed dipoles spaced $\lambda/2$ apart at 30º off-broadside scan.

C. MUTUAL COUPLING FOR AN ARRAY OF THREE CENTER-FED DIPOLES OVER A GROUND PLANE

An array of three dipoles over a finite ground plane is shown in Figure 5.4. The ground plane is a 2λ square plate. The distance between the antennas and the plate is $\lambda/4$. All of the elements are the center-fed dipoles spaced $\lambda/2$ apart.

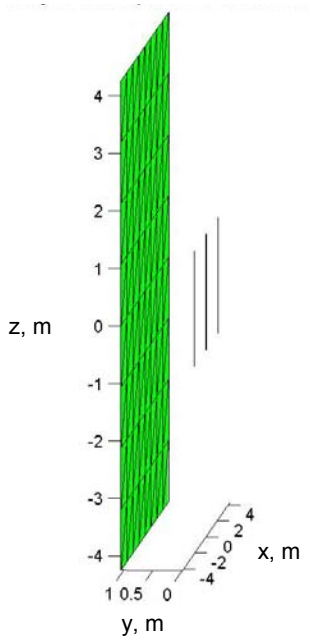

Figure 5.4. An array of three dipoles over a finite ground plane.

The input impedance for broadside scan versus the number of triangles on the plate is shown in Table 5.1. The input impedances have stabilized when the number of triangles is 1248. There is actually a very small amount of difference between the input impedances of dipole 1 (Z_{in1} = 102.70 + j5.07 Ω) and dipole 3 (Z_{in3} = 102.93 + j4.97 Ω) due to the use of a non-symmetrical plate mesh distribution, as shown in Figure 5.5. The input impedances are modified from those in Section B due to the presence of the ground plane. The input impedances obtained for 30º off-broadside scan are Z_{in1} = 72.64 + j20.19 Ω, Z_{in2} = 114.24 + j29.83 Ω, and Z_{in3} = 140.46 + j7.40 Ω. The input impedance versus scan angle is plotted in Figure 5.6. The input impedance varied significantly with the scan angle for all three dipoles.

Number of Triangles	Input Impedance of Dipole 1 (Ω)		Input Impedance of Dipole 2 (Ω)	
128	$102.79 + j7.82$	$103.09 \angle 4.35$	$81.53 - j21.90$	$84.42 \angle -15.04$
512	$102.49 + j5.75$	$102.65 \angle 3.21$	$80.44 - j24.21$	$84.00 \angle -16.75$
1248	$102.70 + j5.07$	$102.83 \angle 2.83$	$80.32 - j24.87$	$84.08 \angle -17.20$
2048	$102.95 + j4.72$	$103.06 \angle 2.63$	$80.33 - j25.26$	$84.21 \angle -17.46$

Table 5.1. Input impedance for an array of three center-fed dipoles spaced $\lambda/2$ apart, over a 2λ square plate with various discretization, at broadside scan.

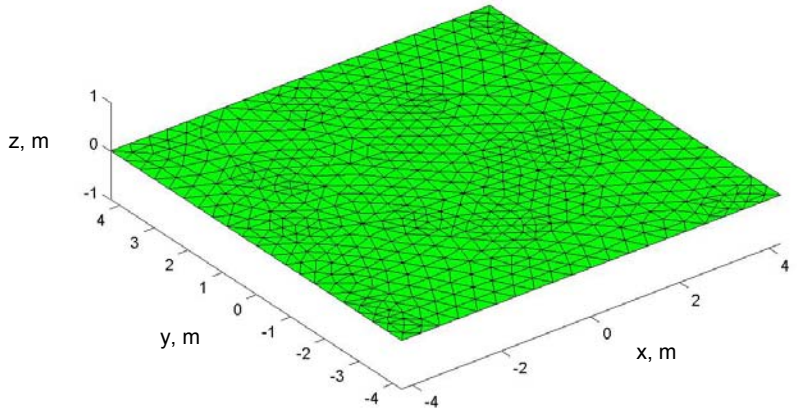

Figure 5.5. A 2λ square plate with 1248 triangles.

The radiation pattern for broadside scan and 30º off-broadside scan are plotted in Figure 5.7. The electromagnetic energy is mostly contained in the region $0° \le \phi \le 180°$, except for a small level of backlobe, due to the presence of the finite ground plane. The gains obtained for broadside scan and 30º off-broadside scan are G = 13.7226 or 11.3744 dB and G = 14.1262 or 11.5003 dB, respectively. The gain for the latter case is slightly higher than the broadside case.

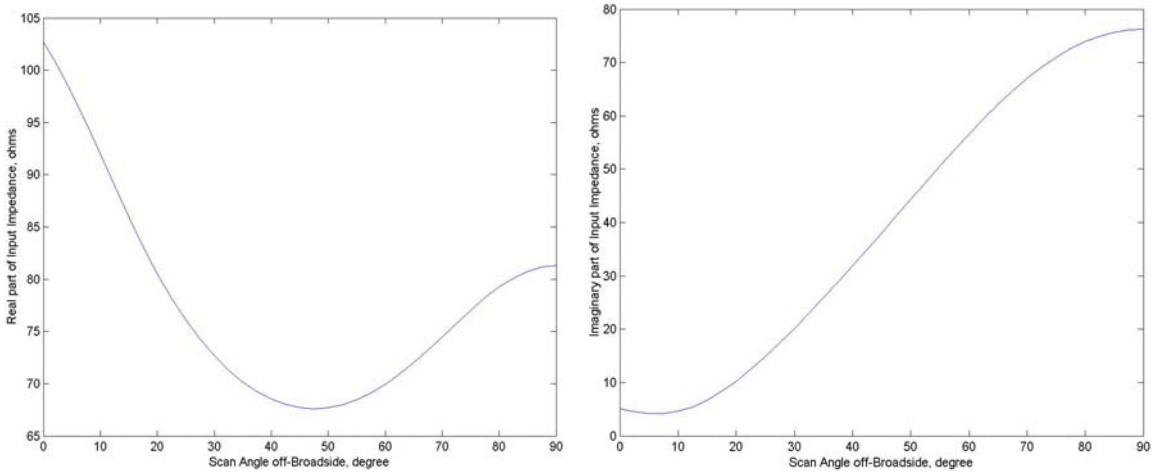
Real part of Input Impedance, ohms
Scan Angle off-Broadside, degree
Imaginary part of Input Impedance, ohms
Scan Angle off-Broadside, degree

(a)

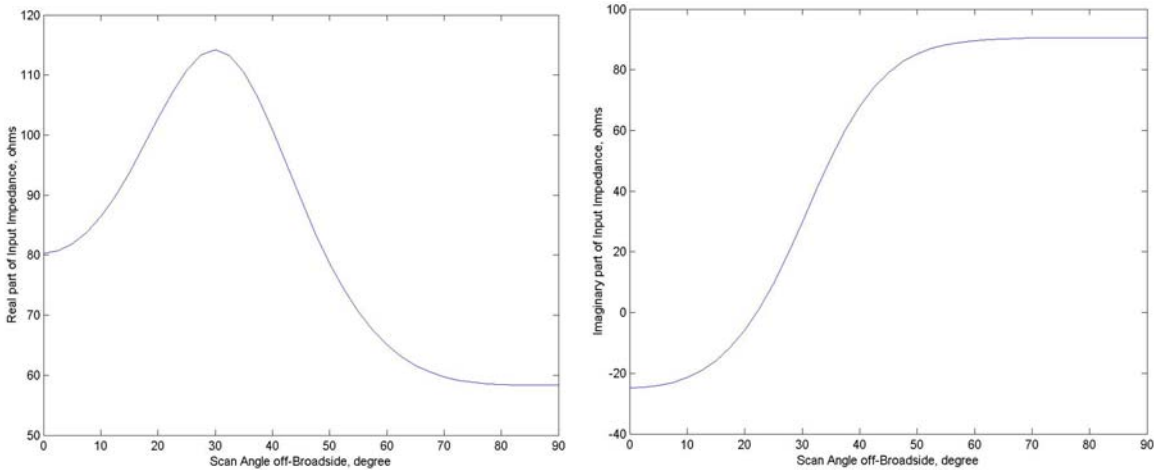
Real part of Input Impedance, ohms
Scan Angle off-Broadside, degree
Imaginary part of Input Impedance, ohms
Scan Angle off-Broadside, degree

(b)

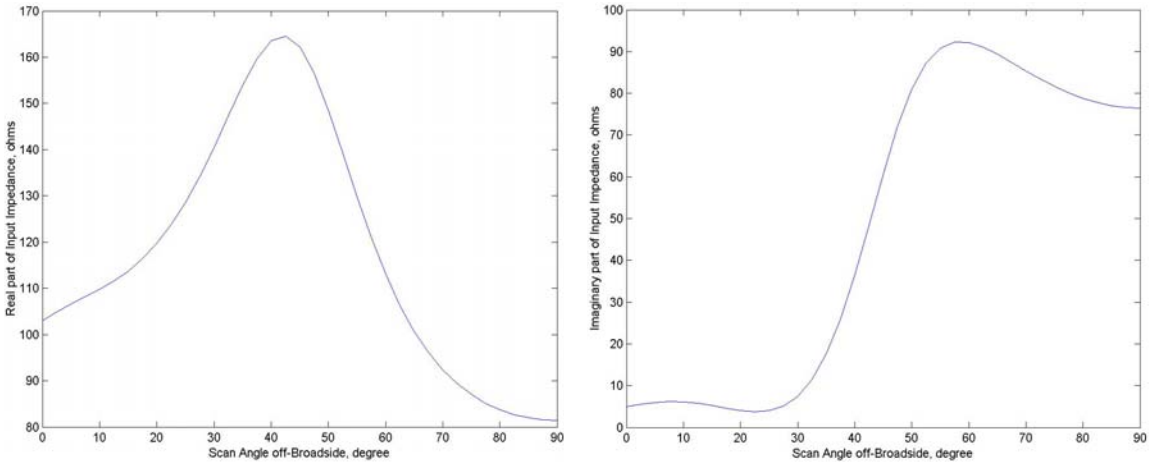
Real part of Input Impedance, ohms
Scan Angle off-Broadside, degree
Imaginary part of Input Impedance, ohms
Scan Angle off-Broadside, degree

(c)

Figure 5.6. Input impedance versus scan angle for an array of three center-fed dipoles spaced $\lambda/2$ apart over a 2λ square plate. Resistance is on the left side and reactance on the right side for (a) dipole 1, (b) dipole 2, and (c) dipole 3.

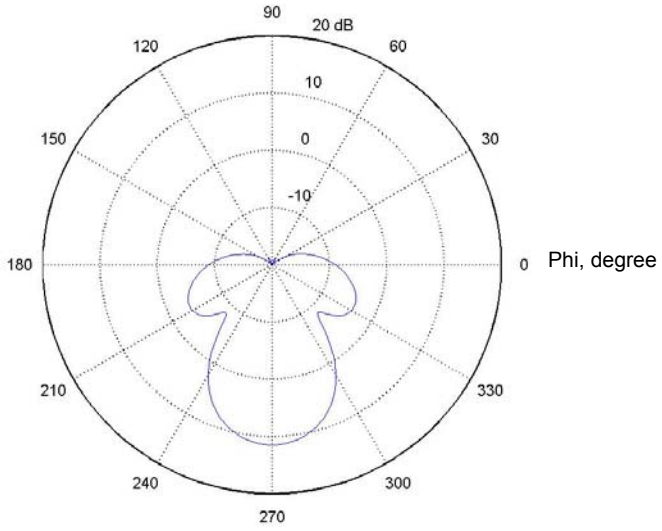

(a)

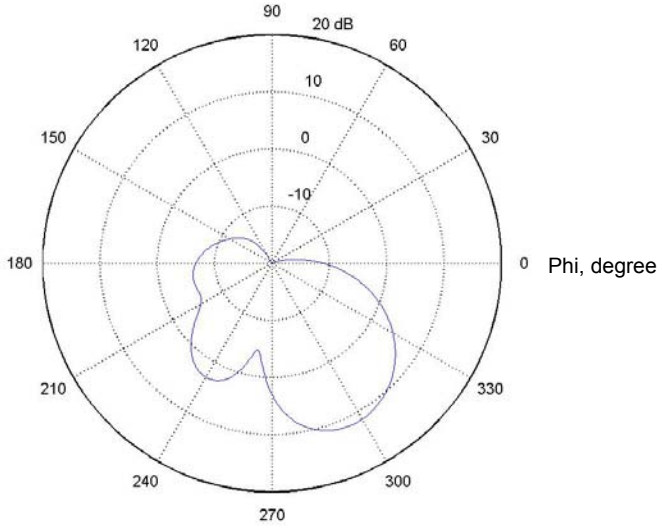

(b)

Figure 5.7. Radiation pattern for an array of three center-fed dipoles spaced $\lambda/2$ apart over a 2λ square plate at (a) broadside scan and (b) 30º off-broadside scan.

D. MUTUAL COUPLING FOR AN ARRAY OF THREE CENTER-FED DIPOLES CONNECTED TO TRANSMISSION LINES OVER A GROUND PLANE

The array of three center-fed dipoles is connected to ideal transmission lines with characteristic impedance Z_o = 75 Ω. Thus, there are six joining equations and six scattering equations, and the procedure in Section C of Chapter III is applied to combine them with MoM. The ground plane is the 2λ square plate (with 1248 triangles) and the dipoles are at a height of $\lambda/4$ over the ground. The input impedances, reflection coefficient, and gain, for both broadside scan and 30º off-broadside scan, are shown in Table 5.2. The input impedances are modified from those obtained in Section C due to additional mutual coupling from reflections introduced by the mismatched feed condition. The gains are also slightly higher than those in Section C. The radiation pattern for broadside scan and 30º off-broadside scan are plotted in Figure 5.8. It is observed that the "nulls" in the pattern are deeper than those in Figure 5.7.

Scan	Parameters	Dipole 1	Dipole 2	Dipole 3	Remarks
Broadside	Input Impedances (Ω)	96.7991 + *j*8.4687	84.7904 – *j*34.4755	97.0134 + *j*8.4075	
	Reflection Coefficient	0.1290 + *j*0.0429	0.1030 – *j*0.1935	0.1301 + *j*0.0425	Symmetrical about the middle dipole
	Gain	14.1407 or 11.5047 dB			
30º off-broadside	Input Impedances (Ω)	67.26 + *j*18.72	102.41 + *j*33.44	141.64 + *j*17.46	
	Reflection Coefficient	-0.0365 + *j*0.1364	0.1835 + *j*0.1539	0.3121 + *j*0.0554	
	Gain	14.6414 or 11.6558 dB			

Table 5.2. Input impedances, return loss, and gain for an array of three center-fed dipoles spaced $\lambda/2$ apart connected to 75-Ω transmission lines over a 2λ square plate.

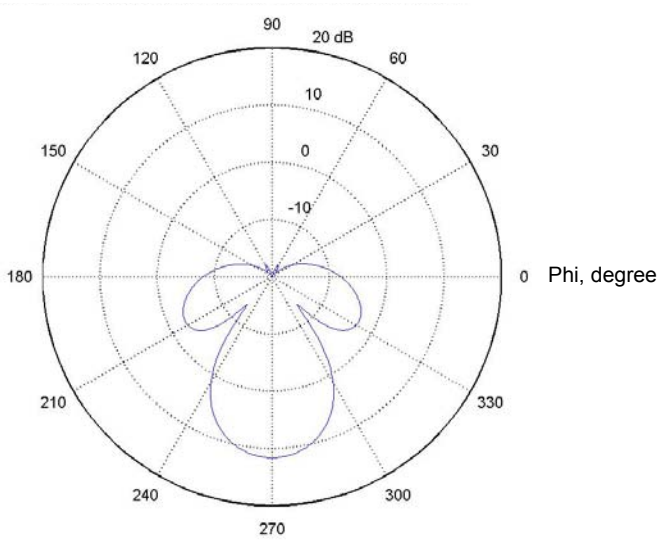

(a)

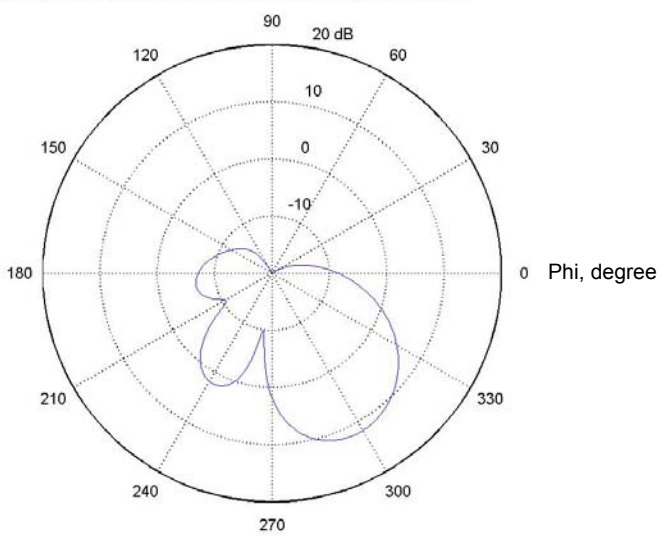

(b)

Figure 5.8. Radiation pattern for an array of three center-fed dipoles spaced $\lambda/2$ connected to 75-Ω transmission lines over a 2λ square plate at (a) broadside scan and (b) 30º off-broadside scan.

E. MUTUAL COUPLING FOR AN ARRAY OF THREE TWO-FEED POINT DIPOLES CONNECTED TO MAGIC-TEES OVER A GROUND PLANE

The array of three two-feed point dipoles is connected to magic-tees with characteristic impedance Z_o = 50 Ω and $A = 1/\sqrt{2}$. There are twelve joining equations and twelve scattering equations, and the procedure in Section C of Chapter III is applied. The ground plane is the 2λ square plate (with 1248 triangles) and the distance to the antennas is $\lambda/4$. The wavelength λ = 4.2236 m is used. In the transmit problem, the operating characteristics of the sum mode will be similar to those observed in Section D. The difference mode is highly inefficient for transmission.

The receive case is investigated here. In the first setup, the plane-wave incidence direction is varied from broadside to end-fire in the *xy*-plane (i.e., $\phi = 90°$ to $180°$ and $\theta = 90°$). The wave polarization is parallel to the dipoles. The outputs of all the three sum ports versus scan angle for this condition are shown in Figure 5.9. The phases for all the sum port outputs are changing smoothly. With zero phase difference, there are no outputs at the difference ports.

In the second setup, the plane-wave incidence direction is varied from $\theta = 90°$ to $0°$ with $\phi = 90°$. The scan angle is set to the incidence direction θ. The outputs of all the three sum ports and all the three difference ports versus scan angle θ for this condition are shown in Figure 5.10 and Figure 5.11, respectively.

It is clear that the sum port output for dipole 1 and dipole 3 are the same. The phases of the sum port outputs are changing smoothly. The phases of all the difference port outputs are also changing smoothly, except when θ is close to 90º and 0º. At $\theta = 90°$, there is no difference in the plane wave path length between all the side arms. At $\theta = 0°$, the magnitudes of all the sum and difference port outputs drop to zero because the plane wave is illuminating the ends of the dipoles. The phases of all the sum and difference port outputs thus change abruptly at θ near zero.

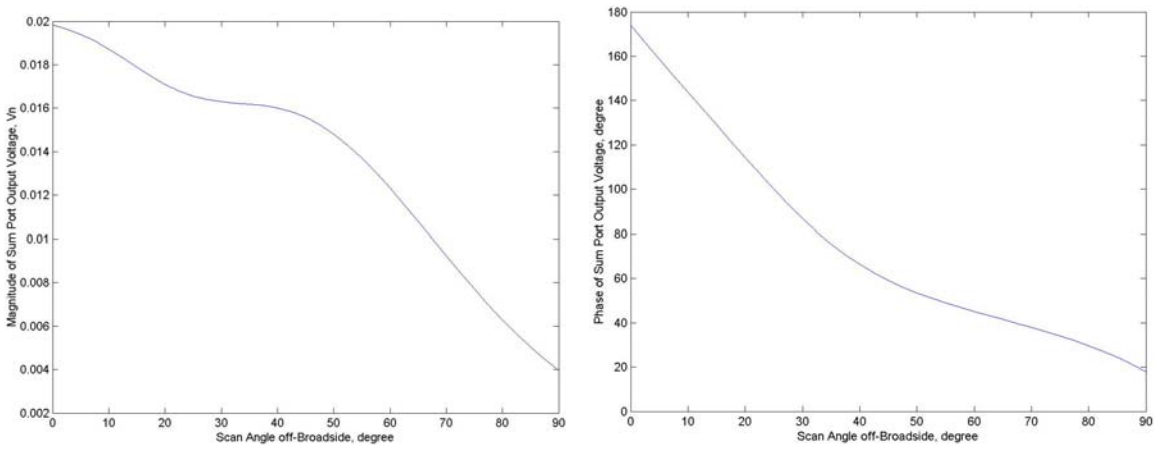
Magnitude of Sum Port Output Voltage, Vh
Scan Angle off-Broadside, degree
Phase of Sum Port Output Voltage, degree
Scan Angle off-Broadside, degree

(a)

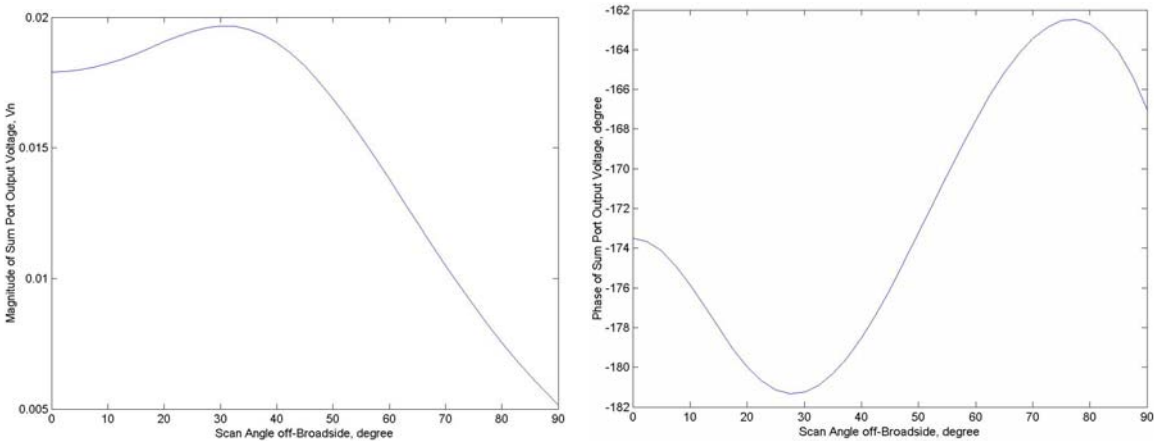
Magnitude of Sum Port Output Voltage, Vh
Scan Angle off-Broadside, degree
Phase of Sum Port Output Voltage, degree
Scan Angle off-Broadside, degree

(b)

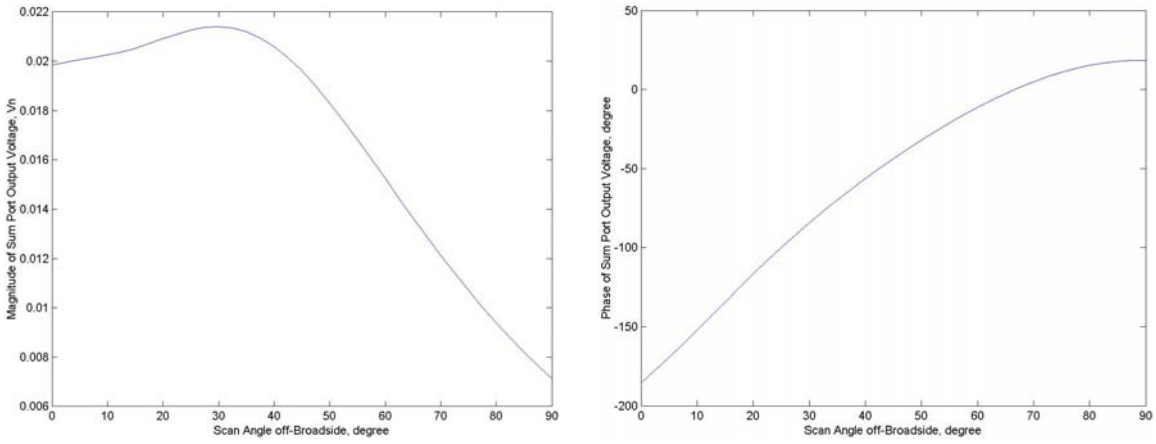
Magnitude of Sum Port Output Voltage, Vh
Scan Angle off-Broadside, degree
Phase of Sum Port Output Voltage, degree
Scan Angle off-Broadside, degree

(c)

Figure 5.9. Sum port outputs for an array of three two-feed point dipoles spaced $\lambda/2$ apart connected to 50-Ω magic-tees over a 2λ square plate. The scan angle (ϕ) is varied from $\phi = 90°$ to $180°$ with $\theta = 90°$. Magnitude of output is on the left side and phase on the right side for (a) dipole 1, (b) dipole 2, and (c) dipole 3.

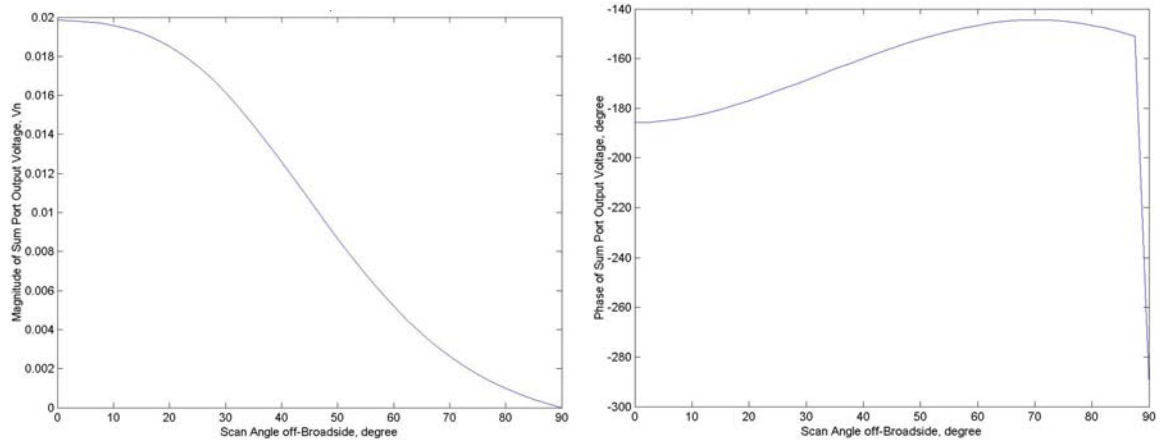
Magnitude of Sum Port Output Voltage, Vn
Scan Angle off-Broadside, degree
Phase of Sum Port Output Voltage, degree
Scan Angle off-Broadside, degree

(a)

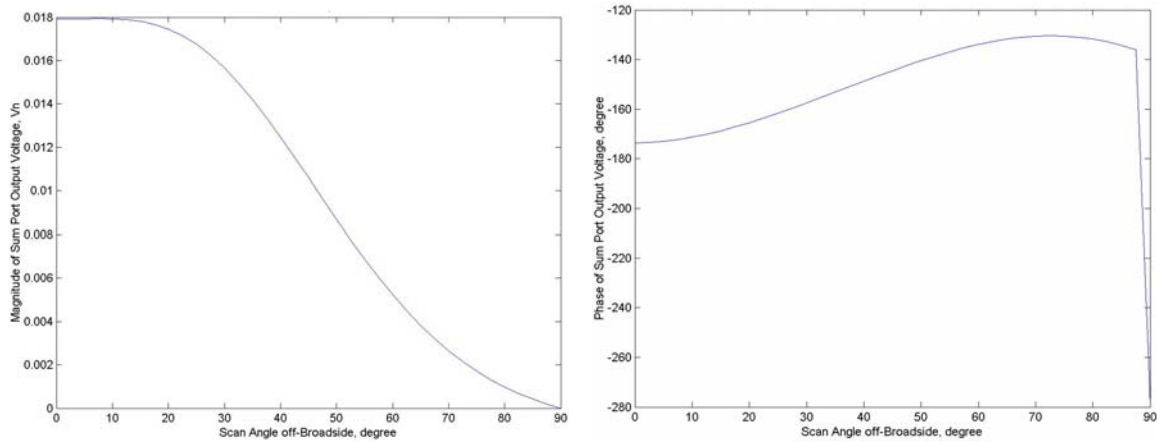
Magnitude of Sum Port Output Voltage, Vn
Scan Angle off-Broadside, degree
Phase of Sum Port Output Voltage, degree
Scan Angle off-Broadside, degree

(b)

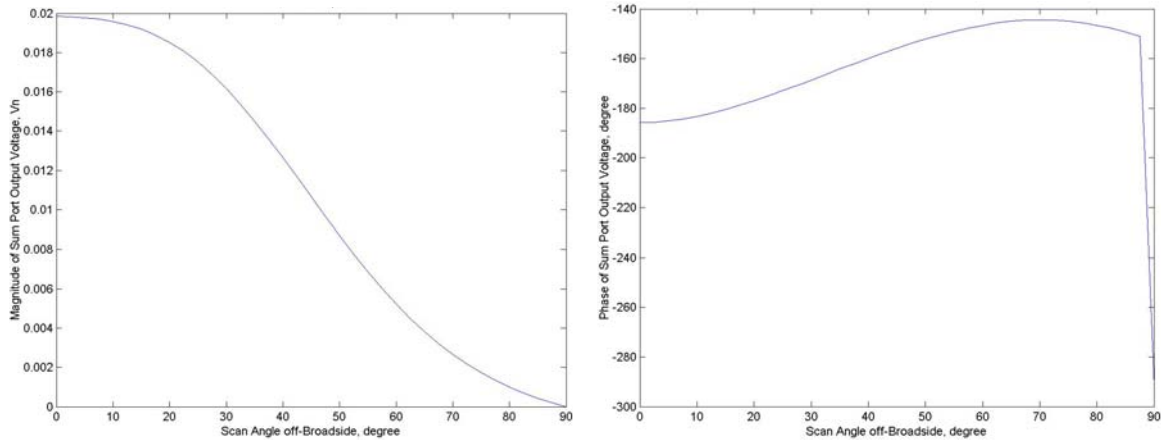
Magnitude of Sum Port Output Voltage, Vn
Scan Angle off-Broadside, degree
Phase of Sum Port Output Voltage, degree
Scan Angle off-Broadside, degree

(c)

Figure 5.10. Sum port outputs for an array of three two-feed point dipoles spaced $\lambda/2$ apart connected to 50-Ω magic-tees over a 2λ square plate. The scan angle (θ) is varied from $\theta = 90°$ to $0°$ with $\phi = 90°$. Magnitude of output is on the left side and phase on the right side for (a) dipole 1, (b) dipole 2, and (c) dipole 3.

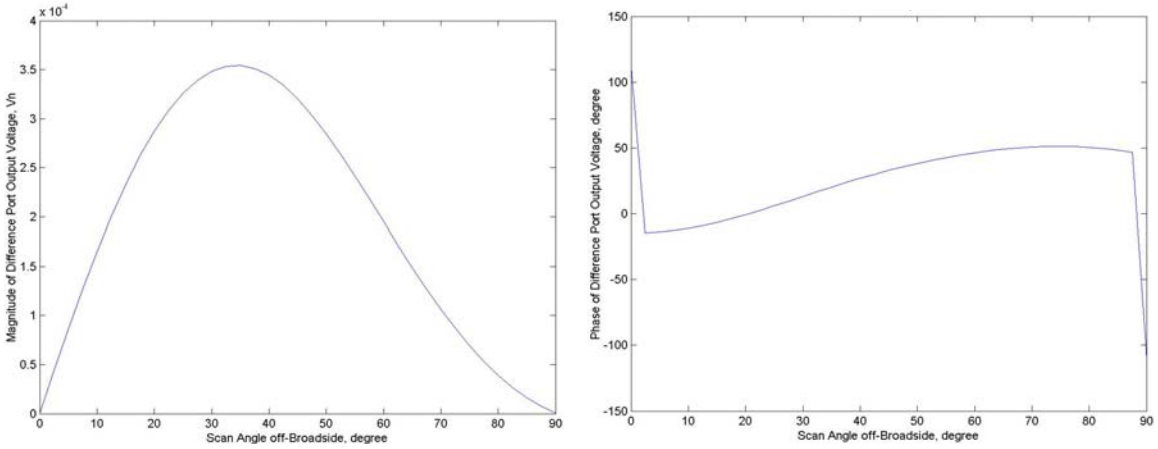
x 10^-4
Magnitude of Difference Port Output Voltage, Vn
Scan Angle off-Broadside, degree
Phase of Difference Port Output Voltage, degree
Scan Angle off-Broadside, degree

(a)

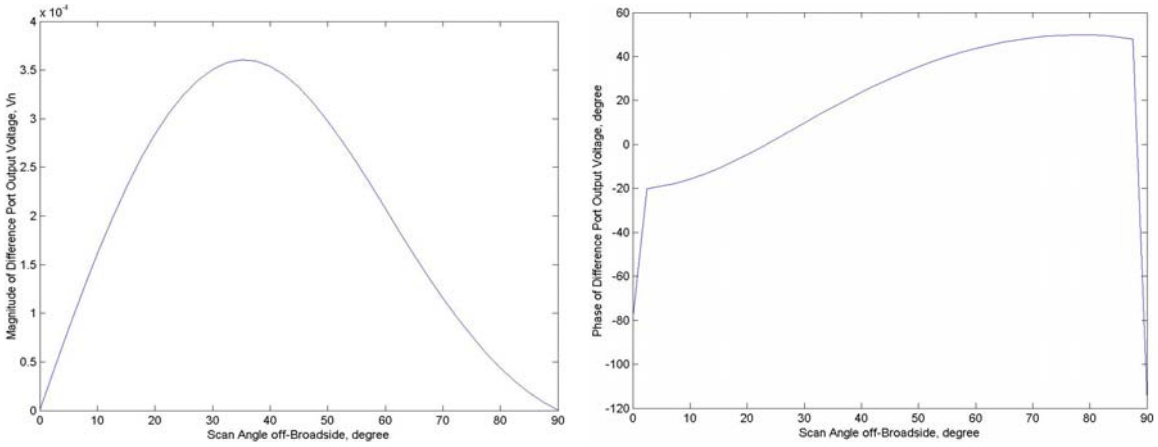
x 10^-4
Magnitude of Difference Port Output Voltage, Vn
Scan Angle off-Broadside, degree
Phase of Difference Port Output Voltage, degree
Scan Angle off-Broadside, degree

(b)

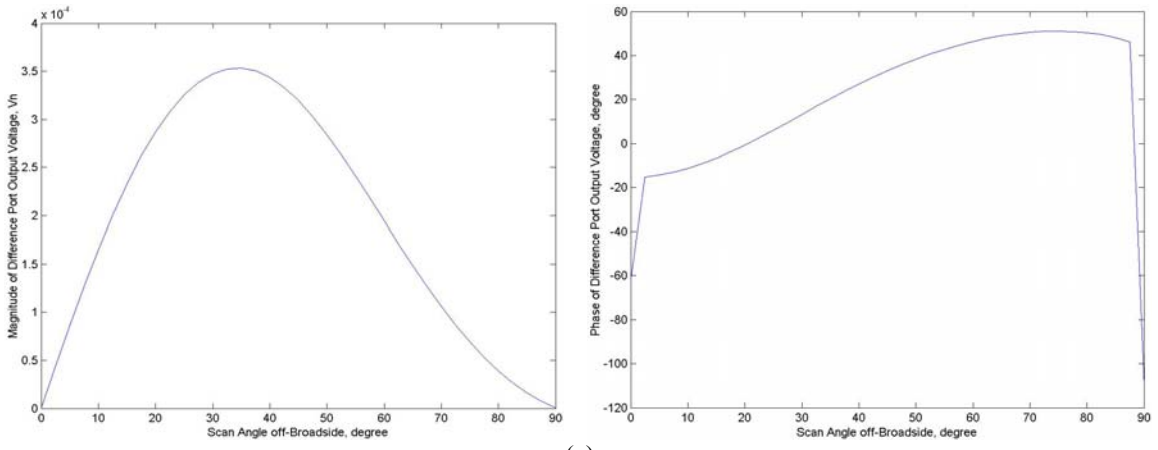
x 10^-4
Magnitude of Difference Port Output Voltage, Vn
Scan Angle off-Broadside, degree
Phase of Difference Port Output Voltage, degree
Scan Angle off-Broadside, degree

(c)

Figure 5.11. Difference port outputs for an array of three two-feed point dipoles spaced $\lambda/2$ apart connected to 50-Ω magic-tees over a 2λ square plate. The scan angle (θ) is varied from $\theta = 90°$ to $0°$ with $\phi = 90°$. Magnitude of output is on the left side and phase on the right side for (a) dipole 1, (b) dipole 2, and (c) dipole 3.

F. CHAPTER SUMMARY

The mutual coupling for an array of three center-fed dipoles was examined. The dipoles were spaced $\lambda/2$ apart along the *x*-axis and aligned parallel to the *z*-axis. In order to scan the main beam, the appropriate phase shift was introduced to the three antenna feeds. As a function of scan angle, the input impedances for an array of three center-fed dipoles were observed to be changing, and different from those of a single dipole, due to the effect of mutual coupling.

The array of three center-fed dipoles was then placed $\lambda/4$ over a 2λ square plate. A convergence test using a broadside scan was performed to determine the discretization requirement for the plate. A discretization of 1248 triangles on the plate ensured that the phase of the input impedances had stabilized. The input impedances were modified due to mutual coupling introduced by the plate. The input impedances were found to vary significantly with scan angle. The radiation into the rear hemisphere behind the plate is largely eliminated due to the presence of the ground plane.

The array of three center-fed dipoles was then connected to 75-Ω transmission lines. The input impedances were further modified due to additional mutual coupling from reflections introduced by the mismatched feed condition. A slight improvement in the radiation pattern was observed, which is probably not real and due to numerical error. If it is real, it is due to the fact that the ground plane is not infinite.

An array of three two-feed point dipoles was connected to 50-Ω magic-tees and placed over the 2λ square plate. The configuration is the same as that for the array of center-fed dipoles. The characteristics for the transmit mode would be similar to those observed for the array of center-fed dipoles. Hence, the receive mode was examined by varying the direction and the polarization of the incidence plane wave. The phases for both the sum port and difference port outputs were observed to change smoothly, except during situations of cross polarization and zero phase difference. The model for an array of three ring-hybrid dipoles has been verified. The conclusions and recommendations for future work are presented in the next chapter.

THIS PAGE INTENTIONALLY LEFT BLANK

VI. CONCLUSIONS AND RECOMMENDATIONS

A. CONCLUSIONS

This thesis project modeled a microstrip ring-hybrid dipole that is capable of simultaneously producing a sum pattern (resonant) and a difference pattern (anti-resonant) using the method of moments (MoM) based on the Rao-Wilton-Glisson (RWG) edge elements. Existing Matlab source codes were modified from [2] to suit the needs of this thesis project. The ring-hybrid dipole is simply a ring-hybrid coupler driving a dipole antenna.

A two-feed point dipole was successfully developed to model the operating characteristics of the ring-hybrid dipole. Two feed points were equally offset by 12 edges from the center of a symmetrical thin-wire strip with 80 segments. The sum pattern and the difference pattern were correctly produced by feeding the excitation voltages in-phase and 180º out-of-phase, respectively.

In the beamforming network modeling, the matrix solution combined the MoM equations on the antenna surfaces and a magic-tee scattering matrix. The joining equations were formed by applying Kirchhoff's voltage and current law at the terminals of the dipole antenna. Once the excitation is specified, the complete system of equations was solved to yield the MoM expansion current coefficients and the signals in the feed network. The feed network interaction with the antenna feed was modeled rigorously.

The effect of mutual coupling for an array of three ring-hybrid dipoles was examined by extending the model. In the receive mode, the direction and the polarization of the incident plane wave were varied. The phases for both the sum port and difference port outputs were observed to be changing smoothly, except during situations of cross polarization and zero phase difference.

A valid antenna model combined with the feed network model has been successfully developed for the ring-hybrid dipole using the method of moments. The effect of mutual coupling in an array of three ring-hybrid dipoles has been studied. The stage is now ready for the design of compensation network to reduce the interferences caused by mutual coupling.

B. RECOMMENDATIONS FOR FUTURE WORK

A potential compensation network concept uses feedback circuits to connect from one dipole to the others. The difference ports can be used as a feedback mechanism to adjust how much mutual coupling the dipoles receive. With this information, the dipoles can adjust their voltage to reduce the phase error due to mutual coupling. This is a type of cancellation; signals are coupled from each element and used to cancel the free space coupling. A possible compensation network is shown in Figure 6.1. This simple network derives a single cancellation signal that is a weighted sum of the difference port outputs. The cancellation signal is then used to adjust the beamforming signal. The network will work over a narrow range of angle due to gross feedback. Better performance can be achieved by incorporating multi-path feedback at the cost of increased complexity.

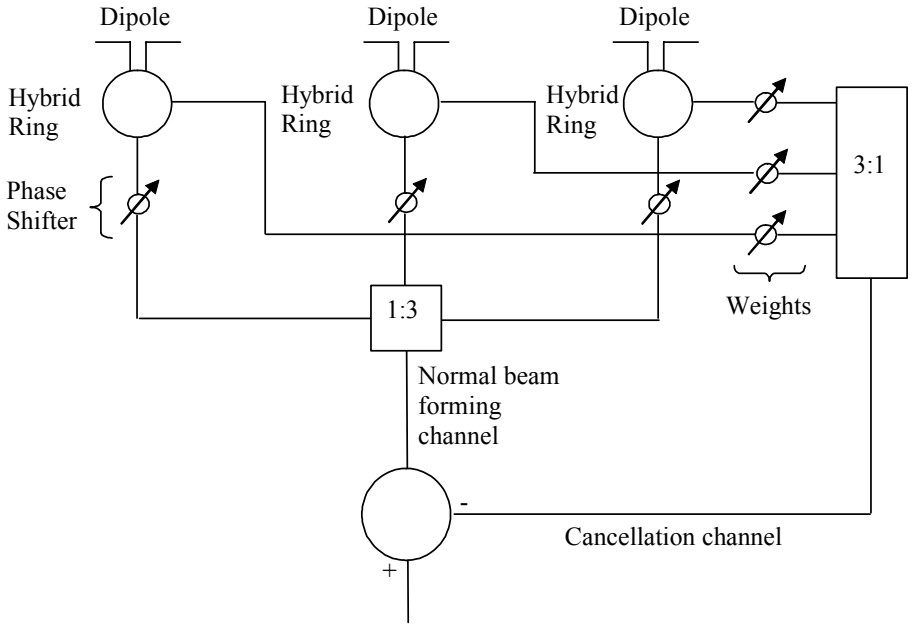

Figure 6.1. An array of three elements with a compensation network (From Ref. [2].).

APPENDIX A: MATLAB SCRIPTS *RWG1.M* TO *RWG5.M* AND *EFIELD1.M* TO *EFIELD3.M*

script *rwg1.m*

```
%RWG1 Geometry calculations - all Chapters
%   Uses the structure mesh file, e.g. platefine.mat,
%   as an input.
%
%   Creates the RWG edge element for every inner edge of
%   the structure. The total number of elements is EdgesTotal.
%   Outputs the following arrays:
%
%   Edge first node number          Edge_(1,1:EdgesTotal)
%   Edge second node number         Edge_(2,1:EdgesTotal)
%   Plus triangle number            TrianglePlus(1:EdgesTotal)
%   Minus triangle number           TriangleMinus(1:EdgesTotal)
%   Edge length                     EdgeLength(1:EdgesTotal)
%   Edge element indicator          EdgeIndicator(1:EdgesTotal)
%
%   Also outputs areas and midpoints of separate triangles:
%   Triangle area                   Area(1:TrianglesTotal)
%   Triangle center                 Center(1:TrianglesTotal)
%
%   This script may handle surfaces with T-junctions
%   including monopoles over various metal surfaces and
%   certain metal meshes
%
%   The modification for Antenna Array passes the array
%   Feed

clear all
tic;

%load('mesh/strip80_sym'); %antenna structure
%load('mesh/strip80syma3g_1248');
load('mesh/twofeed_a3g');
[s1 s2]=size(p);
if(s1==2)
    p(3,:)=0;   %to convert 2D to 3D
end

%Eliminate unnecessary triangles
Remove=find(t(4,:)>1);
t(:,Remove)=[];
TrianglesTotal=length(t);
```

```
%Find areas of separate triangles

for m=1:TrianglesTotal
   N=t(1:3,m);
   Vec1=p(:,N(1))-p(:,N(2));
   Vec2=p(:,N(3))-p(:,N(2));
   Area(m) =norm(cross(Vec1,Vec2))/2;
   Center(:,m)=1/3*sum(p(:,N),2);
end

%Find all edge elements "Edge_" with at least two
%adjacent triangles
Edge_=[];
n=0;
for m=1:TrianglesTotal
    N=t(1:3,m);
    for k=m+1:TrianglesTotal
        M=t(1:3,k);
        a=1-all([N-M(1) N-M(2) N-M(3)]);
        if(sum(a)==2) %triangles m and k have common edge
            n=n+1;
            Edge_=[Edge_ M(find(a))];
            TrianglePlus(n)=m;
            TriangleMinus(n)=k;
        end;
    end
end
EdgesTotal=length(Edge_);

%This block is only meaningful for T junctions
%It leaves only two edge elements at a junction
Edge__=[Edge_(2,:); Edge_(1,:)];
Remove=[];
for m=1:EdgesTotal
    Edge_m=repmat(Edge_(:,m),[1 EdgesTotal]);
    Ind1=any(Edge_  -Edge_m);
    Ind2=any(Edge__ -Edge_m);
    A=find(Ind1.*Ind2==0);
    if(length(A)==3)    %three elements formally exist at a junction
        Out=find(t(4,TrianglePlus(A))==t(4,TriangleMinus(A)));
        Remove=[Remove A(Out)];
    end
end
Edge_(:,Remove)         =[];
TrianglePlus(Remove)    =[];
TriangleMinus(Remove)   =[];
EdgesTotal=length(Edge_)
EdgeIndicator=t(4,TrianglePlus)+t(4,TriangleMinus);

%Find edge length
for m=1:EdgesTotal
   EdgeLength(m)=norm(p(:,Edge_(1,m))-p(:,Edge_(2,m)));
end
toc
```

```
%Save result
save mesh1  p ...
            t ...
            Edge_ ...
            TrianglesTotal ...
            EdgesTotal ...
            TrianglePlus ...
            TriangleMinus ...
            EdgeLength ...
            EdgeIndicator ...
            Area ...
            Center ...
            %Feed %used only for array of antennas
```

script *rwg2.m*

```
%RWG2 Geometry calculations - all Chapters
%   Uses the mesh file from RWG1, mesh1.mat,
%   as an input.
%
%   Creates the following parameters of the RWG edge elements:
%
%   Position vector rho_c_plus from the free vertex of
%   the "plus" triangle to its center
%                                   RHO_Plus(1:3,1:EdgesTotal)
%   Position vector rho_c_minus from the center of the "minus"
%   triangle to its free vertex
%                                   RHO_Minus(1:3,1:EdgesTotal)
%
%   In addition to these parameters creates the following
%   arrays for nine subtriangles (barycentric subdivision):
%
%   Midpoints of nine subtriangles
%                                   Center_(1:3,1:9,1:TrianglesTotal)
%   Position vectors rho_c_plus from the free vertex of
%   the "plus" triangle to nine subtriangle midpoints
%                                   RHO__Plus(1:3,1:9,1:EdgesTotal)
%   Position vectors rho_c_minus from nine subtriangle midpoints
%   to the free vertex of the "minus" triangle
%                                   RHO__Minus(1:3,1:9,1:EdgesTotal)
%
%   See Rao, Wilton, Glisson, IEEE Trans. Antennas and Propagation,
%   vol. AP-30, No 3, pp. 409-418, 1982.
%
%   The modification for Array Antenna passes the array
%   Feed

clear all

%load the data
load('mesh1')
```

```
%Find nine sub-triangle midpoints
IMT=[];
for m=1:TrianglesTotal
    n1=t(1,m);
    n2=t(2,m);
    n3=t(3,m);
    M=Center(:,m);
    r1=    p(:,n1);
    r2=    p(:,n2);
    r3=    p(:,n3);
    r12=r2-r1;
    r23=r3-r2;
    r13=r3-r1;
    C1=r1+(1/3)*r12;
    C2=r1+(2/3)*r12;
    C3=r2+(1/3)*r23;
    C4=r2+(2/3)*r23;
    C5=r1+(1/3)*r13;
    C6=r1+(2/3)*r13;
    a1=1/3*(C1+C5+r1);
    a2=1/3*(C1+C2+M);
    a3=1/3*(C2+C3+r2);
    a4=1/3*(C2+C3+M);
    a5=1/3*(C3+C4+M);
    a6=1/3*(C1+C5+M);
    a7=1/3*(C5+C6+M);
    a8=1/3*(C4+C6+M);
    a9=1/3*(C4+C6+r3);
    Center_(:,:,m)=...
        [a1 a2 a3 a4 a5 a6 a7 a8 a9];
end
%PLUS
for m=1:EdgesTotal
    NoPlus=TrianglePlus(m);
    n1=t(1,NoPlus);
    n2=t(2,NoPlus);
    n3=t(3,NoPlus);
    if((n1~=Edge_(1,m))&(n1~=Edge_(2,m))) NODE=n1; end;
    if((n2~=Edge_(1,m))&(n2~=Edge_(2,m))) NODE=n2; end;
    if((n3~=Edge_(1,m))&(n3~=Edge_(2,m))) NODE=n3; end;
    FreeVertex=p(:,NODE);

    RHO_Plus(:,m)   =+Center(:,NoPlus)-FreeVertex;
    %Nine rho's of the "plus" triangle
    RHO__Plus(:,:,m)  =...
        +Center_(:,:,NoPlus)-repmat(FreeVertex,[1 9]);
end
%MINUS
for m=1:EdgesTotal
    NoMinus=TriangleMinus(m);
    n1=t(1,NoMinus);
    n2=t(2,NoMinus);
    n3=t(3,NoMinus);
    if((n1~=Edge_(1,m))&(n1~=Edge_(2,m))) NODE=n1; end;
    if((n2~=Edge_(1,m))&(n2~=Edge_(2,m))) NODE=n2; end;
    if((n3~=Edge_(1,m))&(n3~=Edge_(2,m))) NODE=n3; end;
    FreeVertex=p(:,NODE);
```

```
    RHO_Minus(:,m)   =-Center(:,NoMinus) +FreeVertex;
    %Nine rho's of the "minus" triangle
    RHO__Minus(:,:,m)=...
        -Center_(:,:,NoMinus)+repmat(FreeVertex,[1 9]);
end

%Save result
save mesh2  p ...
            t ...
            TrianglesTotal ...
            EdgesTotal ...
            Edge_ ...
            TrianglePlus ...
            TriangleMinus ...
            EdgeLength ...
            EdgeIndicator ...
            Area ...
            RHO_Plus ...
            RHO_Minus ...
            RHO__Plus ...
            RHO__Minus ...
            Center ...
            Center_ ...
            %Feed %used only for array of antennas
```

script *rwg3.m*

```
%RWG3 Calculates the impedance matrix using function IMPMET
%   Uses the mesh file from RWG2, mesh2.mat, as an input.
%
%   The following parameters need to be specified prior to
%   calculations:
%
%   Frequency (Hz)                  f
%   Dielectric constant (SI)        epsilon_
%   Magnetic permeability (SI)      mu_

clear all
%Load the data
load('mesh2');

%EM parameters (f=3e8 means that f=300 MHz)
%f=70.98038e6%resonant freq offset 12 for strip80_sym
f=71.18541e6%resonant freq center fed for strip80_sym

epsilon_    =8.854187817e-012;
mu_         =1.256637061e-006;

%Speed of light
c_=1/sqrt(epsilon_*mu_)
c_/f
%Free-space impedance
eta_=sqrt(mu_/epsilon_);
```

```
%Contemporary variables - introduced to speed up
%the impedance matrix calculation
omega       =2*pi*f;
k           =omega/c_;
K           =j*k;
Constant1   =mu_/(4*pi);
Constant2   =1/(j*4*pi*omega*epsilon_);
Factor      =1/9;

FactorA     =Factor*(j*omega*EdgeLength/4)*Constant1;
FactorFi    =Factor*EdgeLength*Constant2;

for m=1:EdgesTotal
    RHO_P(:,:,m)=repmat(RHO_Plus(:,m),[1 9]);   %[3 9 EdgesTotal]
    RHO_M(:,:,m)=repmat(RHO_Minus(:,m),[1 9]);  %[3 9 EdgesTotal]
end
FactorA=FactorA.';
FactorFi=FactorFi.';

%Impedance matrix Z
tic; %start timer

Z=  impmet( EdgesTotal,TrianglesTotal,...
            EdgeLength,K,...
            Center,Center_,...
            TrianglePlus,TriangleMinus,...
            RHO_P,RHO_M,...
            RHO__Plus,RHO__Minus,...
            FactorA,FactorFi);

toc %elapsed time

%Save result
FileName='impedance.mat';
save(FileName, 'f','omega','mu_','epsilon_','c_', 'eta_','Z');
```

script *rwg4.m*

```
%RWG4 Solves MoM equations for the antenna radiation problem
%   Uses the mesh file from RWG2, mesh2.mat, and
%   the impedance file from RWG3, impedance.mat,
%   as inputs.
%
%   Also calculates the "voltage" vector V (the right-
%   hand side of moment equations)
%                                           V(1:EdgesTotal)
%
%   The following parameters need to be specified:
%
%   The feed point position                 FeedPoint(1:3);
%   Number of feeding edges (one for the dipole;
%   two for the monopole)                   INDEX(1:2);

%load the data
load('mesh2');
```

```
load('impedance');

rx=0;%assign 1 for rx otherwise tx

nfeed=2;%assign 2 for two feedpoints (freq change for resonant),
otherwise 1 feedpoint.

sum_diff=-1;%assign 1 for sum and -1 for diff

offset=12;%offset edge for two feedpoints

ztl=72.0887;%assign Rrad to match TL to antenna

%Find the feeding edge(s)(closest to the origin)
FeedPoint=[0; 0; 0];
Index=[];

for m=1:EdgesTotal
    V(m)=0;
    Distance(m)=norm(0.5*sum(p(:,Edge_(:,m)),2)-FeedPoint);
end

 [Y,INDEX]=sort(Distance);
Index=[Index INDEX(1)];

%Define the voltage vector

if (nfeed==2)
    V(Index-offset)=0.5*EdgeLength(Index-offset);
    V(Index+offset)=sum_diff*0.5*EdgeLength(Index+offset);

else
    V(Index)=1.0*EdgeLength(Index);
end

%Dipole - normal incidence
d      =[0 0 -1];
Pol    =[0 1 0];%parallel

k=omega/c_;
kv=k*d;

for m=1:EdgesTotal
   ScalarProduct=sum(kv.*Center(:,TrianglePlus(m))');
   EmPlus =Pol.'*exp(-j*ScalarProduct);
   ScalarProduct=sum(kv.*Center(:,TriangleMinus(m))');
   EmMinus=Pol.'*exp(-j*ScalarProduct);
   ScalarPlus =sum(EmPlus.* RHO_Plus(:,m));
   ScalarMinus=sum(EmMinus.*RHO_Minus(:,m));
   Vr(m)=EdgeLength(m)*(ScalarPlus/2+ScalarMinus/2);%*1.063948;
end

%Solve system of MoM equations
tic;

VV=0;%transmit case
source=1*EdgeLength(Index);
```

```
if (rx==1)
    V=Vr;
    VV=Vr;%receive case with network
    source=0;%turn off Vin for receive case
end

D=[0 1;1 0];%two port device connected to dipole

VV(EdgesTotal+1)=0;
VV(EdgesTotal+2)=-source*D(1,2);
VV(EdgesTotal+3)=-source*D(2,2);

ZZ(1:EdgesTotal+3,1:EdgesTotal+3)=0;
ZZ(1:EdgesTotal,1:EdgesTotal)=Z(1:EdgesTotal,1:EdgesTotal);

ZZ(Index,EdgesTotal+1)=-1;
ZZ(Index,EdgesTotal+2)=-1;
Zo=EdgeLength(Index)^2*ztl;%TL impedance
ZZ(EdgesTotal+1,Index)=+1;
ZZ(EdgesTotal+1,EdgesTotal+1)=+1/Zo;%
ZZ(EdgesTotal+1,EdgesTotal+2)=-1/Zo;%

ZZ(EdgesTotal+2,EdgesTotal+1)=D(1,1);
ZZ(EdgesTotal+2,EdgesTotal+2)=-1;

ZZ(EdgesTotal+3,EdgesTotal+1)=D(2,1);
ZZ(EdgesTotal+3,EdgesTotal+3)=-1;

%Z(Index,Index)=Z(Index,Index)+ EdgeLength(Index)^2*72.0887;

I=Z\V.'; %transmit

II=ZZ\VV.'; %TL feeding Dipole

toc %elapsed time

%Find the antenna input impedance
if (rx==1)

pwr_rec_matched=.5*(II(EdgesTotal+1)*II(EdgesTotal+1)')/EdgeLength(Inde
x)^2/ztl*1000
else
    if(nfeed==1)
    GapCurrent  =I(Index)*EdgeLength(Index)
    GapVoltage  =V(Index)/EdgeLength(Index)
    Impedance   =GapVoltage/GapCurrent
    FeedPower   =1/2*real(GapCurrent*conj(GapVoltage))*1000

    PortCurrent  =II(Index)*EdgeLength(Index)
    PortVoltage  =(II(EdgesTotal+1)+II(EdgesTotal+2))/EdgeLength(Index)
    Impedance   =PortVoltage/PortCurrent
    TxPower   =1/2*real(PortCurrent*conj(PortVoltage))*1000
    RC=II(EdgesTotal+1)/II(EdgesTotal+2)
    RL=-10*log10(abs(RC)^2)
    else
    GapCurrent  =I(Index-offset)*EdgeLength(Index-offset)
    GapVoltage  =V(Index-offset)/EdgeLength(Index-offset)
```

```
    Impedance   =GapVoltage/GapCurrent
    FeedPower   =1/2*real(GapCurrent*conj(GapVoltage))*1000

    GapCurrent  =I(Index+offset)*EdgeLength(Index+offset)
    GapVoltage  =V(Index+offset)/EdgeLength(Index+offset)
    Impedance   =GapVoltage/GapCurrent
    FeedPower   =1/2*real(GapCurrent*conj(GapVoltage))*1000

end
end

if (rx==1)
   I(1:EdgesTotal)=II(1:EdgesTotal);
end

if (rx==1)

FileName='current.mat';
save(FileName, 'f','omega','mu_','epsilon_','c_',
'eta_','I','V','d','Pol');

else

FileName='current.mat';
save(FileName, 'f','omega','mu_','epsilon_','c_', 'eta_',...
    'I','V','GapCurrent','GapVoltage','Impedance','FeedPower');

end
```

script *rwg5.m*

```
%RWG5 or RWG6 Plots the surface current distribution along the dipole
%   Increase the number of sampling points, K, to obtain more
%   accurate results

clear all

%Load the data
load('mesh2');
load('current');

Index=find(t(4,:)<=1);
Triangles=length(Index);

%Find the current density Jx for every triangle
for k=1:Triangles
    i=[0 0 0]';
    for m=1:EdgesTotal
        IE=I(m)*EdgeLength(m);
        if(TrianglePlus(m)==k)
            i=i+IE*RHO_Plus(:,m)/(2*Area(TrianglePlus(m)));
        end
        if(TriangleMinus(m)==k)
            i=i+IE*RHO_Minus(:,m)/(2*Area(TriangleMinus(m)));
        end
```

```
    end
    CurrentNorm(1:2,k)=abs(i(1:2)); %magnitude
    %CurrentNorm(1:2,k)=angle(i(1:2))/pi*180; %phase
end

K=20;
x0=min(p(1,:));
x1=max(p(1,:));
y0=min(p(2,:));
y1=max(p(2,:));

for n=1:K+1
    y(n)=y0+(n-1)*(y1-y0)/K;
    Dist=repmat([0 y(n) 0]',[1,TrianglesTotal])-Center;
    [dummy,Index]=min( sum(Dist.*Dist));
    X(n)=CurrentNorm(1,Index);
    Y(n)=CurrentNorm(2,Index);
end
yi=[y0:(y1-y0)/100:y1];
Xi = interp1(y,X,yi,'cubic');
Yi = interp1(y,Y,yi,'cubic');
%plot(yi,Xi,'*',yi,Yi,'.');
plot(yi,Yi,'.');
xlabel('Dipole length, m')
ylabel('Surface current density, A/m')
grid on
```

function *impmet.m*

```
function [Z]=       impmet( EdgesTotal,TrianglesTotal,...
                            EdgeLength,K,...
                            Center,Center_,...
                            TrianglePlus,TriangleMinus,...
                            RHO_P,RHO_M,...
                            RHO__Plus,RHO__Minus,...
                            FactorA,FactorFi);
%IMPMET Standard impedance matrix (metal surface)
%
%     Returns the complex impedance matrix [EdgesTotal x EdgesTotal]
%     Uses 9 integration points for every triangle
%   (barycentric subdivision)
%
%   The impedance matrix is calculated as a sum of the contributions
%   due to separate triangles (similar to the "face-pair" method).
%   See Appendix B for a detailed algorithm.
%
%   A 9-point quadrature is used for all integrals, including
%   the self-coupling terms. The alternative source code with
%   the analytical approximation of the self-coupling terms
%   is given in Appendix B. The difference between two methods
%   is not significant.

%Memory allocation
Z   =zeros  (EdgesTotal,EdgesTotal)+j*zeros(EdgesTotal,EdgesTotal);
```

```
%Loop over integration triangles
for p=1:TrianglesTotal

    Plus     =find(TrianglePlus-p==0);
    Minus    =find(TriangleMinus-p==0);

    D=Center_-repmat(Center(:,p),[1 9 TrianglesTotal]);
    %[3 9 TrianglesTotal]

    R=sqrt(sum(D.*D));                        %[1 9 TrianglesTotal]
    g=exp(-K*R)./R;                           %[1 9 TrianglesTotal]

    gP=g(:,:,TrianglePlus);                          %[1 9 EdgesTotal]
    gM=g(:,:,TriangleMinus);                         %[1 9 EdgesTotal]

    Fi=sum(gP)-sum(gM);                              %[1 1 EdgesTotal]
    ZF= FactorFi.*reshape(Fi,EdgesTotal,1);          %[EdgesTotal 1]

    for k=1:length(Plus)
        n=Plus(k);
        RP=repmat(RHO__Plus(:,:,n),[1 1 EdgesTotal]);%[3 9 EdgesTotal]
        A=sum(gP.*sum(RP.*RHO_P))+sum(gM.*sum(RP.*RHO_M));
        Z1= FactorA.*reshape(A,EdgesTotal,1);
        Z(:,n)=Z(:,n)+EdgeLength(n)*(Z1+ZF);
    end
    for k=1:length(Minus)
        n=Minus(k);
        RP=repmat(RHO__Minus(:,:,n),[1 1 EdgesTotal]);%[3 9 EdgesTotal]
        A=sum(gP.*sum(RP.*RHO_P))+sum(gM.*sum(RP.*RHO_M));
        Z1= FactorA.*reshape(A,EdgesTotal,1);
        Z(:,n)=Z(:,n)+EdgeLength(n)*(Z1-ZF);
    end
end
```

script *efield1*

```
%EFIELD1 Radiated/scattered field at a point
%   The point is outside the metal surface
%   Uses the mesh file from RWG2, mesh2.mat, and
%   the file containing surface current coefficients,
%   current.mat, from RWG4 as inputs.
%
%   The following parameters need to be specified:
%
%   Observation point           ObservationPoint[X; Y; Z] (m)

clear all
%Load the data
load('mesh2');
load('current');

k=omega/c_;
K=j*k;


for m=1:EdgesTotal
    Point1=Center(:,TrianglePlus(m));
    Point2=Center(:,TriangleMinus(m));
    DipoleCenter(:,m)=0.5*(Point1+Point2);
    DipoleMoment(:,m)=EdgeLength(m)*I(m)*(-Point1+Point2);
end

ObservationPoint=[0; 0; 100];
[E,H]=point(ObservationPoint,eta_,K,DipoleMoment,DipoleCenter);

%find the sum of all dipole contributions
EField=sum(E,2); HField=sum(H,2);

%Common
EField                  %Radiated/scattered electric field
                        %(complex vector at a point, V/m)

HField                  %Radiated/scattered magnetic field
                        %(complex vector at a point, A/m)

Poynting=0.5*real(cross(EField,conj(HField)))
                        %Poynting vector (W/m^2) for radiated/scattered
field

W=norm(Poynting)        %Radiation density (W/m^2) for
radiated/scattered field

U=norm(ObservationPoint)^2*W
                        %Radiation intensity (W/unit solid angle)

%Only scattering
RCS=4*pi*(norm(ObservationPoint))^2*sum(EField.*conj(EField));
                        %Backscattering radar cross-section (scattering)
```

script *efield2*

```
%EFIELD2 Radiated/scattered field over a large sphere
%   Uses the mesh file from RWG2, mesh2.mat, and
%   the file containing surface current coefficients,
%   current.mat, from RWG4 as inputs.
%
%   Uses the structure sphere.mat/sphere1.mat to display
%   radiation intensity distribution over the sphere surface.
%   The sphere doesn't intersect the radiating object.
%
%   The following parameters need to be specified:
%
%   Sphere radius (m)

clear all
%Load the data
load('mesh2');
load('current');
load('sphere');

p=100*p;    %sphere radius is 100 m

k=omega/c_;
K=j*k;

for m=1:EdgesTotal
    Point1=Center(:,TrianglePlus(m));
    Point2=Center(:,TriangleMinus(m));
    DipoleCenter(:,m)=0.5*(Point1+Point2);
    DipoleMoment(:,m)=EdgeLength(m)*I(m)*(-Point1+Point2);
end

TotalPower=0;
%Sphere series
M=length(t);
for m=1:M
    N=t(1:3,m);
    ObservationPoint=1/3*sum(p(:,N),2);
    [E,H]=point(ObservationPoint,eta_,K,DipoleMoment,DipoleCenter);
    ET=sum(E,2); HT=sum(H,2);
    Poynting(:,m)=0.5*real(cross(ET,conj(HT)));
    U(m)=(norm(ObservationPoint))^2*norm(Poynting(:,m));
    Vector1=p(:,N(1))-p(:,N(2));
    Vector2=p(:,N(3))-p(:,N(2));
    Area =0.5*norm(cross(Vector1,Vector2));
    TotalPower=TotalPower+norm(Poynting(:,m))*Area;
    %-----------------------------
    X(1:3,m)=[p(1,N)]';
    Y(1:3,m)=[p(2,N)]';
    Z(1:3,m)=[p(3,N)]';
end

TotalPower*1000

GainLogarithmic     =10*log10(4*pi*max(U)/TotalPower)
```

```
GainLinear          =4*pi*max(U)/TotalPower
%RadiationResistance =2*TotalPower/abs(GapCurrent)^2

FileName='gainpower.mat';
save(FileName, 'TotalPower','GainLogarithmic','GainLinear');

U=U/norm(U);
C=repmat(U,3,1);
h=fill3(X,Y,Z,C);
colormap gray;
axis('equal')
rotate3d on
```

script *efield3*

```
%EFIELD3 2D Radiation patterns
%   Uses the mesh file from RWG2, mesh2.mat, and
%   the file containing surface current coefficients,
%   current.mat, from RWG4 as inputs.
%
%   Additionally uses the value of TotalPower saved
%   in file gainpower.mat (script efield2.m)
%
%   The following parameters need to be specified:
%
%   Radius of the circle (m)            R
%   Plane of the circle:                [x y 0] or
%                                       [x 0 z] or
%                                       [0 y z]
%   Number of discretization points per
%   pattern                             NumPoints

clear all
%Load the data
load('mesh2');
load('current');
load('gainpower');

k=omega/c_;
K=j*k;

for m=1:EdgesTotal
    Point1=Center(:,TrianglePlus(m));
    Point2=Center(:,TriangleMinus(m));
    DipoleCenter(:,m)=0.5*(Point1+Point2);
    DipoleMoment(:,m)=EdgeLength(m)*I(m)*(-Point1+Point2);
end

NumPoints=200;
R=1000; %pattern in m
for ii=1:NumPoints+1
   phi(ii)=(ii-1)*pi/(NumPoints/2);
   y=R*cos(phi(ii));z=R*sin(phi(ii));
   %x=R*cos(phi(ii));z=R*sin(phi(ii));%new
   ObservationPoint=[0 y z]';
```

```
   %ObservationPoint=[x 0 z]';%new
   [E,H]=point(ObservationPoint,eta_,K,DipoleMoment,DipoleCenter);
   ET=sum(E,2); HT=sum(H,2);
   Poynting=0.5*real(cross(ET,conj(HT)));
   W(ii)=norm(Poynting);
   U(ii)=(norm(ObservationPoint))^2*W(ii);
end
Polar_=10*log10(4*pi*U/TotalPower);

GainLogarithmic=max(Polar_) %gain for the particular pattern!

%This is the standard Matlab polar plot
OFFSET=40; polar(phi,max(Polar_+OFFSET,0)); grid on;
Title=strcat('Offset= ', num2str(OFFSET), ' dB');
title(Title);

%This is Balanis' relative power:
%Polar=10*log10(U/max(U)); OFFSET=40; polar(phi,Polar+OFFSET); grid on;

%This is Galenski's polar plot:
%Use with care: outputs an error if Polar is a constant function
%polarhg(phi',Polar','rlim',[min(Polar) 10],'rtick',[-30 -20 -10 0
10],'tstep',90,'color','b');
```

function *point.m*

```
function[EField, HField]=...
    point1(Point,eta_,K,DipoleMoment,DipoleCenter)

%POINT Radiated/scattered field at a point of a dipole array
%   or a single dipole. Gives exact near- and far-fields. Outputs
%   individual contribution of each dipole.
%
%   Observation point                   Point(1:3)
%   Array of dipole moments             DipoleMoment(1:3,1:EdgesTotal)
%   Array of dipole centers             DipoleCenter(1:3,1:EdgesTotal)
%   E-field at the observation point    E(1;3,1:EdgesTotal)
%   H-field at the observation point    H(1;3,1:EdgesTotal)

C=4*pi;
ConstantH=K/C;
ConstantE=eta_/C;

m=DipoleMoment;
c=DipoleCenter;
r       =repmat(Point,[1 length(c)])-c(1:3,:);
PointRM =repmat(sqrt(sum(r.*r)),[3 1]);
EXP     =exp(-K*PointRM);
PointRM2=PointRM.^2;
C=1./PointRM2.*(1+1./(K*PointRM));
D=repmat(sum(r.*m),[3 1])./PointRM2;
M=D.*r;
HField=ConstantH*cross(m,r).*C.*EXP;
EField=ConstantE*((M-m).*(K./PointRM+C)+2*M.*C).*EXP;
```

THIS PAGE INTENTIONALLY LEFT BLANK

APPENDIX B: MATLAB SCRIPTS FOR THE SIMULATIONS OF CHAPTER IV-V

Script *rwg4tl_2.m* (two-feed point dipole connected to two transmission lines)

```
%load the data
load('mesh2');
load('impedance');

rx=1;
zt1=37.5438;%1.0885-8.8658e2i;
zt2=37.5438;%1.0885-8.8658e2i;

%Find the feeding edge(s)(closest to the origin)
FeedPoint=[0; 0; 0];
Index=[];

for m=1:EdgesTotal
    V(m)=0;
    Distance(m)=norm(0.5*sum(p(:,Edge_(:,m)),2)-FeedPoint);
end

[Y,INDEX]=sort(Distance);
Index=[Index INDEX(1)]

%Define the voltage vector
sum_diff=-1;
offset=12;
V(Index-offset)=0.5*EdgeLength(Index-offset);
V(Index+offset)=sum_diff*0.5*EdgeLength(Index+offset);

%Dipole - normal incidence
angz_=-pi/4;
angz=pi+angz_;
angx=pi/2;
d       =[sin(angz)*cos(angx) sin(angz)*sin(angx) cos(angz)]

angz=angz-pi/2;%TEM
Pol     =[sin(angz)*cos(angx) sin(angz)*sin(angx) cos(angz)]

k=omega/c_;
kv=k*d;

for m=1:EdgesTotal
   ScalarProduct=sum(kv.*Center(:,TrianglePlus(m))');
   EmPlus =Pol.'*exp(-j*ScalarProduct);
   ScalarProduct=sum(kv.*Center(:,TriangleMinus(m))');
   EmMinus=Pol.'*exp(-j*ScalarProduct);
   ScalarPlus =sum(EmPlus.* RHO_Plus(:,m));
   ScalarMinus=sum(EmMinus.*RHO_Minus(:,m));
   Vr(m)=EdgeLength(m)*(ScalarPlus/2+ScalarMinus/2);%1.0635
end
```

```
%Solve system of MoM equations
tic;

VV=0;%transmit case
if (rx==1)
    VV=Vr;%receive case
end

D=[0 1;1 0]%two port device connected to dipole

source1=0.5*EdgeLength(Index-offset);%turn off Vin for receive case
source2=sum_diff*0.5*EdgeLength(Index+offset);
if (rx==1)
    source1=0;
    source2=0;
end

VV(EdgesTotal+1)=0;
VV(EdgesTotal+2)=-source1*D(1,2);
VV(EdgesTotal+3)=-source1*D(2,2);
VV(EdgesTotal+4)=0;
VV(EdgesTotal+5)=-source2*D(1,2);
VV(EdgesTotal+6)=-source2*D(2,2);

ZZ(1:EdgesTotal+6,1:EdgesTotal+6)=0;
ZZ(1:EdgesTotal,1:EdgesTotal)=Z(1:EdgesTotal,1:EdgesTotal);

ZZ(Index-offset,EdgesTotal+1)=-1;
ZZ(Index-offset,EdgesTotal+2)=-1;

ZZ(Index+offset,EdgesTotal+4)=-1;
ZZ(Index+offset,EdgesTotal+5)=-1;

Zo1=EdgeLength(Index-offset)^2*zt1;%TL impedance
ZZ(EdgesTotal+1,Index-offset)=+1;
ZZ(EdgesTotal+1,EdgesTotal+1)=+1/Zo1;
ZZ(EdgesTotal+1,EdgesTotal+2)=-1/Zo1;

Zo2=EdgeLength(Index+offset)^2*zt2;%TL impedance
ZZ(EdgesTotal+4,Index+offset)=+1;
ZZ(EdgesTotal+4,EdgesTotal+4)=+1/Zo2;
ZZ(EdgesTotal+4,EdgesTotal+5)=-1/Zo2;

ZZ(EdgesTotal+2,EdgesTotal+1)=D(1,1);
ZZ(EdgesTotal+2,EdgesTotal+2)=-1;

ZZ(EdgesTotal+3,EdgesTotal+1)=D(2,1);
ZZ(EdgesTotal+3,EdgesTotal+3)=-1;

ZZ(EdgesTotal+5,EdgesTotal+4)=D(1,1);
ZZ(EdgesTotal+5,EdgesTotal+5)=-1;

ZZ(EdgesTotal+6,EdgesTotal+4)=D(2,1);
ZZ(EdgesTotal+6,EdgesTotal+6)=-1;
```

```
if (rx==1)
    V=Vr;
End


I=Z\V.'; %transmit

II=ZZ\VV.'; %TL feeding Dipole

toc %elapsed time

%Find the antenna input impedance

if (rx==1)

pwr_rec1=.5*(II(EdgesTotal+1)*II(EdgesTotal+1)')/EdgeLength(Index)^2/zt
1*1000

pwr_rec2=.5*(II(EdgesTotal+4)*II(EdgesTotal+4)')/EdgeLength(Index)^2/zt
2*1000
else
    GapCurrent  =sum(II(Index-offset).*EdgeLength(Index-offset)')
    GapVoltage
=mean((II(EdgesTotal+1)+II(EdgesTotal+2))./EdgeLength(Index-offset))
    Impedance   =GapVoltage/GapCurrent
    FeedPower   =1/2*real(GapCurrent*conj(GapVoltage))*1000
    RC1=II(EdgesTotal+1)/II(EdgesTotal+2)
    RL1=-10*log10(abs(RC1)^2)

    GapCurrent  =sum(II(Index+offset).*EdgeLength(Index+offset)')
    GapVoltage
=mean((II(EdgesTotal+4)+II(EdgesTotal+5))./EdgeLength(Index+offset))
    Impedance   =GapVoltage/GapCurrent
    FeedPower   =1/2*real(GapCurrent*conj(GapVoltage))*1000
    RC2=II(EdgesTotal+4)/II(EdgesTotal+5)
    RL2=-10*log10(abs(RC2)^2)
end


if (rx==1)
    I(1:EdgesTotal)=II(1:EdgesTotal);
end

if (rx==1)

FileName='current.mat';
save(FileName, 'f','omega','mu_','epsilon_','c_',
'eta_','I','V','d','Pol');

else

FileName='current.mat';
save(FileName, 'f','omega','mu_','epsilon_','c_', 'eta_',...
    'I','V','GapCurrent','GapVoltage','Impedance','FeedPower');

end
```

Script *rwg4tl_hr.m* (two-feed point dipole connected to a magic-tee)

```
%load the data
load('mesh2');
load('impedance');

%Find the feeding edge(s)(closest to the origin)
FeedPoint=[0; 0; 0];
Index=[];

for m=1:EdgesTotal
    V(m)=0;
    Distance(m)=norm(0.5*sum(p(:,Edge_(:,m)),2)-FeedPoint);
end

[Y,INDEX]=sort(Distance);
Index=[Index INDEX(1)]         %Center feed - dipole

rx=1;
sum_diff=1;
offset=12;

%Define the voltage vector
V(Index-offset)=+0.5*EdgeLength(Index-offset);
V(Index+offset)=+0.5*EdgeLength(Index+offset)*sum_diff;

angz_=-pi/4;
angz=pi+angz_;
angx=pi/2;
d       =[sin(angz)*cos(angx) sin(angz)*sin(angx) cos(angz)]

angz=angz-pi/2;%TEM
Pol     =[sin(angz)*cos(angx) sin(angz)*sin(angx) cos(angz)]

k=omega/c_;
kv=k*d;

for m=1:EdgesTotal
   ScalarProduct=sum(kv.*Center(:,TrianglePlus(m))');
   EmPlus =Pol.'*exp(-j*ScalarProduct);
   ScalarProduct=sum(kv.*Center(:,TriangleMinus(m))');
   EmMinus=Pol.'*exp(-j*ScalarProduct);
   ScalarPlus =sum(EmPlus.* RHO_Plus(:,m));
   ScalarMinus=sum(EmMinus.*RHO_Minus(:,m));
   Vr(m)=EdgeLength(m)*(ScalarPlus/2+ScalarMinus/2);%1.0635
end

%Solve system of MoM equations
tic;

%hydrid ring input

S_hr=1/sqrt(2)*[0 1 1 0;1 0 0 1;1 0 0 -1;0 1 -1 0]%hybrid ring
connected to dipole
```

```
hr_a1=1;%sum port incidence
hr_a4=0;%difference port incidence

if (rx==1)
    hr_a1=0;
    hr_a4=0;
end

EL=EdgeLength(Index-offset);%symmetrical structure !!!
EL2=EL^2;

VV=0;
if (rx==1)
    VV=Vr;
End


VV(EdgesTotal+1)=0;
VV(EdgesTotal+2)=0;
VV(EdgesTotal+3)=(S_hr(1,1)*hr_a1 + S_hr(1,4)*hr_a4)*EL;
VV(EdgesTotal+4)=(S_hr(2,1)*hr_a1 + S_hr(2,4)*hr_a4)*EL;
VV(EdgesTotal+5)=(S_hr(3,1)*hr_a1 + S_hr(3,4)*hr_a4)*EL;
VV(EdgesTotal+6)=(S_hr(4,1)*hr_a1 + S_hr(4,4)*hr_a4)*EL;

ZZ(1:EdgesTotal+6,1:EdgesTotal+6)=0;
ZZ(1:EdgesTotal,1:EdgesTotal)=Z(1:EdgesTotal,1:EdgesTotal);

%Vn = Vn+ + Vn-
ZZ(Index-offset,EdgesTotal+1)=-1;
ZZ(Index-offset,EdgesTotal+2)=-1;

ZZ(Index+offset,EdgesTotal+3)=-1;
ZZ(Index+offset,EdgesTotal+4)=-1;

%-In = (Vn+ - Vn-)/Zon
Zt1=50;%37.5438;%1.0885-8.8658e2i;
Zt2=50;%37.5438;%1.0885-8.8658e2i;

Zo1=EL2*Zt1;
ZZ(EdgesTotal+1,Index-offset)=1;
ZZ(EdgesTotal+1,EdgesTotal+1)=+1/Zo1;
ZZ(EdgesTotal+1,EdgesTotal+2)=-1/Zo1;

Zo2=EL2*Zt2;
ZZ(EdgesTotal+2,Index+offset)=1;
ZZ(EdgesTotal+2,EdgesTotal+3)=+1/Zo2;
ZZ(EdgesTotal+2,EdgesTotal+4)=-1/Zo2;

ZZ(EdgesTotal+3,EdgesTotal+1)=-S_hr(1,2);
ZZ(EdgesTotal+3,EdgesTotal+2)=0;
ZZ(EdgesTotal+3,EdgesTotal+3)=-S_hr(1,3);
ZZ(EdgesTotal+3,EdgesTotal+4)=0;
ZZ(EdgesTotal+3,EdgesTotal+5)=1;
ZZ(EdgesTotal+3,EdgesTotal+6)=0;
```

```
ZZ(EdgesTotal+4,EdgesTotal+1)=-S_hr(2,2);
ZZ(EdgesTotal+4,EdgesTotal+2)=1;
ZZ(EdgesTotal+4,EdgesTotal+3)=-S_hr(2,3);
ZZ(EdgesTotal+4,EdgesTotal+4)=0;
ZZ(EdgesTotal+4,EdgesTotal+5)=0;
ZZ(EdgesTotal+4,EdgesTotal+6)=0;

ZZ(EdgesTotal+5,EdgesTotal+1)=-S_hr(3,2);
ZZ(EdgesTotal+5,EdgesTotal+2)=0;
ZZ(EdgesTotal+5,EdgesTotal+3)=-S_hr(3,3);
ZZ(EdgesTotal+5,EdgesTotal+4)=1;
ZZ(EdgesTotal+5,EdgesTotal+5)=0;
ZZ(EdgesTotal+5,EdgesTotal+6)=0;

ZZ(EdgesTotal+6,EdgesTotal+1)=-S_hr(4,2);
ZZ(EdgesTotal+6,EdgesTotal+2)=0;
ZZ(EdgesTotal+6,EdgesTotal+3)=-S_hr(4,3);
ZZ(EdgesTotal+6,EdgesTotal+4)=0;
ZZ(EdgesTotal+6,EdgesTotal+5)=0;
ZZ(EdgesTotal+6,EdgesTotal+6)=1;

if (rx==1)
    V=Vr;
end

I=Z\V.';

II=ZZ\VV.';

%I(1:EdgesTotal)=II(1:EdgesTotal);

toc %elapsed time

%Find the antenna input impedance

GapCurrent  =sum(II(Index-offset).*EdgeLength(Index-offset)')
GapVoltage
=mean((II(EdgesTotal+1)+II(EdgesTotal+2))./EdgeLength(Index-offset))
Impedance   =GapVoltage/GapCurrent
FeedPower   =1/2*real(GapCurrent*conj(GapVoltage))*1000

GapCurrent  =sum(II(Index+offset).*EdgeLength(Index+offset)')
GapVoltage
=mean((II(EdgesTotal+3)+II(EdgesTotal+4))./EdgeLength(Index+offset))
Impedance   =GapVoltage/GapCurrent
FeedPower   =1/2*real(GapCurrent*conj(GapVoltage))*1000

sum_out=II(EdgesTotal+5)
diff_out=II(EdgesTotal+6)
sum_out_pwr=0.5*II(EdgesTotal+5)*II(EdgesTotal+5)'/EL2/Zt1*1000
diff_out_pwr=0.5*II(EdgesTotal+6)*II(EdgesTotal+6)'/EL2/Zt2*1000
total_pwr=sum_out_pwr+diff_out_pwr
I(1:EdgesTotal)=II(1:EdgesTotal);

FileName='current.mat';
save(FileName, 'f','omega','mu_','epsilon_','c_', 'eta_',...
    'I','V','GapCurrent','GapVoltage','Impedance','FeedPower');
```

Script *rwg4_Zin_a3.m* (array of three dipoles)

```
clear all
%Load the data
load('mesh2');
load('impedance');

V(1:EdgesTotal)=0;

%Find feeding edges closest to the array Feed
N=length(Feed(1,:));
Index=[];
for k=1:N
    for m=1:EdgesTotal
        Distance(m)=norm(0.5*sum(p(:,Edge_(:,m)),2)-Feed(:,k));
    end
    [Y,INDEX]=sort(Distance);
    Index=[Index INDEX(1)];      %Center feed - dipole
end
Index
N=length(Index);

%Identify phase shift
%The progressive phase shift is 90 for the broadside array:
scan_index=0;
for scan = pi/2:-pi/72:0

    scan_index=scan_index+1;
    phase=-pi*cos(-scan);
    display(scan/pi*180);

%Identify feeding voltages-linear array (dipole array only!)
for n=1:N
    nn=Index(n);
    V(nn)=1.0*EdgeLength(nn)*exp(j*phase*(n-1));
end

%Solve system of MoM equations
tic;
I=Z\V.';
toc %elapsed time

%Terminal impedance (dipole array only!)
for n=1:N
    nn=Index(n);
    GapCurrent(n)=I(nn)*EdgeLength(nn);
    GapVoltage(n)=V(nn)/EdgeLength(nn);
    Impedance(scan_index,n)=GapVoltage(n)/GapCurrent(n); %this is the
terminal impedance
end
display(Impedance(scan_index,:));
end

save ('zin1','Impedance');
```

Script *rwg4tl_ary3.m* (array of three dipoles connected to transmission lines)

```
clear all
%Load the data
load('mesh2');
load('impedance');

V(1:EdgesTotal)=0;

%Find feeding edges closest to the array Feed
N=length(Feed(1,:));
Index=[];
for k=1:N
    for m=1:EdgesTotal
        Distance(m)=norm(0.5*sum(p(:,Edge_(:,m)),2)-Feed(:,k));
    end
    [Y,INDEX]=sort(Distance);
    Index=[Index INDEX(1)];      %Center feed - dipole
end
Index
V(Index)=1.0*EdgeLength(Index);
N=length(Index);

%Identify phase shift
%The progressive phase shift is 90 for the broadside array:
phase=-pi*cos(0);%reference to horizontal

%Identify feeding voltages-linear array (dipole array only!)
for n=1:N
    nn=Index(n);
    V(nn)=V(nn)*exp(j*phase*(n-1));
end

%Solve system of MoM equations
tic;

VV=0;

D=[0 1;1 0]%two port device connected to dipole
source=V(Index)

VV(EdgesTotal+2)=source(1)*D(1,2);
VV(EdgesTotal+3)=source(1)*D(2,2);

VV(EdgesTotal+5)=source(2)*D(1,2);
VV(EdgesTotal+6)=source(2)*D(2,2);

VV(EdgesTotal+8)=source(3)*D(1,2);
VV(EdgesTotal+9)=source(3)*D(2,2);

ZZ(1:EdgesTotal+9,1:EdgesTotal+9)=0;
ZZ(1:EdgesTotal,1:EdgesTotal)=Z(1:EdgesTotal,1:EdgesTotal);

ZZ(Index(1),EdgesTotal+1)=-1;
ZZ(Index(1),EdgesTotal+2)=-1;
```

```
ZZ(Index(2),EdgesTotal+4)=-1;
ZZ(Index(2),EdgesTotal+5)=-1;

ZZ(Index(3),EdgesTotal+7)=-1;
ZZ(Index(3),EdgesTotal+8)=-1;

%Zo=1e2*[1.0270+0.0507i 0.8032-0.2487i 1.0293+0.0497i];%broadside scan
Zo=[75 75 75];

Zo1=EdgeLength(Index(1))^2*Zo(1);
ZZ(EdgesTotal+1,Index(1))=+1;
ZZ(EdgesTotal+1,EdgesTotal+1)=-1/Zo1;
ZZ(EdgesTotal+1,EdgesTotal+2)=+1/Zo1;

ZZ(EdgesTotal+2,EdgesTotal+1)=+1;
ZZ(EdgesTotal+2,EdgesTotal+2)=-D(1,1);

ZZ(EdgesTotal+3,EdgesTotal+2)=-D(2,1);
ZZ(EdgesTotal+3,EdgesTotal+3)=+1;

Zo2=EdgeLength(Index(2))^2*Zo(2);
ZZ(EdgesTotal+4,Index(2))=+1;
ZZ(EdgesTotal+4,EdgesTotal+4)=-1/Zo2;
ZZ(EdgesTotal+4,EdgesTotal+5)=+1/Zo2;

ZZ(EdgesTotal+5,EdgesTotal+4)=+1;
ZZ(EdgesTotal+5,EdgesTotal+5)=-D(1,1);

ZZ(EdgesTotal+6,EdgesTotal+5)=-D(2,1);
ZZ(EdgesTotal+6,EdgesTotal+6)=+1;

Zo3=EdgeLength(Index(3))^2*Zo(3);
ZZ(EdgesTotal+7,Index(3))=1;
ZZ(EdgesTotal+7,EdgesTotal+7)=-1/Zo3;
ZZ(EdgesTotal+7,EdgesTotal+8)=+1/Zo3;

ZZ(EdgesTotal+8,EdgesTotal+7)=+1;
ZZ(EdgesTotal+8,EdgesTotal+8)=-D(1,1);

ZZ(EdgesTotal+9,EdgesTotal+8)=-D(2,1);
ZZ(EdgesTotal+9,EdgesTotal+9)=+1;

II=ZZ\VV.';

toc %elapsed time

RL1=(II(EdgesTotal+2)/II(EdgesTotal+1))
Za1=(II(EdgesTotal+2)+II(EdgesTotal+1))/(EdgeLength(Index(1))^2*II(Inde
x(1)));

RL2=(II(EdgesTotal+5)/II(EdgesTotal+4))
Za2=(II(EdgesTotal+5)+II(EdgesTotal+4))/(EdgeLength(Index(2))^2*II(Inde
x(2)));

RL3=(II(EdgesTotal+8)/II(EdgesTotal+7))
Za3=(II(EdgesTotal+8)+II(EdgesTotal+7))/(EdgeLength(Index(3))^2*II(Inde
x(3)));
```

```
Impedance=[Za1 Za2 Za3]

I(1:EdgesTotal)=II(1:EdgesTotal);

FileName='current.mat';
save(FileName, 'f','omega','mu_','epsilon_','c_', 'eta_',...
    'I','V');%,'GapCurrent','GapVoltage','Impedance','FeedPower');
```

Script *rwg4hr_ary3_rx_loop1.m* (array of three two-feed point dipoles connected to magic-tees)

```
clear all
%Load the data
load('mesh2');
load('impedance');

V(1:EdgesTotal)=0;

%Find feeding edges closest to the array Feed
N=length(Feed(1,:));
Index=[];
for k=1:N
    for m=1:EdgesTotal
        Distance(m)=norm(0.5*sum(p(:,Edge_(:,m)),2)-Feed(:,k));
    end
    [Y,INDEX]=sort(Distance);
    Index=[Index INDEX(1)];      %Center feed - dipole
end
Index
N=length(Index);

count=0;
%parallel pol scan from 0-90 deg
for angz_ = pi/2:-pi/72:0
angx=pi/2;
angz=angz_;
d       =[sin(angz)*cos(angx) sin(angz)*sin(angx) cos(angz)];

angz=-pi/2+angz_;%TEM
Pol     =[sin(angz)*cos(angx) sin(angz)*sin(angx) cos(angz)];

k=omega/c_;
kv=k*d;

for m=1:EdgesTotal
   ScalarProduct=sum(kv.*Center(:,TrianglePlus(m))');
   EmPlus =Pol.'*exp(-j*ScalarProduct);
   ScalarProduct=sum(kv.*Center(:,TriangleMinus(m))');
   EmMinus=Pol.'*exp(-j*ScalarProduct);
   ScalarPlus =sum(EmPlus.* RHO_Plus(:,m));
   ScalarMinus=sum(EmMinus.*RHO_Minus(:,m));
   V(m)=EdgeLength(m)*(ScalarPlus/2+ScalarMinus/2);
end
```

```
%Solve system of MoM equations
tic;

S_hr=1/sqrt(2)*[0 1 1 0;1 0 0 1;1 0 0 -1;0 1 -1 0]%hybrid ring
connected to dipole

hr1_a1=0;%sum input
hr2_a1=0;%sum input
hr3_a1=0;%sum input
hr_a4=0;%diff input


%voltage vector - scattering parameters on right hand side
VV=V;

VV(EdgesTotal+1)=0;
VV(EdgesTotal+2)=0;
VV(EdgesTotal+3)=S_hr(1,1)*hr1_a1 + S_hr(1,4)*hr_a4;
VV(EdgesTotal+4)=S_hr(2,1)*hr1_a1 + S_hr(2,4)*hr_a4;
VV(EdgesTotal+5)=S_hr(3,1)*hr1_a1 + S_hr(3,4)*hr_a4;
VV(EdgesTotal+6)=S_hr(4,1)*hr1_a1 + S_hr(4,4)*hr_a4;

VV(EdgesTotal+7)=0;
VV(EdgesTotal+8)=0;
VV(EdgesTotal+9)=S_hr(1,1)*hr2_a1 + S_hr(1,4)*hr_a4;
VV(EdgesTotal+10)=S_hr(2,1)*hr2_a1 + S_hr(2,4)*hr_a4;
VV(EdgesTotal+11)=S_hr(3,1)*hr2_a1 + S_hr(3,4)*hr_a4;
VV(EdgesTotal+12)=S_hr(4,1)*hr2_a1 + S_hr(4,4)*hr_a4;

VV(EdgesTotal+13)=0;
VV(EdgesTotal+14)=0;
VV(EdgesTotal+15)=S_hr(1,1)*hr3_a1 + S_hr(1,4)*hr_a4;
VV(EdgesTotal+16)=S_hr(2,1)*hr3_a1 + S_hr(2,4)*hr_a4;
VV(EdgesTotal+17)=S_hr(3,1)*hr3_a1 + S_hr(3,4)*hr_a4;
VV(EdgesTotal+18)=S_hr(4,1)*hr3_a1 + S_hr(4,4)*hr_a4;

ZZ(1:EdgesTotal+18,1:EdgesTotal+18)=0;
ZZ(1:EdgesTotal,1:EdgesTotal)=Z(1:EdgesTotal,1:EdgesTotal);

os=12;
%%a+b
ZZ(Index(1)-os,EdgesTotal+1)=-1;
ZZ(Index(1)-os,EdgesTotal+2)=-1;

ZZ(Index(1)+os,EdgesTotal+3)=-1;
ZZ(Index(1)+os,EdgesTotal+4)=-1;

ZZ(Index(2)-os,EdgesTotal+7)=-1;
ZZ(Index(2)-os,EdgesTotal+8)=-1;

ZZ(Index(2)+os,EdgesTotal+9)=-1;
ZZ(Index(2)+os,EdgesTotal+10)=-1;

ZZ(Index(3)-os,EdgesTotal+13)=-1;
ZZ(Index(3)-os,EdgesTotal+14)=-1;

ZZ(Index(3)+os,EdgesTotal+15)=-1;
```

```
ZZ(Index(3)+os,EdgesTotal+16)=-1;

%%a-b

Ztl=[50 50 50]
Zo=EdgeLength(Index(1)-os)^2*Ztl;%symmetry

ZZ(EdgesTotal+1,Index(1)-os)=1;
ZZ(EdgesTotal+1,EdgesTotal+1)=+1/Zo(1);
ZZ(EdgesTotal+1,EdgesTotal+2)=-1/Zo(1);

ZZ(EdgesTotal+2,Index(1)+os)=1;
ZZ(EdgesTotal+2,EdgesTotal+3)=+1/Zo(1);
ZZ(EdgesTotal+2,EdgesTotal+4)=-1/Zo(1);

ZZ(EdgesTotal+7,Index(2)-os)=1;
ZZ(EdgesTotal+7,EdgesTotal+7)=+1/Zo(2);
ZZ(EdgesTotal+7,EdgesTotal+8)=-1/Zo(2);

ZZ(EdgesTotal+8,Index(2)+os)=1;
ZZ(EdgesTotal+8,EdgesTotal+9)=+1/Zo(2);
ZZ(EdgesTotal+8,EdgesTotal+10)=-1/Zo(2);

ZZ(EdgesTotal+13,Index(3)-os)=1;
ZZ(EdgesTotal+13,EdgesTotal+13)=+1/Zo(3);
ZZ(EdgesTotal+13,EdgesTotal+14)=-1/Zo(3);

ZZ(EdgesTotal+14,Index(3)+os)=1;
ZZ(EdgesTotal+14,EdgesTotal+15)=+1/Zo(3);
ZZ(EdgesTotal+14,EdgesTotal+16)=-1/Zo(3);

%%scattering parameters on left hand side

%%
ZZ(EdgesTotal+3,EdgesTotal+1)=-S_hr(1,2);
ZZ(EdgesTotal+3,EdgesTotal+2)=0;
ZZ(EdgesTotal+3,EdgesTotal+3)=-S_hr(1,3);
ZZ(EdgesTotal+3,EdgesTotal+4)=0;
ZZ(EdgesTotal+3,EdgesTotal+5)=1;
ZZ(EdgesTotal+3,EdgesTotal+6)=0;

ZZ(EdgesTotal+4,EdgesTotal+1)=-S_hr(2,2);
ZZ(EdgesTotal+4,EdgesTotal+2)=1;
ZZ(EdgesTotal+4,EdgesTotal+3)=-S_hr(2,3);
ZZ(EdgesTotal+4,EdgesTotal+4)=0;
ZZ(EdgesTotal+4,EdgesTotal+5)=0;
ZZ(EdgesTotal+4,EdgesTotal+6)=0;

ZZ(EdgesTotal+5,EdgesTotal+1)=-S_hr(3,2);
ZZ(EdgesTotal+5,EdgesTotal+2)=0;
ZZ(EdgesTotal+5,EdgesTotal+3)=-S_hr(3,3);
ZZ(EdgesTotal+5,EdgesTotal+4)=1;
ZZ(EdgesTotal+5,EdgesTotal+5)=0;
ZZ(EdgesTotal+5,EdgesTotal+6)=0;
```

```
ZZ(EdgesTotal+6,EdgesTotal+1)=-S_hr(4,2);
ZZ(EdgesTotal+6,EdgesTotal+2)=0;
ZZ(EdgesTotal+6,EdgesTotal+3)=-S_hr(4,3);
ZZ(EdgesTotal+6,EdgesTotal+4)=0;
ZZ(EdgesTotal+6,EdgesTotal+5)=0;
ZZ(EdgesTotal+6,EdgesTotal+6)=1;

%%
ZZ(EdgesTotal+9,EdgesTotal+7)=-S_hr(1,2);
ZZ(EdgesTotal+9,EdgesTotal+8)=0;
ZZ(EdgesTotal+9,EdgesTotal+9)=-S_hr(1,3);
ZZ(EdgesTotal+9,EdgesTotal+10)=0;
ZZ(EdgesTotal+9,EdgesTotal+11)=1;
ZZ(EdgesTotal+9,EdgesTotal+12)=0;

ZZ(EdgesTotal+10,EdgesTotal+7)=-S_hr(2,2);
ZZ(EdgesTotal+10,EdgesTotal+8)=1;
ZZ(EdgesTotal+10,EdgesTotal+9)=-S_hr(2,3);
ZZ(EdgesTotal+10,EdgesTotal+10)=0;
ZZ(EdgesTotal+10,EdgesTotal+11)=0;
ZZ(EdgesTotal+10,EdgesTotal+12)=0;

ZZ(EdgesTotal+11,EdgesTotal+7)=-S_hr(3,2);
ZZ(EdgesTotal+11,EdgesTotal+8)=0;
ZZ(EdgesTotal+11,EdgesTotal+9)=-S_hr(3,3);
ZZ(EdgesTotal+11,EdgesTotal+10)=1;
ZZ(EdgesTotal+11,EdgesTotal+11)=0;
ZZ(EdgesTotal+11,EdgesTotal+12)=0;

ZZ(EdgesTotal+12,EdgesTotal+7)=-S_hr(4,2);
ZZ(EdgesTotal+12,EdgesTotal+8)=0;
ZZ(EdgesTotal+12,EdgesTotal+9)=-S_hr(4,3);
ZZ(EdgesTotal+12,EdgesTotal+10)=0;
ZZ(EdgesTotal+12,EdgesTotal+11)=0;
ZZ(EdgesTotal+12,EdgesTotal+12)=1;

%%
ZZ(EdgesTotal+15,EdgesTotal+13)=-S_hr(1,2);
ZZ(EdgesTotal+15,EdgesTotal+14)=0;
ZZ(EdgesTotal+15,EdgesTotal+15)=-S_hr(1,3);
ZZ(EdgesTotal+15,EdgesTotal+16)=0;
ZZ(EdgesTotal+15,EdgesTotal+17)=1;
ZZ(EdgesTotal+15,EdgesTotal+18)=0;

ZZ(EdgesTotal+16,EdgesTotal+13)=-S_hr(2,2);
ZZ(EdgesTotal+16,EdgesTotal+14)=1;
ZZ(EdgesTotal+16,EdgesTotal+15)=-S_hr(2,3);
ZZ(EdgesTotal+16,EdgesTotal+16)=0;
ZZ(EdgesTotal+16,EdgesTotal+17)=0;
ZZ(EdgesTotal+16,EdgesTotal+18)=0;

ZZ(EdgesTotal+17,EdgesTotal+13)=-S_hr(3,2);
ZZ(EdgesTotal+17,EdgesTotal+14)=0;
ZZ(EdgesTotal+17,EdgesTotal+15)=-S_hr(3,3);
ZZ(EdgesTotal+17,EdgesTotal+16)=1;
ZZ(EdgesTotal+17,EdgesTotal+17)=0;
ZZ(EdgesTotal+17,EdgesTotal+18)=0;
```

```
ZZ(EdgesTotal+18,EdgesTotal+13)=-S_hr(4,2);
ZZ(EdgesTotal+18,EdgesTotal+14)=0;
ZZ(EdgesTotal+18,EdgesTotal+15)=-S_hr(4,3);
ZZ(EdgesTotal+18,EdgesTotal+16)=0;
ZZ(EdgesTotal+18,EdgesTotal+17)=0;
ZZ(EdgesTotal+18,EdgesTotal+18)=1;
%%

II=ZZ\VV.';

toc %elapsed time

count=count+1
sum_out(count,1)=II(EdgesTotal+5);
sum_out(count,2)=II(EdgesTotal+11);
sum_out(count,3)=II(EdgesTotal+17);

diff_out(count,1)=II(EdgesTotal+6);
diff_out(count,2)=II(EdgesTotal+12);
diff_out(count,3)=II(EdgesTotal+18);

save (‘sumdiff’,‘sum_out’,‘diff_out’);
```

LIST OF REFERENCES

[1] W. L. Stutzman and G. A. Thiele, *Antenna Theory and Design*, 2nd Edition, Wiley, New York, 1998.

[2] Chua Eng Hock, "Reduction of mutual coupling in small dipole array antennas," Master's Thesis, Naval Postgraduate School, Monterey, California, March 2003.

[3] S. N. Makarov, *Antenna and EM Modeling with MATLAB®*, Wiley, New York, 2002.

[4] S. M. Rao, D. R. Wilton, and A.W. Glisson, "Electromagnetic scattering by surfaces of arbitrary shapes," *IEEE Transactions on Antennas and Propagation*, vol. 30, no. 3, pp 409-418, 1982.

[5] D. Z. Du and F.K. Hwang, *Computing in Euclidean Geometry*, 2nd Edition, World Scientific, pp. 47-123, 1995.

[6] C. A. Balanis, *Antenna Theory Analysis and Design*, 2nd Edition, Wiley, New York, 1997.

[7] D. C. Jenn, "A complete matrix solution for antenna analysis," *1989 IEEE AP-S International Symposium Digest*, vol. I, p. 152, June 1989

[8] D. M. Pozar, *Microwave Engineering*, 2nd Edition, Wiley, New York, 1998.

THIS PAGE INTENTIONALLY LEFT BLANK

INITIAL DISTRIBUTION LIST

1. Defense Technical Information Center
   Ft. Belvoir, Virginia

2. Dudley Knox Library
   Naval Postgraduate School
   Monterey, California

3. Professor John P. Powers
   Chairman, Department of Electrical and Computer Engineering
   Code EC
   Naval Postgraduate School
   Monterey, California

4. Professor Yeo Tat Soon
   Director, Temasek Defense Systems Institute
   Block E1, #05-05
   1, Engineering Drive 2
   Singapore 117576

5. Professor David C. Jenn
   Department of Electrical and Computer Engineering
   Code EC/Jn
   Naval Postgraduate School
   Monterey, California

6. Professor Roberto Cristi
   Department of Electrical and Computer Engineering
   Code EC/Cx
   Naval Postgraduate School
   Monterey, California

7. MAJ Ong Chee Hwee
   Republic of Singapore Navy
   Ministry of Defense
   Singapore